

The University of Nottingham

UNITED KINGDOM · CHINA · MALAYSIA

Formulation and Stabilization of Protein-Loaded Nanoparticles and Potential Therapeutic Applications Thereof

K M Khairul Alam, MPharm

Thesis submitted to the University of Nottingham

for the degree of

Doctor of Philosophy

AUGUST 2016

Abstract

Myocardial infarction is a medical emergency and needs an immediate treatment with reperfusion therapy. But, reperfusion itself causes damage to the myocardium by overproduction of reactive oxygen species (ROS). These excessive ROS generated during reperfusion lead to oxidative stress in the myocardium and damage to the cardiomyocytes. Reperfusion injury has been suggested to be responsible for up to 50% of the final infarct size of the myocardium and this resultant infarct size is highly related with the development of chronic heart failure. Although both the superoxide anion and hydrogen peroxide are elevated following myocardial infarction, the levels of their endogenous scavenger enzymes, superoxide dismutase and catalase, decrease even more. Catalase is a major antioxidant enzyme in the body's endogenous antioxidant defence systems and this enzyme is considered to be responsible for most of the peroxidase activities in the cardiomyocytes.

Delivery of active proteins such as catalase to the myocardium is challenging as they can easily be inactivated by proteases, aggregation and natural inhibitors. Delivery of therapeutic proteins using polymeric nanoparticles can offer an attractive approach. No studies on evaluation of the cardio-protective effect of catalase-loaded nanoparticles in conserving cardiomyocytes from the oxidative stress induced by reperfusion injury have been reported yet. Poly(lactic-co-glycolic acid) (PLGA) is a US Food & Drug Administration (US FDA)-approved biocompatible and biodegradable polymer, and this polymer was used in this study to prepare catalase-loaded nanoparticles.

In the double emulsion method of fabricating protein-loaded nanoparticles, emulsification process induces denaturation of proteins. No reports have showed the effects of trehalose and bovine serum albumin on the encapsulation of catalase into PLGA nanoparticles and comparison of their effects yet. This study showed that trehalose and bovine serum albumin added to the initial aqueous phase as a stabilizer of the catalase activity were observed to be effective in reducing loss of enzymatic activity of catalase during emulsification steps of the enzyme

encapsulation process in the double emulsion method. Surprisingly, unlike BSA-stabilized catalase-loaded PLGA nanoparticles, trehalose-stabilized nanoparticles showed very low enzymatic activity which was comparable to the catalase activity of the unstabilized nanoparticles.

Freeze-drying is a useful technique to stabilize the nanoparticles and proteins. But, the process of freeze-drying itself exerts stresses resulting in aggregation of the nanoparticles and denaturation of the proteins. Cryoprotectants are added to protect the nanoparticulate systems from the damage induced by the freeze-drying process. Trehalose is a well-known cryoprotectant. No studies on the cryoprotective effect of trehalose in reducing the loss of enzymatic activity of the encapsulated catalase upon freeze-drying of the catalase-loaded PLGA nanoparticles have been reported yet. In this study, trehalose added as a cryoprotectant minimized the loss of enzymatic activity of the encapsulated catalase of catalase-loaded nanoparticles in a dose-dependent manner.

Cryoprotected catalase-loaded nanoparticles were found to be effective in reducing oxidative stress-induced damage in a widely recognized hydrogen peroxide-induced cellular model of oxidative stress in HL-1 cardiomyocytes. This protective response was dose-dependent. The nanoparticles also demonstrated efficacy in reducing apoptosis that plays an important role in myocardial cell death during reperfusion of the myocardium and is linked with the development of heart failure following myocardial infarction. Structural study of the encapsulated catalase of catalase-loaded nanoparticles was performed by Attenuated Total Reflectance-Fourier Transform Infrared (ATR-FTIR) spectroscopy and fluorescence spectroscopy which showed that trehalose could reduce the encapsulated enzyme's structural alterations induced by freeze-drying of the nanoparticles.

The promising cardioprotective effect demonstrated by the cryoprotected catalase-loaded PLGA nanoparticles in rescuing cardiomyocytes from oxidative stress, makes this catalase-loaded nanoparticle a valuable candidate for the treatment of reperfusion injury and warrants further investigation including animal trials.

Acknowledgements

Firstly, I would like to thank my supervisors, Professor Phil Williams and Dr Jonathan Aylott, for their continuous intellectual guidance, advice and discussion they provided during working towards my PhD. I am grateful to them for the support they ensured for me in both academic and non-academic fields. I thankfully acknowledge the Government of the Peoples Republic of Bangladesh for financing my PhD study.

I am grateful to Dr James Dixon for providing cells and cell culture training, and his support in my cell culture work. I gratefully acknowledge Dr David Onion's assistance, advice and training in flow cytometry analysis.

My thanks go to Dr Veeren Chauhan, Dr Mohammad Mounir, Dr Arrandeep Singh Basra and other colleagues of the D38 lab for making a great environment to work in the lab. I am also thankful to my friend, Mohammed Khaled Tumbi for his continuous extra-ordinary support and motivation.

I must thank Robert Markus, School of Life Sciences Imaging (SLIM) for his help in super-resolution microscopy and as well as thank the BBSRC which funded the microscope facility (ref# BB/L013827/1).

Finally, I gratefully thank my family members especially my wife and parents for their love, inspiration and motivational support which helped me to undertake and complete this PhD study.

Contents

Abstract…...……..i

Acknowledgements…….……...…iii

Contents…….……iv

List of Figures……..….. ix

List of Tables……...…xv

List of Abbreviations……..xvi

1 General Introduction 1

1.1 Heart disease and oxidative stress 1

1.1.1 Myocardial infarction 1

1.1.2 Heart failure followed by myocardial infarction 10

1.1.3 ROS and Oxidative stress 10

1.1.4 Myocardial ischemia/reperfusion injury 17

1.1.5 Experimental manipulative approaches in signalling pathways of different death modes 21

1.1.6 Therapeutic approaches in reducing myocardial I/R injury 23

1.2 Formulation of nanoparticles 26

1.2.1 Polymeric nanoparticles 26

1.2.2 Poly(lactic-co-glycolic acid) 27

1.2.3 Instability of the protein-loaded nanoparticles 31

1.2.4 Freeze-drying of protein-loaded PLGA nanoparticles 34

1.3 Structural characterization of protein-loaded nanoparticles 36

1.3.1 Protein's secondary structural characterization by infrared spectroscopy 37

1.3.2 Protein's tertiary structural characterization by fluorescence spectroscopy 38

1.4 Aims 42

2 Preparation and Characterization of Protein-Loaded PLGA Nanoparticles 44

2.1 Introduction 44

2.2 Materials and methods 48

2.2.1 Chemicals 48

2.2.2 Formulation of nanoparticles 48

2.2.3 Freeze-drying 56

2.2.4 Analysis of catalase activity 57

2.2.5 Reconstitution and analysis of particle size and zeta potential of the nanoparticles 58

2.2.6 Transmission electron microscopy 60

2.2.7 Statistical analysis 61

2.3 Results 62

2.3.1 Plain PLGA nanoparticles by nanoprecipitation method 62

2.3.2 Catalase-loaded PLGA nanoparticles 67

2.3.3 Role of trehalose on lyophilization of bovine serum albumin-stabilized catalase-loaded nanoparticles 76

2.3.4 Particle size, zeta potential and morphology of reconstituted BSA-stabilized catalase-loaded nanoparticles 78

2.4 Discussion 80

2.5 Conclusion 89

3 Evaluation of Potential Therapeutic Use of Cryoprotected BSA-Stabilized Catalase-Loaded PLGA Nanoparticles in Myocardial Ischemia/Reperfusion Injury 91

3.1 Introduction 91

3.2 Materials and methods 95

3.2.1 Materials 95

3.2.2 Cell culture 95

3.2.3 Reconstitution of freeze-dried nanoparticles 96

3.2.4 Induction and treatment of oxidative stress 96

3.2.5 Induction and treatment of apoptosis 98

3.2.6 Cytotoxicity of nanoparticles 101

3.2.7 Co-exposure of cardiomyocytes with 1000µM of H_2O_2 and 200 µg/well of nanoparticles 102

3.2.8 Cellular uptake of nanoparticles 103

3.2.9 Statistical analysis 108

3.3 Results 109

3.3.1 Cytotoxicity upon exposure to hydrogen peroxide 109

3.3.2 Cryoprotected BSA-stabilized catalase-loaded nanoparticles protected cardiomyocytes from hydrogen peroxide-induced cytotoxicity .. 111

3.3.3 Cryoprotected BSA-stabilized catalase-loaded nanoparticles protected cardiomyocytes from hydrogen peroxide-induced apoptosis 116

3.3.4 Cytotoxicity of the cryoprotected BSA-stabilized catalase-loaded nanoparticles 121

3.3.5 Presence of the cryoprotected BSA-stabilized catalase-loaded nanoparticles neutralized H_2O_2 of higher strength in contact with the cardiomyocytes 123

3.3.6 Alexa Fluor 488-stained BSA-stabilized catalase-loaded PLGA nanoparticles 124

3.4 Discussion 129

3.5 Conclusion 138

4 Investigation of Structural Changes of Encapsulated Catalase upon Lyophilization and Cryoprotection of Unstabilized Catalase-Loaded PLGA Nanoparticles 139

4.1 Introduction 139

4.2 Materials and methods 141

4.2.1 Unstabilized Catalase-loaded PLGA nanoparticles 141

4.2.2 ATR-FTIR spectroscopy analysis 143

4.2.3 Fluorescence spectroscopy analysis 144

4.3 Results 146

4.3.1 Effect of trehalose on lyophilization of unstabilized catalase-loaded PLGA nanoparticles 146

4.3.2 ATR-FTIR spectroscopic study 148

4.3.3 Fluorescence spectroscopic study 151

4.4 Discussion 157

4.5 Conclusion 162

5 Summary and future work 164

5.1 Summary 164

5.2 Future work 176

6 References 179

List of Figures

Figure 1: Reversible and irreversible injury of the cardiomyocytes in response to the duration of ischemia. 2

Figure 2: The 'wave-front' of necrosis due to ischemia in canine models..... 3

Figure 3: Diagrammatic view of apoptotic and necrotic cells..... 4

Figure 4: Schematic diagram of intrinsic and extrinsic pathways of apoptosis. 6

Figure 5: Pathway of necroptosis 8

Figure 6: Pathways of forming endogenous superoxide anion 13

Figure 7: Cellular defence system against ROS 15

Figure 8: Diagrammatic representation of area at risk, myocardial infarct size and myocardial salvage 18

Figure 9: Diagrammatic illustration of myocardial ischemia/reperfusion injury .. 19

Figure 10: Hydrolysis of PLGA 28

Figure 11: Fabrication of PLGA nanoparticles by different methods 30

Figure 12: Tryptophan emission spectra of Apoazurin Pfl, Ribonuclease T1, Staphylococcal nuclease and Glucagon (from 1 to 4, respectively) showing effect of the tryptophan microenvironment on their emission spectra 40

Figure 13: Diagrammatic presentation of preparing catalase-loaded PLGA nanoparticles. 51

Figure 14: Representative photographs of reconstituted plain PLGA NPs after mixing by vortex. 62

Figure 15: Comparison of non-cryoprotected and cryoprotected of plain PLGA NPs after reconstitution by vortex & probe sonication. 63

Figure 16: Representative TEM image of freshly prepared plain PLGA NPs. 66

Figure 17: Representative TEM image of reconstituted plain PLGA NPs cryoprotected by trehalose. 67

Figure 18: Activity of catalase retained in the nanoparticles after formulation without stabilizer and cryoprotection. 69

Figure 19: Effect of the emulsification procedure. 69

Figure 20: Effect of the absence of dichloromethane. 70

Figure 21: Effect of the absence of ultrasonication. 71

Figure 22: Comparative detrimental effects of vortex followed by ultrasonication and only vortex. 72

Figure 23: Effect of trehalose added to the initial aqueous phase. 73

Figure 24: Effect of BSA added to the initial aqueous phase. 74

Figure 25: Comparison of the activities of stabilized and unstabilized nanoparticles. 75

Figure 26: Role of trehalose in preserving catalase activity of BSA-stabilized catalase-loaded nanoparticles upon freeze-drying. 77

Figure 27: Representative TEM image of cryoprotected BSA-stabilized catalase-loaded PLGA NPs after reconstitution. 79

Figure 28: Effect of H_2O_2 on HL-1 cell viability upon exposure for 3 hours. 109

Figure 29: Effect of H_2O_2 on HL-1 cell viability upon exposure for 24 hours. .. 110

Figure 30: Effect of catalase-loaded nanoparticles in protecting the cardiomyocytes from oxidative stress induced by H_2O_2 when the cells were incubated for 3 hours with the BSA-stabilized catalase-loaded PLGA nanoparticles. 112

Figure 31: Comparison of the protective effects provided by the three formulations of the cryoprotected BSA-stabilized catalase-loaded nanoparticles. 114

Figure 32: Protective effect of catalase-loaded nanoparticles in oxidative stress of cardiomyocytes induced by H_2O_2 for 3 hours followed by treating them with the BSA-stabilized catalase-loaded PLGA nanoparticles. 115

Figure 33: Representative flow cytometric analysis showing protective effect of the nanoparticles in reducing caspase-positive apoptotic HL-1 cells upon exposure to H_2O_2..... 117

Figure 34: Summary of changes in the percentages of caspase-positive apoptotic HL-1 cells as evaluated in the experiments shown in Figure 33. 117

Figure 35: Representative flow cytometric analysis showing no visible protective effect of the nanoparticles in reducing apoptosis of HL-1 cells observed after 6 hours of exposure to H_2O_2. 119

Figure 36: Summary of the percentages of apoptotic cells observed after 6 hours of exposure to H_2O_2 as evaluated in the experiments shown in Figure 35. 119

Figure 37: Representative flow cytometric analysis showing protective effect of the nanoparticles in reducing apoptosis of HL-1 cells observed after 24 hours of exposure to H_2O_2. 120

Figure 38: Summary of changes in the percentages of the apoptotic cells observed after 24 hours of exposure to H_2O_2 as evaluated in the experiments shown in Figure 37. 121

Figure 39: Effect of the cryoprotected BSA-stabilized catalase-loaded nanoparticles on cell viability of the HL-1 cardiomyocytes upon incubating them with the nanoparticles for 24 hours. 122

Figure 40: Effect of the co-treatment of the cryoprotected BSA-stabilized catalase-loaded nanoparticles and H_2O_2 on cell viability of the HL-1 cardiomyocytes. .. 123

Figure 41: Role of trehalose in preserving catalase activity of BSA-stabilized catalase-loaded nanoparticles containing Alexa Fluor 488 upon freeze-drying. 125

Figure 42: Representative flow cytometric histograms showing uptake of the cryoprotected BSA-stabilized catalase-loaded PLGA nanoparticles labelled with Alexa Fluor 488 by HL-1 cells. 126

Figure 43: Representative super-resolution microscopy (3D SIM) image of HL-1 cardiomyocytes showing adsorption of the Alexa Fluor 488-labelled catalase-loaded PLGA nanoparticles on the cell membranes. 127

Figure 44: Representative super-resolution microscopy (3D SIM) reconstructed images of HL-1 cells showing with orthogonal sections that cluster of Alexa Fluor 488-labelled nanoparticles were in the focal plane of nucleus indicating internalization of particles. 128

Figure 45: Role of trehalose in lyophilization of unstabilized catalase-loaded PLGA nanoparticles. 147

Figure 46: Baseline-corrected and area-normalized amide I spectra of native catalase, non-cryoprotected (1.0) and cryoprotected unstabilized catalase-loaded nanoparticles. 149

Figure 47: Comparison of the spectra of freeze-dried trehalose and cryoprotected nanoparticles (1.60). 150

Figure 48: Effect of GdnHCl on tryptophan fluorescence intensity of catalase solution observed at 335 nm. 151

Figure 49: Effect of GdnHCl on tryptophan fluorescence intensity of catalase solution observed at 328 nm. 152

Figure 50: Comparison of tryptophan fluorescence intensities of 1:0 and 1:60 formulations of NPs 153

Figure 51: Changes in tryptophan maximum emission wavelength of catalase with raising concentration of GdnHCl. 154

Figure 52: Comparison of the tryptophan maximum emission wavelengths of the native catalase solution and solutions extracted from NPs. 156

List of Tables

Table 1: Body's oxygen free radicals and their electronic structures 11

Table 2: Endogenous antioxidant enzymes and compounds 15

Table 3: A bird’s eye view of variants of the modified double emulsion method applied in this study 52

Table 4: Action of trehalose in resisting aggregation of NPs upon lyophilization ..... .64

Table 5: Effect of cryoprotection on zeta potential of NPs 65

List of Abbreviations

AAR	Area at risk
AMI	Acute myocardial infarction
ATR-FTIR	Attenuated total reflectance-fourier transform infrared spectroscopy
BSA	Bovine serum albumin
Bcl-2	B-cell lymphoma 2
Bax	Bcl-2–associated protein x
CAT	Catalase
CD	Circular dichromism
eNOS	Endothelial nitric oxide synthase
FD	Freeze-drying
FTIR	Fourier transform infrared
GdnHCl	Guanidine hydrochloride
GPx	Glutathione peroxidase
GR	Glutathione reductase
GSH	Glutathione
GSSG	Glutathione disulfide

IHD	Ischemic heart disease
I/R	Ischemic/Reperfusion
MI	Myocardial infarction
MLKL	Mixed lineage kinase domain-like
MPTP	Mitochondrial permeability transition pore
mTOR	Mammalian target of rapamycin
NADPH	Nicotinamide-adenine dinucleotide phosphate
NOX	NADPH oxidase
NPs	Nanoparticles
OMM	Outer mitochondrial membrane
PCL	Polycaprolactone
PDI	Polydispersity index
PGA	Poly(glycolic acid)
PI	Propidium iodide
PLA	Poly(lactic acid)
PLGA	Poly(lactic-co-glycolic acid)
PMMA	Poly(methyl methacrylate)

PVA	Poly(vinyl alcohol)
RIPK	Receptor-interacting protein kinase
ROS	Reactive oxygen species
SOD	Superoxide dismutase
TEM	Transmission electron microscopy
TNF-α	Tumour necrosis factor-α
Trp	Tryptophan
TRAIL	TNF-related apoptosis-inducing ligand
XD	Xanthine dehydrogenase
XO	Xanthine oxidase

1 General Introduction

1.1 Heart disease and oxidative stress

Ischemic heart disease currently occupies the top position among the leading causes of mortality worldwide. About 7.4 million people died in 2012 due to ischemic heart diseases (IHD) in the world.[1] It is also a major cause of morbidity in the world.[2] Acute myocardial infarction (MI) is the most serious form of IHD.[3]

1.1.1 Myocardial infarction

Myocardial infarction or acute myocardial infarction is defined as sudden cellular death of myocardial tissue because of prolonged myocardial ischemia.[4-6] Blockage of coronary artery is a common cause of myocardial infarction.[7] Histological cell death is not immediately ensued after ischemia. It takes a certain time after starting the ischemic attack.[4] If the ischemic duration is <15-20 minutes, changes in the myocardial tissues due to the ischemia is reversed when coronary blood flow is restored and myocardial cells can survive the insult.[6] Prolonging ischemic period after 20 minutes results in a 'wavefront' of cellular death in the myocardium that starts from the subendocardium and spreads towards the pericardium.[8] Lack of oxygen during ischemia triggers anaerobic respiration in the cardiomyocytes resulting in increased lactate and reduced ATP level.[9]

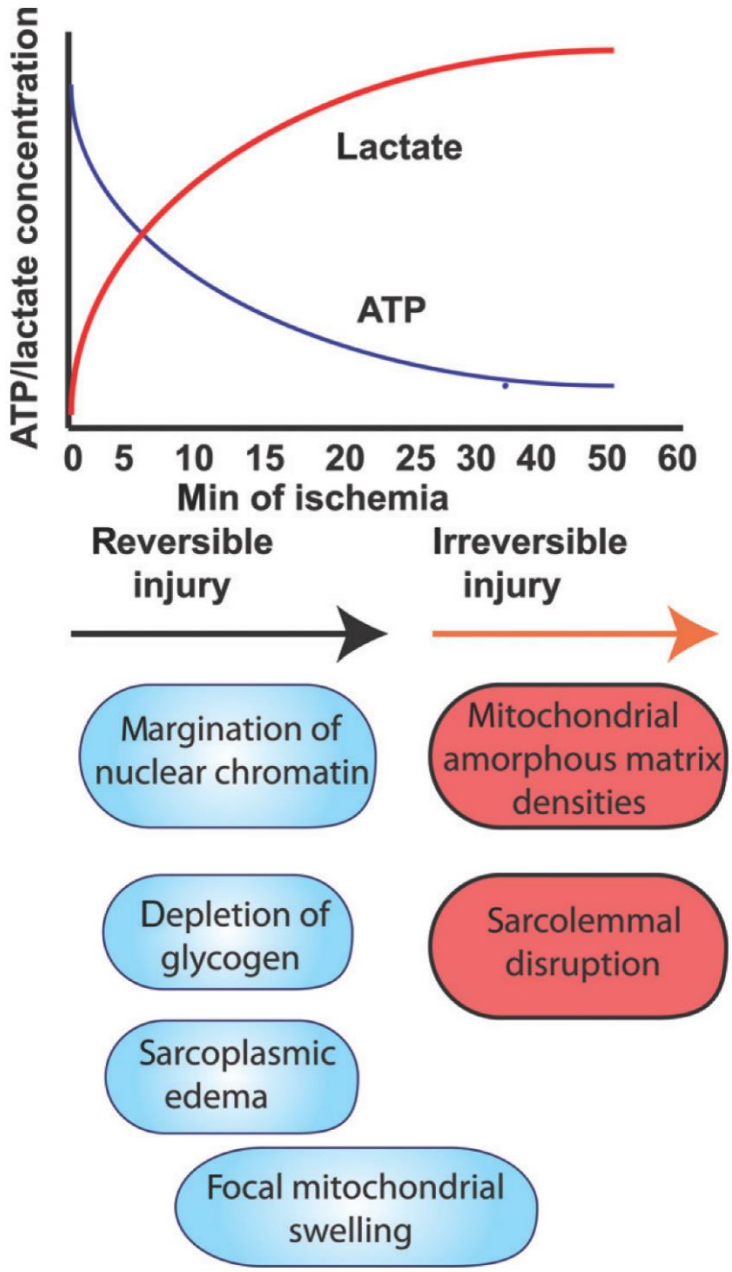

Figure 1: Reversible and irreversible injury of the cardiomyocytes in response to the duration of ischemia. With declining ATP levels in the ischemic myocardium, susceptible subendocardial cardiomyocytes lose structural integrity and present ultrastructural transformations indicative of irreversible cardiomyocyte injury like sarcolemmal disruption and marked changes in the mitochondrial structure such as drastic swelling of mitochondria and representation of amorphous matrix densities. Reproduced from[6]

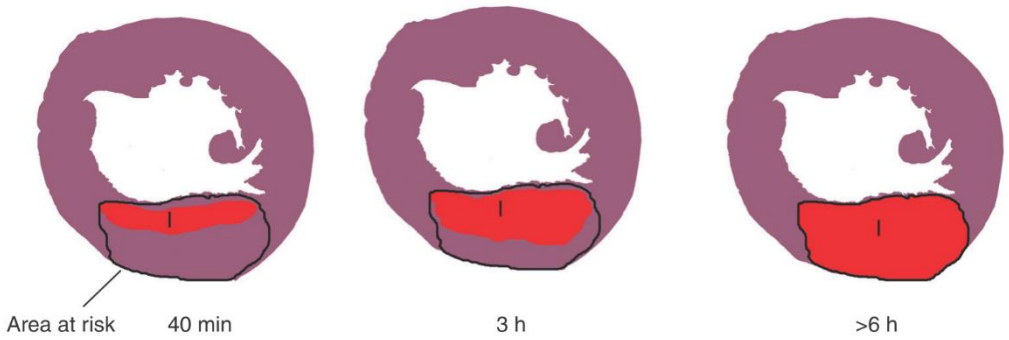

Figure 2: The 'wave-front' of necrosis due to ischemia in canine models, showing progression towards the subepicardium from the subendocardium with increasing the duration of ischemia. Reproduced from[6]

During MI cardiomyocytes in the ischemic area die by necrosis and apoptosis. Comparative contribution of the individual death form is not known yet.[10] A massive surge of cellular death of cardiomyocytes happens in the ischemic area in the first 6-24 hours.[11] Due to the consequence of residual ischemia, a less intense cellular death happens in the peri-infarct zone, which continues because of cardiac remodelling. Afterwards, a lower degree of myocardial cellular death persists in a distant area of the myocardium as a process of cardiac remodelling.[12]

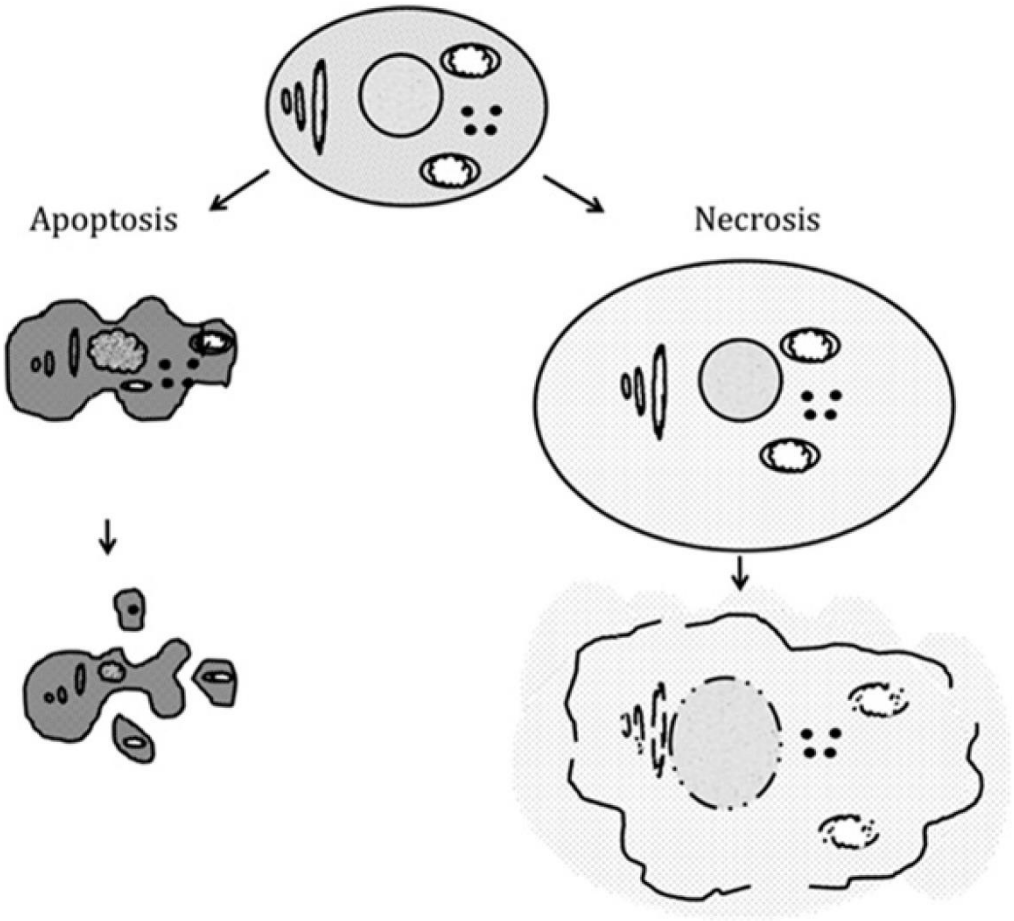

Figure 3: Diagrammatic view of apoptotic and necrotic cells. Reproduced from[13]

Apoptosis is a programmed and regulated death process where apoptotic bodies containing cellular components are formed. Apoptosis is presented with cellular and nuclear shrinkage followed by apoptotic body formation. The apoptotic bodies are removed by phagocytes. As plasma membrane integrity is maintained and no intracellular components are released in apoptotic death, it does not trigger an inflammatory cascade or causes very little inflammatory response.[14]

Apoptosis in the infarcted myocardium is mediated through both intrinsic and extrinsic pathways. Intrinsic pathways involve mitochondrial signalling, whereas

extrinsic pathways involve binding of death ligands to the death receptors located on the cellular surface.[6,10,15]

In the intrinsic pathway, pro-apoptotic members of the B-cell lymphoma 2 (Bcl-2) proteins, Bcl-2 associated X protein (Bax) and Bcl-2 homologous antagonist/killer (Bak) cause permeabilization of the outer mitochondrial membrane resulting in release of mitochondrial apoptogens most importantly cytochrome c into the cytoplasm from the intermembrane space of mitochondria.[16] In contrast, antiapoptotic members of the Bcl-2 family, Bcl-extra large (Bcl-Xl) helps to stabilize the outer mitochondrial membrane to inhibit apoptosis in the intrinsic pathway. The cytochrome c released from the intermembrance space of mitochondria binds to the apoptotic protease activating factor 1 (apaf-1) resulting in oligomerization of the protein which in turn mediates recruiting procaspase-9. Caspase-9 induces activation of caspase-3, -6 and -7 leading to apoptotic death of the cell.[13] In the extrinsic pathway, death ligands such as Fas ligand and Trail, activate their cognate receptors on the cell membrane upon binding to them. The death receptors containing intracellular death domain recruit and activate caspase-8 and ultimately results in apoptotic death by activating downstream caspases.[17,18]

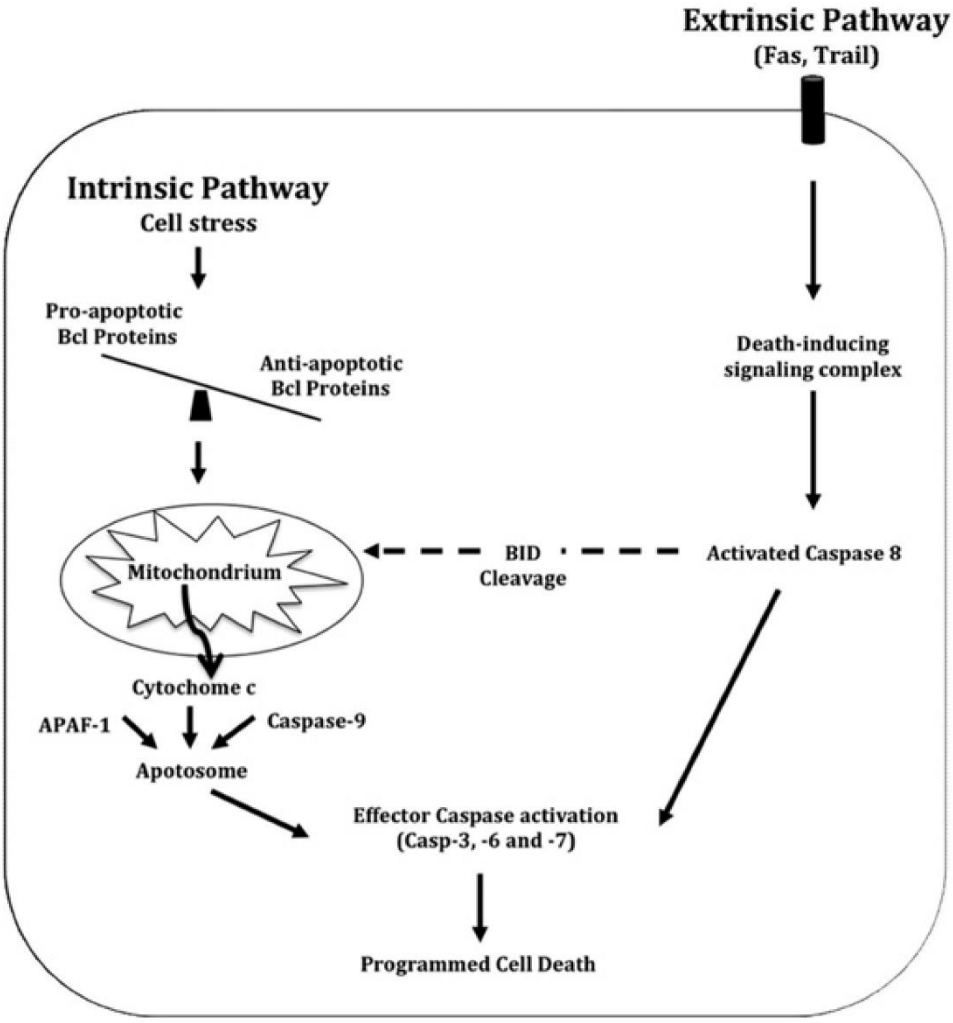

Figure 4: Schematic diagram of intrinsic and extrinsic pathways of apoptosis. Reproduced from[13]

Necrosis is a passive and unregulated process where the cell membrane integrity is lost and the cellular contents are leaked into the neighbouring areas. This process triggers an inflammatory cascade. Cellular and mitochondrial swelling are presented in necrotic process. Necrosis has been suggested to be the main cause of cardiomyocyte death during ischemia, whereas apoptosis has been strikingly accentuated through activation of pro-apoptotic pathways by reperfusion of the myocardium.[6,14,19,20]

In necrosis, mitochondrial permeability transition pore (MPTP) is opened in the inner mitochondrial membrane, which is impermeable to ions, water and protons in healthy mitochondria. Forming of MPTP causes water intrusion into the matrix of mitochondria leading to swelling of the mitochondria that ultimately results in necrosis. Stimuli of necrosis like calcium (Ca^{2+}) trigger MPTP opening in the inner mitochondrial membrane.[21] Alkalosis, ROS and deficiency of ATP or ADP can enhance the calcium ion-induced opening of MPTP.[22,23] Intrusion of Ca^{2+} into the mitochondria of ischemic cardiomyocytes causes MPTP opening that results in rapid drop of mitochondrial membrane potential and consequent halt of ATP synthesis. Opening of MPTP also lets inward rush of water into the matrix of mitochondria, resulting in swelling of mitochondria. Unrestrained entry of water into the mitochondria may cause rupture of the outer mitochondrial membrane (OMM) and this rupture causes releasing apoptogens like cytochrome c with consequent activation of caspases.[24] The mechanism that regulates opening of MPTP in cardiomyocytes is not understood well yet. A peptidyl-prolyl cis-trans isomerase, cyclophilin D, located in the matrix positively regulates the MPTP opening and it is involved in swelling of the mitochondria and ischemia-related necrosis of cardiomyocytes.[24,25]

Autophagy is the process whereby the cells deliver their own proteins and lipids which are needless and non-functional, to lysosomes.[26] This is a way of disposing cellular wastes like long-lived proteins and also a quality control mechanism of proteins. The process of autophagy serves as an alternative source of energy and nutrients when exposed to stress and starvation.[27,28] Both I/R injury and permanent coronary artery occlusion induce autophagy in the myocardium. But, the

mechanisms and effects of the process are different. In permanent coronary artery occlusion, activation of 5' AMP-activated protein kinase (AMPK) followed by inhibition of mammalian target of rapamycin (mTOR) occurs and the process of autophagy is activated.[29] Beclin-1 level is increased in I/R injury to activate autophagy and this is not dependent on AMPK. Studies have indicated that autophagy has a significant role in survival of cardiomyocytes in myocardial infarction, but this role is highly dependent on circumstances.[29,30]

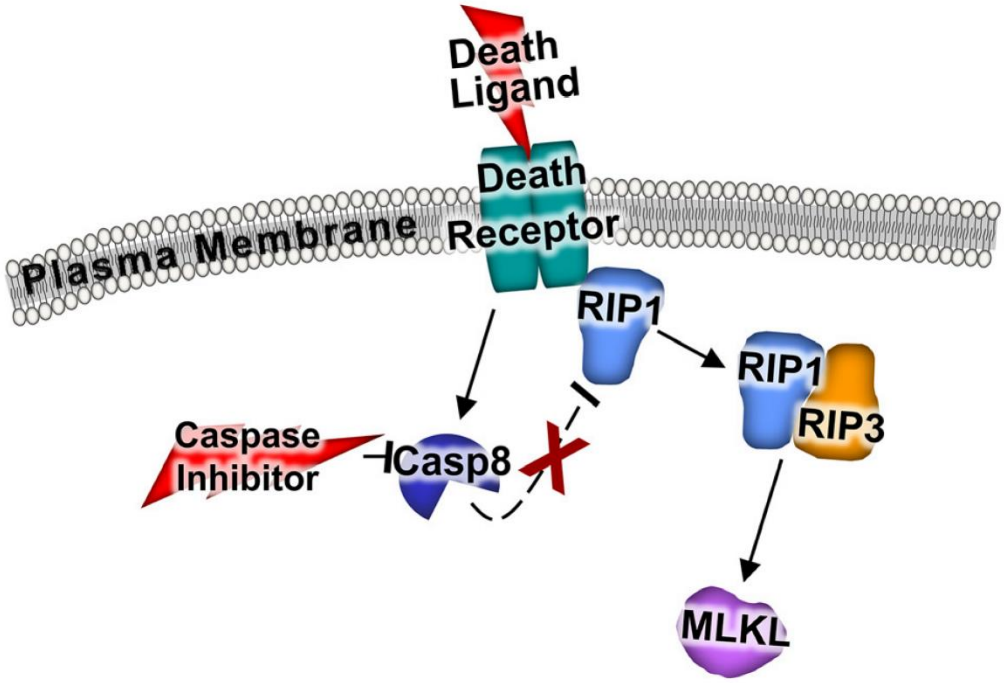

Figure 5: Pathway of necroptosis. Reproduced from[31]

Necroptosis, a new mechanism of cell death, has an important role in mediating death of cardiomyocytes.[32] It combines the features of both necrosis and apoptosis. Like apoptosis, it is highly regulated by specific molecules. At the same time, the process results in the same morphological features of necrosis of losing membrane integrity and inflammation.[32-36] The molecular pathway in the process of regulated

necrosis is not clearly understood. The most extensively studied pathway was that of the tumour necrosis factor-α (TNF-α)-induced necroptosis. *In vitro* investigations demonstrated that two members of the receptor-interacting protein kinases are involved in this TNF-α-induced necroptosis. They are Receptor-Interacting Protein Kinase-1 (RIPK-1) and Receptor-Interacting Protein Kinase-3 (RIPK-3). When the apoptotic death receptor (TNF receptor 1) is stimulated with the death ligand (TNF-α) in the presence of a caspase inhibitor, this stimulation of the apoptotic death receptor causes activation of RIPK-1 which in turn interacts with RIPK-3. The interaction of RIPK-1 and RIPK-3 promotes recruitment of mixed lineage kinase domain-like (MLKL) protein. The MLKL protein is then phosphorylated by RIPK-3.[37-40] Tetramers are formed by this phosphorylated MLKL, translocate to the cell membrane and triggers influx of calcium, an initial episode of necroptosis induced by TNF.[37,39] In absence of caspase inhibitor, RIP-1 would usually be cleaved and inactivated by caspase 8 and consequently necroptosis is inhibited. The cell's necroptotic machinery can circumvent this inhibition of necroptosis produced by caspase 8 through endogenous cellular FLICE-inhibitory protein (cFLIP) that causes inactivation of caspase 8. There are considerable interaction between the pathways of necroptosis and apoptosis by which they are co-regulated by each other.[41]

Other forms of regulated necrosis are emerging, e.g., parthanatos, NETosis, ferroptosis, pyronecrosis, oxytosis and pyroptosis.[40] There are cross-talks among the different modes of myocardial cellular death.[10]

1.1.2 Heart failure followed by myocardial infarction

The major cause of chronic heart failure is acute myocardial infarction (AMI).[42] This is a common complication of AMI. With the advancement of reperfusion therapy, patients with severely deteriorated cardiac function after myocardial infarction survive now, but live with a damaged heart leading to chronic heart failure.[43] Studies suggested that apoptosis not only contributes to the death of cardiomyocytes in acute stage of AMI, but also is responsible for progressive death of surviving cardiomyocytes in the sub-acute and chronic stages. It has also been suggested that attenuation of apoptosis in the surviving cardiomyocytes can minimize the cardiac remodelling and heart failure after myocardial infarction.[44]

After myocardial infarction, cardiac remodelling continues for months and is represented by a gradual dilatation of the heart, thinning of infarct wall and manifestation of heart failure. This is attributed to the gradual loss of cardiomyocytes in the peri-infarct region of the heart. Animal studies and human autopsy studies showed a continuously higher apoptosis process persisted for months after acute myocardial infarction in the peri-infarct and remote regions of the myocardium although apoptosis is lower in the remote myocardium, but still higher than the control hearts.[45-50]

1.1.3 ROS and Oxidative stress

1.1.3.1 Reactive oxygen species (ROS)

Free radicals are atomic or molecular species those are unstable and contain unpaired electron(s) in their outer orbitals. The reactive free radical derived from

metabolic processes may donate its unpaired electron to other molecule or may take away an electron from another molecule. Greater than 95% of the free radicals in our body contain oxygen. Oxygen free radicals play a key role in regulating cellular functions, cell signalling pathways and body's defence mechanism against pathogens.[51,52] Superoxide anion ($O_2^{\bullet -}$), hydroxyl radical ($^{\bullet}OH$), perhydroxyl radical ($HO_2^{\bullet}$), alkyl peroxide radical ($ROO^{\bullet}$), alkoxyl radical ($RO^{\bullet}$) are common oxygen free radicals.

Table 1: Body's oxygen free radicals and their electronic structures. Reproduced from[53]

Radicals	Chemical formulas	Electron structures
Superoxide anion	$^{\bullet}O_2^-$	
Hydroxyl radical	$HO^{\bullet}$	
Perhydroxyl radical	$HO_2^{\bullet}$	
Alkoxyl radical	$RO^{\bullet}$	
Alkyl peroxide radical	$ROO^{\bullet}$	
Hydrogen peroxide	H_2O_2	
Singlet oxygen	$^1O_2$	

Superoxide anion is highly unstable and it can be converted to hydrogen peroxide by the enzyme superoxide dismutase (SOD). The superoxide anion can also be protonated spontaneously to form perhydroxyl radical ($HO_2^{\bullet}$) although at a very low magnitude.[54] The perhydroxyl radical is more reactive than the superoxide anion and can damage biomolecules.[55,56] Hydrogen peroxide forms the most damaging free radical, hydroxyl radical via Fenton Reaction in the presence of iron cations (Fe^{2+}) and can react with any biomolecule.[57] Hydrogen peroxide and singlet

oxygen ($^1O_2$) can also be considered as oxygen free radicals though they are actually not free radicals.[58] Singlet oxygen can react with cellular proteins, lipids and nucleic acids.[59]

1.1.3.2 Sources of ROS

Reactive oxygen species are constantly formed and some of them are essential for normal cellular functions.[51] But, overproduction of ROS causes damage to cells.[60,61] The main intracellular ROS source is mitochondria. Greater than 90% of oxygen is utilized for ATP production in oxidative phosphorylation and 2% of the oxygen is converted to ROS as byproducts.[62]

NADPH oxidase is another source of generating ROS in cells. This enzyme catalyses formation of superoxide anion from molecular oxygen through transfer of one electron from NADPH. Although NADPH activity mostly occurs on phagocytic cell membrane, it is also observed in cardiomyocytes and heart endothelial cells. The NADPH oxidase system normally remaining latent can be activated by stimulating factors like endotoxin, leukotrienes, calcium and complement, and produces ROS from molecular oxygen.[15,63-65]

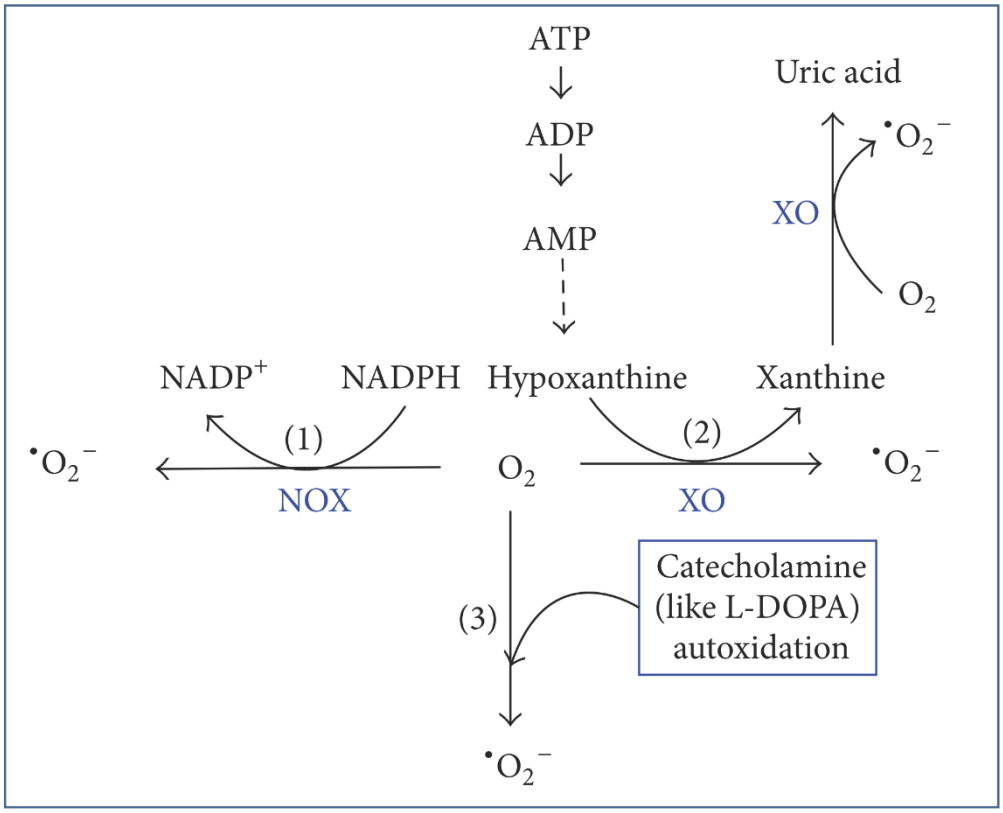

Figure 6: Pathways of forming endogenous superoxide anion. (1) NADPH oxidase (NOX)-catalysed formation of superoxide anion from molecular oxygen using NADPH as donor of electron. (2) Xanthine oxidase (XO)-catalysed formation of superoxide anion where hypoxanthine is converted to xanthine and xanthine to uric acid. (3) Formation of superoxide anion by autoxidation of catecholamine. Reproduced from[53]

Two interconvertible forms of xanthine oxidoreductase, xanthine dehydrogenase and xanthine oxidase, exist in cells.[66] Between the two forms, only xanthine oxidase can generate ROS. Xanthine oxidase produces more hydrogen peroxide than superoxide during hypoxic condition.[67] Use of a xanthine oxidase blocker improved myocardial function in isolated reperfused rat hearts.[68] The oxidase form is reported

to be upregulated in heart failure and inhibition of the enzyme produces improvement in cardiac remodelling and increased efficacy.[69,70]

Autooxidation of catecholamine can produce ROS which could be damaging to the cells.[71] Myeloperoxidase (MPO) produces a powerful oxidant hypochlorite (HOCl) using hydrogen peroxide as a substrate. Other sources of ROS are uncoupled endothelial nitric oxide synthase (eNOS), lipoxygenase, pyruvate dehydrogenase and flavoprotein acyl-CoA dehydrogenase.[15,72-75]

1.1.3.3 Endogenous defences against ROS and oxidative stress

The cellular antioxidant defence system normally regulates ROS level and maintains the balance between production and elimination of ROS. Oxidative stress develops when ROS are overproduced and exceed the rate of ROS removal by the cellular antioxidant defence system.[76] This resultant oxidative stress because of the imbalance of production and removal of ROS, is damaging to the cardiomyocytes.[77]

Table 2: Endogenous antioxidant enzymes and compounds. Reproduced from[78-81]

Antioxidant enzymes	Antioxidant compounds
Superoxide dismutase (SOD)	Ascorbic acid
Catalase (CAT)	Glutathione (GSH)
Glutathione peroxidase (GPx)	Alpha-tocopherol
Glutathione reductase (GR)	Uric acid

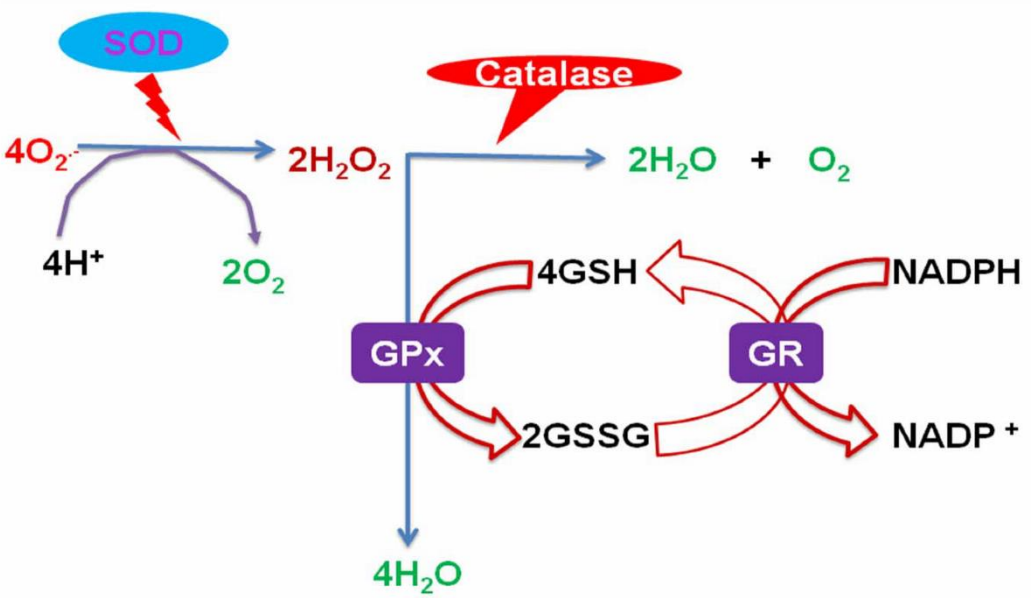

Figure 7: Cellular defence system against ROS. Reproduced from[80]

Oxygen delivery in brain is about three times of its consumption. In the myocardium, oxygen delivery is 1.5 to 1.6 times of its consumption reflecting the

scenario of skeletal muscle engaged in moderate exercise. This is indicative of the myocardial consumption of excess amount of oxygen.[82] The cardiac myocytes encounter a low-level of superoxide anion generation and convert the anion to H_2O_2 by enzymatic action of superoxide dismutase in the cytoplasm or mitochondria. The hydrogen peroxide generated from the superoxide anion is neutralized to water either by catalase or by glutathione peroxidase (GPx) system.[83] Hydrogen peroxide more likely interacts with iron cations (Fe^{2+}) via Fenton reaction to form the most damaging free radical species, the hydroxyl radical ($^{\bullet}OH$), instead of being neutralized by catalase or glutathione peroxidase. Hydroxyl radical, generated excessively during myocardial ischemia-reperfusion, promptly reacts with nucleic acids, lipids and proteins of cardiomyocytes.[84] By means of glutathione (GSH), GPx catalyses hydrogen peroxide and neutralizes it by converting it to water. Oxidized form of glutathione, glutathione disulphide (GSSG) is again reduced back to its reduced form, GSH by glutathione reductase (GR) where NADPH donates an electron.[85] Glutathione (GSH) is abundant in organisms that neutralize ROS in an enzymatic or non-enzymatic way. The heart's low antioxidant enzymatic activities of catalase and GPx, and lower content of glutathione (GSH) than other tissues indicate that the heart is highly susceptible to oxidative stress-induced damage of cardiomyocytes.[86] It has been reported that cardiac cells normally maintain very poor catalase activity which is as little as 2% of the catalase activity observed in liver cells.[87-89]

Oxidative stress plays a key role in cellular death of cardiomyocytes in cardiac pathologies of ischemia/reperfusion injury and heart failure.[90,91] This is an important determinant in expanding myocardial damage during reperfusion after

myocardial ischemia. Oxidative stress of cardiomyocytes strongly influences the ultimate size of the myocardial infarct by inducing death of cardiomyocytes through apoptosis and necrosis.[92-96]

Intracellular levels of both superoxide and hydrogen peroxide are raised following myocardial infarction, and the levels of their endogenous antioxidant enzymatic scavengers, superoxide dismutase and catalase, decline.[97,98] In spite of its low content in the cardiac cells, catalase enzyme is mainly accountable for the peroxidase activities in cardiomyocytes.[89]

1.1.4 Myocardial ischemia/reperfusion injury

After occlusion of an epicardial coronary artery which formerly perfused myocardium cannot maintain the previous perfusion of the myocardium and the affected myocardium is at risk. This hypoperfused zone of the myocardium during myocardial infarction is termed as the area at risk (AAR). When the affected coronary artery is not immediately reperfused and there is no collateral circulation in that area, maximum portion of the area at risk becomes necrotic. Still a portion of the AAR remains necrosis-free in patients received timely reperfusion and this necrosis-free portion of the AAR is the salvaged myocardium.[99]

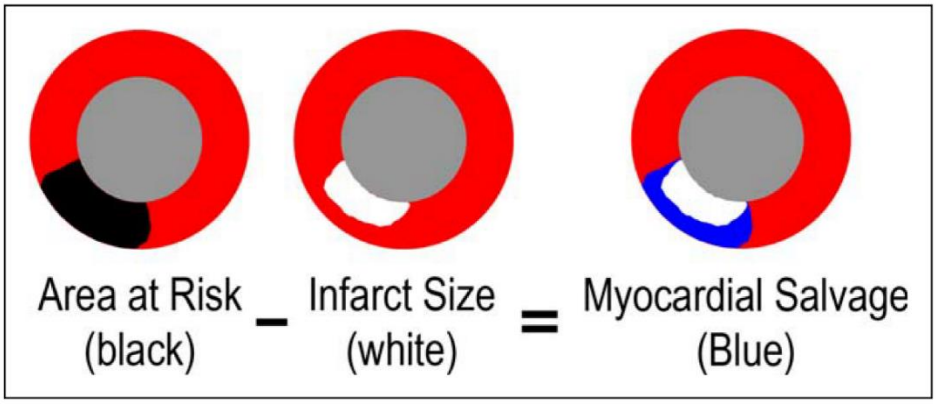

Figure 8: Diagrammatic representation of area at risk, myocardial infarct size and myocardial salvage. Reproduced from[100]

Infarct size after acute myocardial infarction is the most important consideration for prognosis of the disease.[42,101] Studies recognised the factors that determine the size of myocardial infarct are as follows:

i. Size of the area at risk,[102]
ii. Time span of the ischemic period,[8,103]
iii. Degree of collateral blood flow,[102,103]
iv. Temperature of the myocardial tissue in ischemic period and
v. Haemodynamic condition in ischemic period.[104]

After myocardial infarction, reduction of the myocardial infarct size and myocardial ischemic injury can be partially achieved by a prompt initiation of effective reperfusion therapy with thrombolytics, antiplatelets and/or percutaneous coronary intervention (PCI). Though timely and effective reperfusion decreases size of the myocardial infarct, saves cardiac function and increases survival of the MI patients, the reperfusion, i.e., restoration of blood supply to the ischemic myocardium, itself

induces an insult to the ischemic myocardium. This reperfusion therapy-induced damage is termed as ischemia/reperfusion injury (I/R injury). The reperfusion elicits a localized oxidative burst and regional inflammatory responses causing injury of the myocardium and even death of the cardiac myocytes that ultimately results in significant myocardial damage which is reflected in the infarct size. This I/R injury may stimulate development of arrhythmias, myocardial stunning, microvascular injury and inflammatory response.[105-112] It has been reported that apoptosis dominated as the main mode of cardiomyocytes death in myocardial I/R injury.[113]

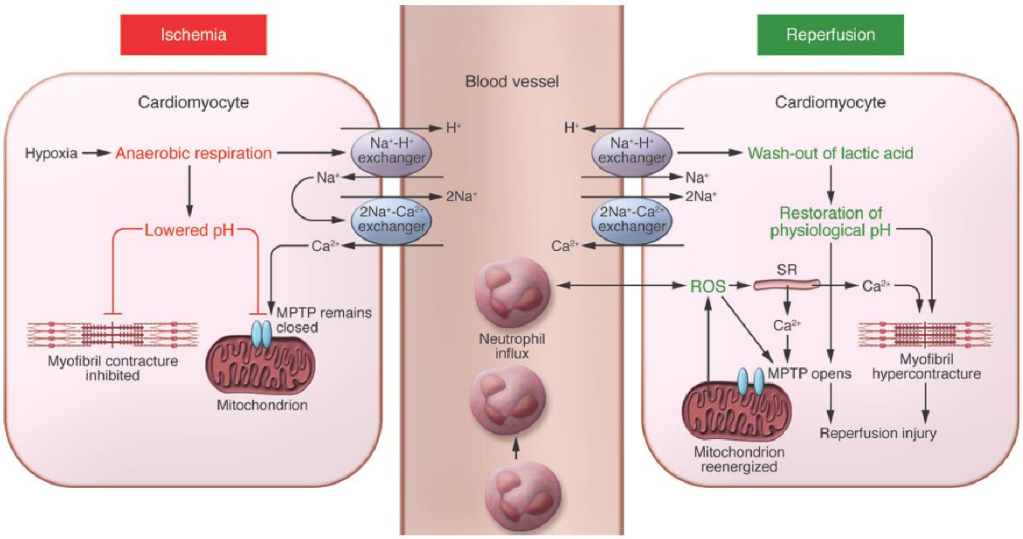

Figure 9: Diagrammatic illustration of myocardial ischemia/reperfusion injury. Reproduced from[9]

Aerobic respiration of cardiomyocytes switches to anaerobic respiration during ischemia of the myocardium due to a lack of oxygen. This anaerobic respiration causes lactate production leading to a fall in intracellular pH. This low intracellular pH induces the Na^+-H^+ exchanger to expel out H^+ from the cell with concomitant rise in the intracellular level of Na^+. This intracellular overload of Na^+ in turn

activates the $2Na^+$-Ca^{2+} exchanger to expel Na^+ out from the cell and results in overload of intracellular Ca^{2+}. The Na^+-K^+ ATPase is stopped to work in ischemic condition that aggravates the intracellular overload of Na^+. The acidic environment during the ischemic period inhibits opening of MPTP and hypercontracture of cardiomyocytes. Electron transport chain of mitochondria is activated again in reperfusion and generates ROS. ROS are also generated from other sources like xanthine oxidase of endothelial cells and NADPH oxidase of neutrophils. ROS cause reperfusion injury of the myocardium by inducing opening of MPTP, playing the role of a neutrophil chemoattractant and inducing damage to the sarcoplasmic reticulum. This exacerbates the overload of intracellular Ca^{2+}. Also ROS cause damage to the plasma membrane by lipid peroxidation, denature enzymes and produce oxidative damage to nucleic acids. Upon reperfusion, the Na^+-H^+ exchanger is reactivated and lactic acid is washed out that leads to recovery of physiological pH. This rapid change in pH results in opening of MPTP and contracture of cardiomyocytes. Recovery of the mitochondrial membrane potential induced by mitochondrial reenergization causes intrusion of calcium into the mitochondria through the mitochondrial calcium uniporter, which can also persuade the opening of MPTP.[9,114] It has been reported that administering antagonists of the mitochondrial calcium uniporter and sarcolemmal calcium channel in the beginning of reperfusion could reduce the size of myocardial infarct.[115,116]

1.1.5 Experimental manipulative approaches in signalling pathways of different death modes

In response to I/R injury, mice hearts that lacked Fas presented infarcts of smaller size, when investigated *in vivo* and as isolated hearts.[117,118] It was reported that overexpression of cardiac-specific Bcl-2 reduced apoptosis of cardiomyocytes and the size of the myocardial infarct with concomitant improvement in cardiac function in mouse model of I/R injury.[119,120] In contrast, ablation of Bax decreased apoptosis of cardiomyocytes and reduced post-ischemic dysfunction in isolated hearts undergone ischemia-reperfusion injury.[121] Obliteration of Bax was also reported to result in a reduction in the infarct size and reduced myocardial dysfunction in a non-reperfused infarction model.[122] The anti-apoptotic protein Bcl-2 has been suggested to reduce not only apoptotic cell death but also necrotic and autophagic cell death.[121,123-127]

In cellular death mediated by apoptosis, caspases play a crucial role. A big variation in the infarct sizes was observed after I/R injury when pan-caspase inhibitors were used.[128-131] Inhibition of caspases produced a moderate reduction in the size of infarct, which was less than that found when anti-apoptotic proteins were overexpressed.[132] Nevertheless, many studies observed that caspase inhibitors could attenuate the size of myocardial infarct supporting the important role of caspases played in the I/R injury.[128,133,134] During the period of ischemia, caspase 9 was reported to be activated, while during reperfusion, caspase 8 and caspase 9 were reported to be activated.[134]

Lacking of cardiac-specific cyclophilin D in mice subjected to I/R injury showed a reduction of 40% in the infarct size and overexpression of cardiac-specific cyclophilin D produced swelling of mitochondria and spontaneous cell death.[24] It has been reported that cyclosporine A or sanglifehrin A could reduce the size of myocardial infarct by inhibiting cyclophilin D.[135-138] Although it was thought that necrosis is an uncontrollable process, later studies suggested that this is also a regulated process and it is possible to decrease the cell death through necrosis by interventions in the process.[110,139]

Some studies showing that inhibition of autophagy in ischemia or anoxia is damaging, are suggestive of the favourable role of the autophagy process in ischemia.[140,141] In contrast to the findings of these reports, a reduction in the autophagy inducing protein, Beclin-1, decreases autophagy induced by I/R and death of cardiomyocytes.[111] In permanent coronary artery occlusion, inhibition of the process of autophagy by means of cardiac-specific overexpressing dominant negative 5' AMP-activated protein kinase caused a deterioration in the infarct size.[29] Similar findings were observed in reduced autophagy induced by overexpressing Rheb and ablating one allele of glycogen synthase kinase-3β.[142,143] The findings of these studies indicate that autophagy is stimulated in ischemia through AMPK-dependent mechanism, while it is stimulated in I/R through another mechanism dependent on Beclin 1 and independent on AMPK. Moreover, the role of autophagy is distinct in ischemia and I/R. Autophagy can be protective in ischemia, while it can be harmful during I/R.

Inhibition or ablation of caspase 8 in mice caused no cleavage of RIP-1 and maintained its ability to interact with RIP-3 leading to necroptosis.[34,35] It has been

demonstrated in a recent report that mice lacking RIP-3 showed higher ejection fraction and less cardiac hypertrophy after infarction by coronary artery occlusion.[144] Mice and cells deficient of mixed lineage kinase domain-like (MLKL) have been reported to be resistant to the death process of necroptosis.[37,145] Necrostatins, inhibitor of RIP-1 activity, have been reported to decrease size of the myocardial infarct and inhibit death of cardiomyocytes in segregated perfused mouse hearts.[146] Koshinuma *et al.* reported that simultaneous treatment with a necroptosis inhibitor, necrostatin-1 and an apoptosis inhibitor, Z-VAD resulted in a reduction in the size of myocardial infarct after I/R injury in isolated guinea pig hearts.[147] Administration of necrostatin-1 at the beginning of reperfusion in a mouse model of I/R injury, inhibited necroptosis dependent on RIP-1 and successfully reduced myocardial infarct size with preserving ejection fraction.[148]

1.1.6 Therapeutic approaches in reducing myocardial I/R injury

Antioxidants can counteract oxidative stress and reduce ischemia/reperfusion injury.[149] Based on the role of ROS in the pathophysiology of myocardial I/R injury and demonstration of promising results in experimental studies, it was expected that exogenous antioxidants could reduce the myocardial I/R injury in clinical settings. But, a number of clinical studies failed to show any beneficial effect of the antioxidants in myocardial I/R injury because of their non-specificity and insufficient potency to detoxify the ROS excessively produced during myocardial I/R injury.[150,151] Cardiac-specific overexpression of superoxide dismutase in transgenic mice showed a protective effect of reducing infarct size in *in vivo* models

of I/R injury[152] and a similar result was observed in case of glutathione peroxidase. After myocardial ischemia/reperfusion injury, transgenic mice with overexpression of glutathione peroxidase demonstrated a lower myocardial infarct size in isolated perfused hearts.[153] It has also been demonstrated that overexpression of catalase in transgenic mice could provide beneficial effect in hypoxia-reoxygenation cardiotoxicity, cardiac dysfunctions induced by ischemia/reperfusion, and even reduce doxorubicin-induced damage to cardiomyocytes.[154-157] Catalase is mainly responsible for peroxidase activities in the heart.[89] However, this transgenic expression is a proof of principle that implies the therapeutic potential of catalase in ameliorating the myocardial ischemia/reperfusion injury and this is not realistic for therapeutic application. In order to obtain the best therapeutic effect of the enzyme in myocardial I/R injury, the most applicable way could be the development of a delivery system that can protect the enzyme from degradation and deliver the enzyme to the affected area of the myocardium shortly before generation of oxidative stress triggered by ischemia/reperfusion injury.

Delivery of an adequate amount drug to the diseased area in a controlled way is challenging. Use of nanotechnology-based drug delivery systems could offer advantages over conventional drug delivery systems in this regard. Interest is increasing in delivery of drugs to the heart with the help of improved specificity and bioavailability offered by nanotechnology.[158-161] Approaches of polymeric nanoparticles, dendrimers, liposomes and micelles were tried to deliver drugs to the myocardium. Kan *et al.* demonstrated that liposomes containing phenyl-2-aminoethylselenide, a selenium-based antioxidant, could reduce damage to cardiomyocytes induced by doxorubicin in mouse model and H9c2

cardiomyocytes. Another study employing a similar model of doxorubicin toxicity showed that Pluronic F-127 micelles containing a combination of two antioxidants, resveratrol and quercetin, provided protection against cardiotoxicity-induced by doxorubicin. In both studies, free drugs were less effective than their encapsulated counterparts.[162,163] Co-enzyme Q10 (ubiquinone) encapsulated PLGA nanoparticles of around 150 nm size, have been reported to improve ejection fraction after left anterior descending coronary artery occlusion in rats.[164] A very recent report published by Ikeda *et al.* demonstrated that treatment with the mitochondrial permeability transition pore (MPTP) opening inhibitor, cyclosporine A-loaded PLGA nanoparticles at the onset of reperfusion enhanced protection of the cardiomyocytes in an in vivo murine IR model and this cardioprotection was superior to cyclosporine A alone.[165] Clemons *et al.* synthesized AID peptide, a peptide directed against α-interacting domain (AID) of the L-type Ca^{2+} channel and electrostatically conjugated the AID peptide with multifunctional magnetite (Fe_3O_4) encapsulated rhodamine B-polyglycidal methacrylate nanoparticles. They showed that the AID peptide on the polymeric complex was promptly uptaken by the cardiomyocytes and distributed well throughout the myocardium and could reduce ischemia/reperfusion injury damage in an ex vivo model of I/R injury in guinea pigs.[166] The same group loaded a potent antioxidant, curcumin into the same AID conjugated multifunctional rhodamine B-polyglycidal methacrylate nanoparticles containing magnetite (Fe_3O_4) encapsulated into the polymer and showed that this combination of the AID peptide and antioxidant curcumin were effective in reducing damage to the myocardium and attenuated generation of superoxide and oxidative stress in isolated rat hearts after I/R injury. The protective effect was more potent with the combination of AID and curcumin than with only

the curcumin-loaded nanoparticles.[167] Nakano *et al.* reported that irbesartan-loaded PLGA nanoparticles decreased the myocardial infarct size and improved left ventricular remodelling in a mouse model of ischemia/reperfusion injury, irbesartan solution failed to produce any protective response.[168] Another recent study showed that pitavastatin-loaded PLGA nanoparticles reduced myocardial infarct size and improved LV dysfunction and cardiac remodelling in a rat model of myocardial I/R injury. On the contrary, free pitavastatin administered intravenously failed to show any protective effect in such condition, and this advocates in support of the nanoparticle-mediated drug delivery systems in myocardial ischemia/reperfusion injury.[169]

There have been no studies reported yet on evaluation of any protective effect of catalase-loaded nanoparticles in conserving cardiomyocytes from oxidative stress-induced cellular damage.

1.2 Formulation of nanoparticles

1.2.1 Polymeric nanoparticles

Drug delivery using nanoparticles offers great prospects in pharmaceutical science. A number of products using nano-drug delivery systems are already on the market.[170] Using a nanoparticulate approach, hydrophilic and hydrophobic drug molecules, biological macromolecules and vaccines can be delivered to specific target organs or cells for prolonged release of the drugs.[171,172] Nanoparticles can be

fabricated from natural or synthetic polymers. Natural polymers those are usually used for fabricating nanoparticles are

- Chitosan[173]
- Albumin[174]
- Calcium and sodium alginate[175,176]
- Gelatin[177]
- Dextran[178]

Natural polymers vary in physicochemical properties from batch to batch and possess the risk of immunogenicity and viral infections.[179-181] In contrast, synthetic polymers can be made flexibly and reproducibly with tunable properties.[182] Poly(glycolic acid) (PGA), Poly(lactic acid) (PLA), Poly(lactic-co-glycolic acid) (PLGA), Poly(methyl methacrylate) (PMMA) and Poly(caprolactone) are commonly used for fabrication of nanoparticles.[183]

1.2.2 Poly(lactic-co-glycolic acid)

Poly(lactic-co-glycolic acid) (PLGA) is the most extensively used polymer for fabricating nanoparticles because of biodegradability, biocompatibility and a very good ability of prolonged release of drugs.[182,183] PLGA is the polymer of attention due its favourable properties and USFDA approval.[184]

1.2.2.1 Physicochemical properties of PLGA

PLGA is soluble in chlorinated solvents including dichloromethane, ethyl acetate, tetrahydrofuran and acetone.[185] The biodegradation pathway of this polymer is hydrolysis. PLGA is hydrolysed in the body and produces the two original monomers, lactic acid and glycolic acid which are body's metabolites formed as by-products in different metabolic pathways.[186]

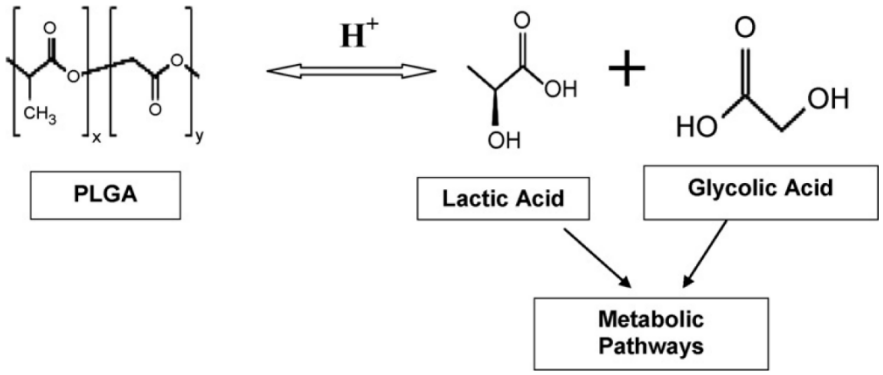

Figure 10: Hydrolysis of PLGA, x is the no. of lactic acid units and y is the no. of glycolic acid units in PLGA polymer. Reproduced from[186]

Degradation of PLGA is dependent on several factors. When the molecular weights of PLGAs were increased from 10 – 20 kDa to 100 kDa, their degradation rates decreased and ranged from few weeks to couple of months. Synthesis of PLGA with different degradation rates is performed by manipulating the ratio of the monomers in the polymerization process. PLGA containing higher content of glycotide units show faster degradation. Degradation of PLGA 50:50 is the fastest, which is an exception. PLGA polymer that is end-capped with ester groups shows a degradation half-life which is longer than the one that is end-capped with free carboxylic acid groups.[187-189] Geometry or shape of the polymeric device also

greatly influences the degradation pattern of the device by the way of water accessibility. Low pH of the media speeds the degradation process of PLGA by autocatalysis.[190]

1.2.2.2 Pharmacokinetics and biodistribution

It has been reported that the pharmacokinetic profile followed by PLGA nanoparticles is non-linear and dependent on dose. Studies suggested that clearance from the blood and uptake of the PLGA nanoparticles by mononuclear phagocyte system (MPS) depend on the dose applied. Reduction in the clearance from blood and uptake by MPS with increasing dose indicated that a saturation of MPS was induced at the increased doses of nanoparticles. Depending on the dose applied, nanoparticles were distributed between blood and mononuclear phagocyte system (liver).[191] It was reported that after 7 days of oral administration of PLGA nanoparticles, nanoparticles were detectable in the mice. The highest percentage of the particles were detected in the liver which was 40.04% of the particles and the lowest percentage was detected in the spleen. 25.97%, 12.86% and 11.92% were detected in the kidney, the brain and the heart respectively. Nanoparticles were also detected in the lungs.[192]

1.2.2.3 Fabrication of PLGA nanoparticles

The most commonly used techniques to prepare PLGA nanoparticles are emulsification/solvent evaporation, emulsification/solvent diffusion and nanoprecipitation methods.[193-195]

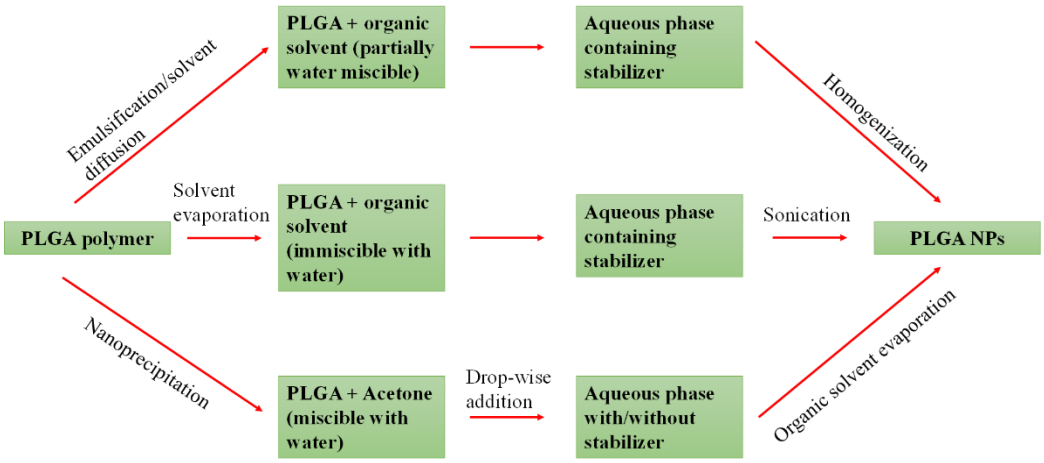

Figure 11: Fabrication of PLGA nanoparticles by different methods. Reproduced from[186]

The PLGA polymer is first dissolved in a partially water miscible organic solvent like propylene carbonate in emulsification/solvent diffusion method.[196] The polymer solution is added and separated in aqueous phase containing stabilizer followed by emulsification with a homogenizer. For solvent evaporation method, a PLGA polymer solution is prepared first by dissolving the polymer in a volatile water immiscible solvent like dichloromethane or ethyl acetate. This polymer solution is the added to an aqueous phase containing an emulsifier or stabilizer followed by high-speed homogenization or ultrasonication. In the nanoprecipitation method, also termed as solvent displacement method, PLGA polymer is dissolved in a water miscible organic solvent like acetone. This polymer solution is added

drop-wise to the aqueous phase with or without stabilizer under continuous magnetic stirring.[186,197]

Double emulsion method (w/o/w) is the most commonly used technique for preparing protein-loaded PLGA nanoparticle by encapsulating hydrophilic proteins into the hydrophobic PLGA polymer. In this method, the protein solution was added to the polymer solution prepared in a water immiscible solvent and emulsified by homogenization or ultrasonication. This primary emulsion is further emulsified with an aqueous phase containing a stabilizer usually PVA by homogenization or ultrasonication followed by evaporation of the organic solvent.[184,198] Fonte *et al.* encapsulated insulin into PLGA nanoparticles by double emulsion method.[199,200] Azizi *et al.* prepared bovine serum albumin-loaded PLGA nanoparticles following the double emulsion method.[184] Alpha 1- antitrypsin-loaded PLGA nanoparticles was also formulated by double emulsion method.[201]

1.2.3 Instability of the protein-loaded nanoparticles

1.2.3.1 Instability of polymeric nanoparticles

Although offering many advantages over the conventional drug delivery systems, delivery systems based on nanoparticles are not free of obstacles. Some major problems restrict the wide-spread use of the nanoparticles-based drug delivery systems. Physical instability like nanoparticles agglomerate formation and fusion of particles, chemical instability of hydrolytic degradation of the polymeric backbone of the nanoparticles, leaking of drugs from the delivery systems, and

reactivity of drug molecules during storage of the delivery systems, are not uncommon when these nanoparticles-based drug delivery systems are kept for long periods of time in the form of suspensions in water.[202]

1.2.3.2 Instability of protein

Role of therapeutic proteins are gradually emerging. Protein-based therapeutics are incredibly successful in medical fields.[203] Potency and high specificity of their activities are the two crucial strengths of protein therapeutics.[204] Protein therapeutics is keeping its footsteps in many pathological conditions and diseases. Therapeutic proteins are utilized in diabetes, anaemia, haemophilia, neutropenia, leukopenia, thrombocytopenia, fibrinolysis, immune disorders, endocrine disorders, viral infections, multiple sclerosis, cancer, spinal fusion surgery, bone injury repair, varicose ulcers and many other diseases.[205] However, proteins are labile in nature. They are in risk of easily inactivation by proteases, aggregation and natural inhibitors.[206] Delivery of the therapeutic proteins under unfavourable conditions could lead to denaturation or aggregation of the proteins, which may ultimately produce unwanted effects. This instability problem of the therapeutic proteins could at least be minimized by employing the nanoparticle-based protein delivery, where proteins are formulated as protein-encapsulated polymeric nanoparticles made of either synthetic or natural polymers.[207]

1.2.3.3 Instability of the protein during encapsulation

It is very usual that proteins lose their native structures while they are being encapsulated into polymeric particles in the double emulsion method as the encapsulation process involves an organic solvent. The structural changes are attributable to exposure of the proteins to organic solvents, manufacturing shear stresses employed for emulsification and interaction of the protein with hydrophobic interfaces of the polymers.[208] Incorporation of a protectant molecule in the encapsulation procedure can enhance protein stability. For example, addition of a decoy protein in the encapsulation process can conserve activity of the encapsulated protein, because protein inactivation happens in part owing to its denaturation in the hydrophobic/hydrophilic interface. Serum albumin is an example of decoy protein.[209]

In the double emulsion method of protein encapsulation for producing protein-loaded nanoparticles, compared to secondary emulsification step, primary emulsification is the detrimental step when most protein denaturation occurs.[210] It was reported that most of the activity of glucose oxidase was lost during the primary emulsification step which was 28% and, 20% lost in the second emulsification step.[211] Interface formed between the aqueous and organic phases during the emulsification process of the encapsulation procedure, is a major cause of destabilization of the protein leading to its denaturation and aggregation. Aggregation tendency is developed when proteins migrate and adsorb at the interface and ultimately become unfolded with exposure of the proteins' hydrophobic region to the organic phase.[210,212]

Proteins are also sensitive to ultrasonication.[210,213] It has been demonstrated that sonication was more detrimental on the activity of protein C, compared to vortexing.[193] Formation of an interface between the aqueous and organic phases is more harmful to proteins than ultrasonication.[213] Ultrasonication generates stress of cavitation that results in local temperature rising and free radical formation, leading to degradation of protein.[214,215] Additives are commonly incorporated into the encapsulation process of nanoparticle formulation in order to minimize protein damage induced by the emulsification procedure.[216] Trehalose has been reported to be a stabilizer in the emulsification process of protein-loaded nanoparticles.[217,218] Studies demonstrated that bovine serum albumin could also prevent emulsification-induced damage to protein in the encapsulation process of protein-loaded PLGA particles.[219,220]

1.2.4 Freeze-drying of protein-loaded PLGA nanoparticles

Due to having some favourable properties like biocompatibility and biodegradability, prolonged release properties, tunable mechanical properties and above all having no toxicity, Poly(lactic-co-glycolic acid) (PLGA) is a largely used synthetic polymer for nanoparticle fabrication.[207,221] But, the hydrolytically unstable polyester structure of PLGA makes the PLGA nanoparticles unstable particularly if the nanoparticles are stored in an aqueous medium.[222] In addition, aggregates of nanoparticles can be formed in an aqueous environment during storage period, even though surfactants are present in the formulation to stabilize the nanosuspensions.[223]

Freeze-drying, also known as lyophilization, is a common and valuable technique to handle and properly stabilize nanoparticulate systems. In the freeze-drying process, water is removed by sublimation and desorption from a nanosuspension kept in its frozen state under vacuum in a freeze-drier.[224] Besides stabilizing the polymeric nanoparticulate systems, lyophilization of the protein-loaded nanoparticles also minimizes the loss of stability of the protein loaded into the polymeric nanoparticles. However, lyophilization itself is a stress for stability of the polymeric nanoparticles as well as for stability of the encapsulated protein of the nanoparticles. The process of lyophilization can adversely influence properties of the nanoparticles and conformational state of the loaded protein.[200] Protectant compounds are incorporated into the nanosuspensions of protein-loaded nanoparticles before lyophilization in order to reduce instability of both the polymeric nanoparticles and the encapsulated protein associated with the stress induced by the lyophilization process. The protectant compounds protect the nanoparticles from mechanical stress of ice crystals and decrease aggregation tendency of the nanoparticles.[199] A number of studies reported that protecting molecules were able to inhibit the aggregation of nanoparticles, impart good redispersibility of the particles after reconstitution and most importantly minimized changes in the native structure of the encapsulated protein upon freeze-drying.[199,200,225-227] Sugars such as trehalose, sucrose, glucose and mannitol are the most commonly used protectants for freeze-drying of nanoparticles.[228] Trehalose is considered as a very good protectant for freeze-drying of biomolecules. It has been demonstrated that trehalose is very effective in stabilizing labile proteins during lyophilisation.[229] It is more advantageous than other sugars because of its low hygroscopicity and very low chemical reactivity. Due to the absence of internal

hydrogen bonds in the trehalose molecule, this protectant molecule can more flexibly form hydrogen bonds with the nanoparticles during lyophilization.[230]

1.3 Structural characterization of protein-loaded nanoparticles

NMR spectroscopy and X-ray crystallography are very powerful tools for studying detailed structures of proteins. X-ray crystallography can provide elaborate and precise structural information of a protein up to atomic level, but it is limited to proteins which can form a high-quality crystal. NMR is not suitable for proteins of high molecular weight.[231,232] Circular dichroism spectroscopy is employed to study secondary structure of proteins, yet this spectroscopy suffers from problems of inconsistency in determining absolute secondary structures. CD spectroscopy is also restricted by the optical clarity of protein solution.[233-235] In contrast, IR spectroscopy is advantageous, because this technique can provide secondary structural information of a protein irrespective of the protein's condition whether it is in solution or crystal or in solid forms.[236-241] Fluorescence spectroscopy is also a useful tool and commonly used in the field of protein study because of its non-invasiveness and sensitivity. Fluorescence spectroscopy cannot give detailed structure of protein, but this technique can provide information on tertiary structure and conformational state of a protein.[242-244]

1.3.1 Protein's secondary structural characterization by infrared spectroscopy

Investigation of stress-induced conformational alterations of protein has been performed by IR spectroscopy. It is also used for determining secondary structural composition of proteins.[199,245,246] Secondary structural information is acquired by examining the amide I band of the IR spectra of protein. Between 1700 and 1600 cm^{-1}, this band is positioned. In the IR spectrum of protein, this amide I is the most sensitive region for protein's secondary structural composition. The amide I band emerges from the protein's amide group's C=O stretching vibrations, coupled with the in-plane N—H bending and C—N stretching vibrations.[247,248] Every form of secondary structures of proteins, α-helices, β-sheets, β-turns and random coil structures, produce the characteristic band positons caused by rising to the frequencies of different C=O stretching vibrations. These characteristic band positions are utilized in resolving secondary structural composition of proteins.[245]

Fonte *et al.* performed secondary structural analysis of cryoprotected insulin-loaded PLGA nanoparticles by ATR-FTIR.[199,200] Secondary structural characterization of lysozyme- and bovine serum albumin-loaded PLGA microspheres with FTIR spectroscopy was also reported.[249] Carrasquillo *et al.* demonstrated FTIR spectroscopic secondary structural characterization of BSA encapsulated into the PLGA microspheres.[250] Castellanos *et al.* used FTIR spectroscopy to determine secondary structure of γ-chymotrypsin of γ-chymotrypsin-loaded PLGA microspheres.[251]

With the technique of IR spectroscopy, secondary structure of protein can only be detected. Lyophilization of protein drugs may induce very little alterations in the tertiary structures, which may not go with changes in the secondary structures and consequently may not be detectable by the IR spectroscopy. These small changes in tertiary structures with no noticeable alterations in secondary structures may influence a protein's conformational stability.[252-254]

1.3.2 Protein's tertiary structural characterization by fluorescence spectroscopy

In studying conformational states of proteins, fluorescence spectroscopy is commonly used. Analysis of protein becomes possible with very low concentration of the sample protein due to the sensitivity of fluorescence and, hence it can reduce quantity of the sample required for analysis along with the problems linked with low solubility.[242]

Fluorescence signals generated by proteins are highly sensitive to the surrounding microenvironments of the fluorescent probes contained in proteins, and suggest conformational states of the proteins.[242,244] Tryptophan, tyrosine and phenylalanine are the three amino acid residues which are intrinsically fluorescent. Among these three intrinsically fluorescent amino acid residues, tryptophan is the most suitable for fluorescence studies of proteins.[244] Tryptophan's indole group is mostly accountable for absorbing UV and emitting fluorescence.[255] Investigation of fluorescence from phenylalanine and tyrosine amino acids in a protein that contains the three amino acids, is generally difficult because of the tryptophan's interference

due to resonance energy transfer.[256,257] So, usage of phenylalanine and tyrosine fluorescence is usually restricted to the proteins that are free of tryptophan although exceptions are available.[258] In contrast to tryptophan fluorescence, tyrosine fluorescence is poorly sensitive to its surrounding microenvironment.[259,260] Phenylalanine fluorescence is not strong and rarely used in study of proteins.[257] So, intrinsic fluorescence of protein is usually related with tryptophan fluorescence.[260]

Intrinsic tryptophan fluorescence emission is dependent on the polarity of its surrounding microenvironment and any changes in this microenvironment of the tryptophan residue(s) are reflected in the tryptophan fluorescence emission. Consequently, intrinsic tryptophan fluorescence is very useful in exploring changes in the tertiary structure of proteins.[242,261-264] Fluorescence intensity and maximum emission wavelength are frequently examined to study proteins.[264-267] When a protein containing multiple tryptophan residues is unfolded it may lose or gain in its tryptophan fluorescence intensity compared to the native state of the protein. This reduction or increment of fluorescence intensity is dependent on the quenching or energy transfer processes.[268]

Tryptophan maximum emission wavelength (λ_{max}) varies with the position of tryptophan residue(s) in proteins. Shorter wavelength of Trp λ_{max} suggests that tryptophan(s) are buried in a hydrophobic environment and longer wavelength Trp λ_{max} indicates tryptophan(s) are very much exposed to the aqueous environment which is polar. Intermediate Trp λ_{max} is indicative of partial buried condition of tryptophan(s).[269-271]

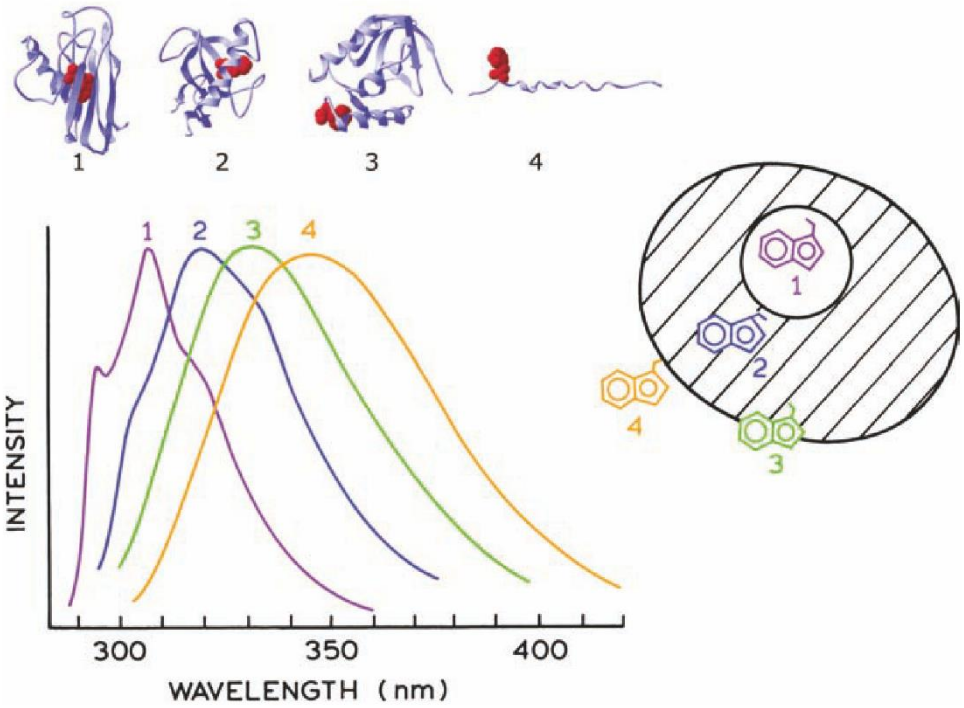

Figure 12: Tryptophan emission spectra of Apoazurin Pfl, Ribonuclease T1, Staphylococcal nuclease and Glucagon (from 1 to 4, respectively) showing effect of the tryptophan microenvironment on their emission spectra. Reproduced from[272]

Unfolding of proteins generally changes the microenvironment of the tryptophan(s) from a comparatively hydrophobic core to a polar aqueous microenvironment. This changes in polarity of the microenvironment of tryptophan(s) produces a red-shift of the tryptophan fluorescence maximum emission wavelength (λ_{max}).[264] It was reported that unfolding of bovine liver catalase by guanidine hydrochloride made a red-shift of the Trp λ_{max}.[273] Enzymatic activity was progressively lost with increasing concentration of GdnHCl and a complete loss of activity was observed at 1.5 M GdnHCl.[273,274] Gaudadana *et al.* investigated tertiary structure of bovine serum albumin of bovine serum albumin encapsulated PLGA nanoparticles.[275]

Swed *et al.* evaluated structural integrity of the lysozyme loaded into the lysozyme-loaded PLGA nanoparticles.[276]

1.4 Aims

Reperfusion therapy is an indispensable part of the management of myocardial infarction, but this reperfusion therapy itself creates an oxidative stress to the myocardium by inducing excessive generation of reactive oxygen species (ROS). Catalase, a vital enzyme in the body's endogenous antioxidant defence system, is considered to perform most of the peroxidase activities in the cardiac myocytes. It was hypothesized that catalase, if could be delivered at the onset or soon after the reperfusion therapy, might protect the cardiac myocytes from the oxidative stress-induced damage caused by reperfusion therapy.

Delivery of catalase to the myocardium using polymeric nanoparticles made of the US Food & Drug Administration (US FDA)-approved biodegradable polymer, PLGA, might be an effective approach to overcome the difficulty of delivering active protein. In the formulation procedure of catalase-loaded nanoparticles, both the emulsification and lyophilization steps could induce denaturation of catalase. Trehalose and bovine serum albumin (BSA) were reported to protect proteins from the emulsification-induced denaturation. Trehalose is a well-known cryoprotectant for labile proteins, and it offers the advantages of low hygroscopicity, very low chemical reactivity and can form hydrogen bonds with the nanoparticles during lyophilization.

The overall aim of the work performed in this thesis was to develop a catalase encapsulated nanoparticulate drug delivery system made of a biodegradable polymer, and explore its therapeutic potential in oxidative stress-induced damage to cardiac myocytes.

Formulation of the enzyme encapsulated nanoparticles are explored in Chapter 2. Chapter 3 describes investigation of the therapeutic efficacy of the formulated nanoparticles in reducing oxidative stress-induced cardiac damage. Finally, Chapter 4 studies structural changes of the protein upon lyophilization of the nanoparticles with and without cryoprotection. More specifically the aims of this thesis work were as follows:

- To encapsulate catalase into the nanoparticles.
- To investigate the detrimental effect of the encapsulation processing steps on the enzymatic activity of the antioxidant enzyme.
- To assess the stabilizing effects of the two commonly used additives, trehalose and bovine serum albumin on the encapsulation process related loss of enzymatic activity.
- To explore the effects of lyophilization on enzymatic activity of the encapsulated enzyme in the absence and presence of a cryoprotectant, trehalose.
- To evaluate the ability of the enzyme-loaded nanoparticles in rescuing cardiomyocytes from oxidative stress-induced damage.
- To examine the potential effect of the nanoparticles on apoptosis-induced death of cardiomyocytes.
- To study cellular uptake of the nanoparticles.
- To explore secondary and tertiary structural changes of the encapsulated enzyme upon lyophilization with and without cryoprotection.

2 Preparation and Characterization of Protein-Loaded PLGA Nanoparticles

2.1 Introduction

A wide range of hydrophilic and hydrophobic drugs, biological macromolecules (e.g., nucleic acids, proteins and peptides) and vaccines can be delivered to specific organs or cells for a prolonged time using nanoparticles.[171,172] Nevertheless, there are major problems that restrict the use of nanoparticulate systems. Physical instability of aggregate formation and particle fusion, chemical instability of hydrolysis of the polymeric materials, leaking of drugs from nanoparticulate systems, and reactivity of drugs during storage, are often observed when these nanoparticulate systems in the form of suspensions in water are kept for long periods of time.[202] In order to stabilize the nanoparticulate systems, lyophilization technique is widely used. In this technique, water is eliminated by sublimation and desorption from a frozen sample of nanosuspension under the condition of vacuum.[224]

Protein-based therapeutics are getting success in many fields of medicine.[203] Therapeutic proteins are used in different pathological conditions and diseases.[205] But, proteins are labile in nature and can easily be inactivated.[206] Their delivery may occur under unfavourable stress conditions which could lead to aggregation or denaturation, and that may cause undesirable adverse effects. To overcome these problems, proteins can be formulated as protein-encapsulated polymeric nanoparticles.[207] Because of the advantageous properties like biocompatibility and biodegradability, prolonged release properties, variable mechanical properties and

non-toxic properties, Poly(lactic-co-glycolic acid) (PLGA) is largely used to fabricate nanoparticles.[207,221]

PLGA is degraded by hydrolysis of its ester linkage. Because of the hydrolytically unstable polyester structure, PLGA nanoparticles are not stable if stored in aqueous media.[222] Furthermore, nanoparticles may form aggregates in aqueous environment during storage, even though surfactants are employed as a stabilizer in the nanosuspensions.[223]

Freeze-drying not only stabilizes the nanoparticulate systems but also reduces instability of the loaded protein of protein-loaded nanoparticles. However, freeze-drying itself is a process that can negatively affect properties of the nanoparticles and stability of the loaded protein.[200] Protectants are added before freeze-drying of nanoparticulate systems to minimize the instability of the nanoparticles associated with lyophilization. They protect the nanoparticles from mechanical stress of ice crystals and decrease aggregation of particles.[199] It has been shown that protectants have been able to prevent aggregation of nanoparticles, impart satisfactory redispersibility after reconstitution and most notably minimize alterations in the encapsulated protein's native structure upon freeze-drying.[199,200,225-227] Trehalose, sucrose, glucose and mannitol are commonly employed as protectant in the freeze-drying of nanoparticles.[228] Trehalose is a well-known protectant of biomolecules in their freeze-drying process. It was reported to be very effective in stabilizing labile proteins during lyophilisation.[229] Trehalose offers many advantages over other sugars, e.g., low hygroscopicity and very low chemical reactivity. Also, trehalose can form hydrogen bonds with nanoparticles during lyophilization as internal hydrogen bonds are absent in trehalose molecule.[230]

Protein's native structure can be altered when it is encapsulated during fabrication of protein-loaded nanoparticles. This alteration in the native structure may be due to a contact of the protein with the organic solvent, shear stresses applied in the emulsification process and protein's interaction with the polymer's hydrophobic interface.[208] Addition of a protecting molecule to the protein's encapsulation process can improve stability of the protein. Incorporating a decoy protein such as serum albumin into the emulsification process of fabricating protein-loaded nanoparticles, can preserve the encapsulated protein's activity, because inactivation of the protein partly happens due to denaturation that occurs in the hydrophobic/hydrophilic interface.[209]

PLGA has been selected as the polymer to prepare nanoparticles for this study. Trehalose has been chosen as the protectant for lyophilization in this study as it is considered to be the best cryoprotectant among the carbohydrates available.[228] It has been demonstrated that trehalose could protect the secondary structure of bovine serum albumin upon freeze-drying.[249] Besides selecting bovine serum albumin as a decoy protein, trehalose has also been chosen as a protecting molecule in the encapsulation process for its protein stabilizing capacity hypothesizing that trehalose could provide both roles of protecting the protein molecule in the encapsulation process and in the lyophilization process as well.

Oxidative stress plays a pivotal role in various diseases including neurological and cardiovascular diseases. Oxidative stress occurs when the ROS are overproduced and cannot be removed by the endogenous antioxidant defence systems.[76] Catalase controls the level of H_2O_2 in the myocardium and it is responsible for almost 80% of all the peroxidase activity in the heart cells.[89] Recently, it has been shown that

catalase-loaded nanoparticles could protect neurons from oxidative stress induced by H_2O_2.[277] No studies have been reported yet on the stability study of catalase-loaded nanoparticles upon freeze-drying. So, catalase has been selected as a model protein for encapsulation of a protein into PLGA nanoparticles. In this work, it was aimed to explore the protective effects of trehalose and bovine serum albumin on catalase activity during encapsulation procedure of catalase-loaded PLGA nanoparticles, and alteration of activity of the loaded catalase induced by lyophilization, and also to evaluate the potential protective action of trehalose in preserving catalase activity of catalase-loaded PLGA nanoparticles upon freeze drying.

2.2 Materials and methods

2.2.1 Chemicals

Poly(D,L-lactide-co-glycolide) acid terminated, lactide:glycolide 50:50, Mw 24,000-38,000 (Resomer® RG 503 H), Catalase from bovine liver (2000–5000 units/mg protein), D-(+)-Trehalose dehydrate, Hydrogen peroxide solution 30% (w/w) in water, Bovine serum albumin, PBS Tablet and Poly(vinyl alcohol) (PVA, 87%-89% hydrolysed with a Mw of 13,000-23,000), Lysozyme from chicken egg-white (protein ≥90 %, ≥40,000 units/mg protein) were purchased from Sigma-Aldrich (Poole, UK).

Dichloromethane, acetone and acetonitrile were obtained from Fisher Scientific, UK. Water used was de-ionised water (Maxima Elga HPLC grade, resistivity 18.2 MΩ cm).

2.2.2 Formulation of nanoparticles

2.2.2.1 Preparation of plain PLGA nanoparticles

Plain PLGA nanoparticles were fabricated by a solvent-displacement method as described by Fessi *et al.*[278] In brief, 10 mg of PLGA was dissolved in 1 mL of acetone. This solution was added, in a drop-wise manner, to 10 mL of water under moderate magnetic stirring. Magnetic stirring was continued overnight, at room temperature, to evaporate the acetone. The resultant nanosuspensions were taken out followed by filtration through syringe filters of 0.45 μm size (Minisart single

use filter unit, Sartorius Stedim Biotech, Germany) to remove any aggregates. The nanosuspensions were then freeze-dried with and without trehalose.

2.2.2.2 Formulation of catalase-loaded PLGA nanoparticles

2.2.2.2.1 Formulation of catalase-loaded PLGA nanoparticles by nanoprecipitation method

Catalase-loaded PLGA nanoparticles were formulated using a two-step nanoprecipitation method developed by Cruz *et al.*[279] Briefly, 25 mg of catalase was dissolved in 1 mL of water to prepare the catalase solution. In 0.8 mL of catalase solution, acetonitrile was added at 1:4 volume ratio under slow stirring. The protein suspension resulted was stirred for 5 minutes with a magnetic stirring bar. 2 mL of a PLGA solution prepared as 190 mg/mL in acetonitrile was added to the protein suspension prepared in the previous step. The resultant mixture was then added through a syringe pump (SP 260PZ Syringe Pump, World Precision Instruments Ltd., UK) to 240 mL of a 10% PVA solution under stirring. The mixture was then immediately centrifuged at 8,000 rpm (Rotor JA-17, Beckman J2-21 centrifuge, Beckman Coulter Inc., CA, USA) for 10 minutes. The pellet was resuspended in water followed by centrifugation again. Washing step of resuspending and centrifuging were repeated thrice. The pellet found after the last centrifugation was resuspended again in water and freeze-dried. In an effort to fabricate lysozyme-loaded PLGA nanoparticles, the same procedure was followed.

2.2.2.2.2 Formulation of catalase-loaded PLGA nanoparticles by a double emulsion method

2.2.2.2.2.A Encapsulation of catalase without stabilizer

Catalase-loaded nanoparticles were formulated following a modified double emulsion method.[277,280] Briefly, a PLGA polymer solution was prepared by dissolving 81 mg of PLGA polymer in 3 mL of dichloromethane. To prepare polyvinyl alcohol solution, 5 gm of PVA was added to 100 mL of water with magnetic stirring on a hot plate and 70–80ºC heat was applied to dissolve it completely in the water. After preparation of the solution of polyvinyl alcohol, it was kept in the room temperature to cool down to room temperature. Then the solution of PVA was passed through a syringe filter of 0.2 μm size (Minisart single use filter unit, Sartorius Stedim Biotech, Germany). A solution of bovine liver catalase (8 mg) in 300 μL of water was prepared. The protein solution was then added to the polymer solution and vortexed for 30 seconds. After vortexing for 30 seconds, the mixture was sonicated for 1minute on an ice bath with a probe sonicator (SONOPULS HD 2070, BANDELIN electronic, Germany) and a primary emulsion was formed. This primary emulsion was added to 18 mL solution of PVA, vortexed for 30 seconds followed by sonication in the same way as mentioned above to form the secondary emulsion. The resultant emulsion was kept stirring in a fume hood overnight for evaporation of the entire dichloromethane. The nanoparticles were recovered by centrifuging the dispersion at 39,800 x g for 30 minutes at 4ºC (Rotor JA-17, Beckman J2-21 centrifuge, Beckman Coulter Inc., CA, USA). After centrifugation, the supernatant was removed and the pellet was resuspended in water followed by vortexing and sonication in the same way as

mentioned above. The suspension was then again centrifuged at 39,800 x g for 30 minutes at 4ºC (Rotor JA-17, Beckman J2-21 centrifuge, Beckman Coulter Inc., CA, USA). This washing step was repeated two times. Finally, the pellet was redispersed in water, vortexed and sonicated on an ice bath in the same way as mentioned above. The final nanosuspension was then freeze-dried.

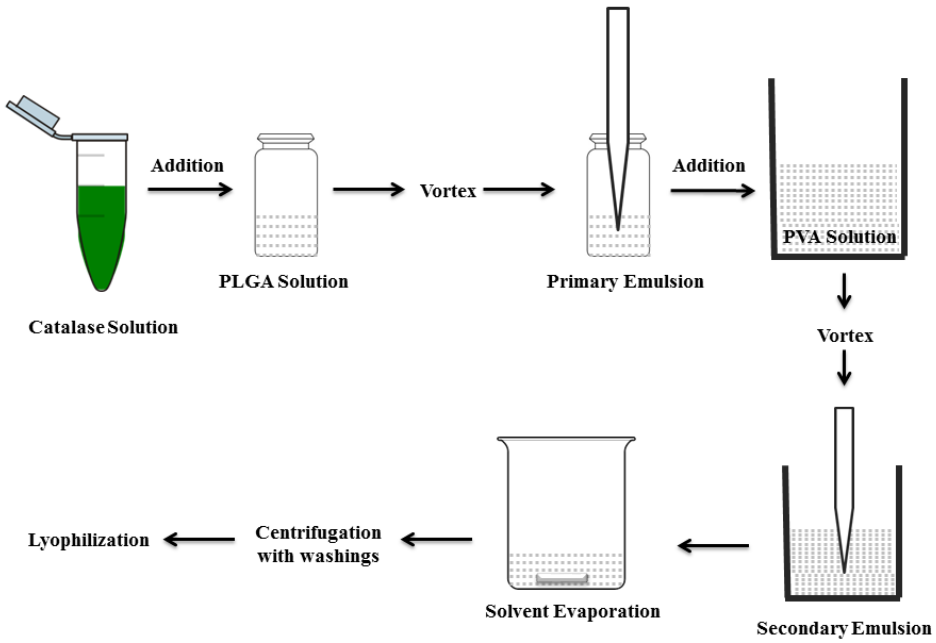

Figure 13: Diagrammatic presentation of preparing catalase-loaded PLGA nanoparticles.

A number of variants of the modified double emulsion method were applied in this study to fabricate different types of catalase-loaded PLGA nanoparticles, and also to investigate the effects of formulation parameters on catalase activity (Table 3).

Table 3: A bird's eye view of variants of the modified double emulsion method applied in this study

Formulation Objective	Stabilizer	Primary Aqueous Phase	Primary Oil Phase	Secondary Aqueous Phase	Shear Stresses Applied	Freeze-Drying
Encapsulation of catalase without stabilizer	None	8 mg of catalase in 300 µL of water	81 mg of PLGA in 3 mL of dichloromethane	18 mL of 5% PVA solution	Vortex and probe sonication	Freeze-dried without cryoprotection
Encapsulation of catalase with trehalose	Trehalose 50 mg/mL	8 mg of catalase in 300 µL of trehalose solution	81 mg of PLGA in 3 mL of dichloromethane	18 mL of 5% PVA solution	Vortex and probe sonication	Freeze-dried without cryoprotection
Encapsulation of catalase with bovine serum albumin (BSA)	BSA 25 mg/mL	8 mg of catalase in 300 µL of BSA solution	81 mg of PLGA in 3 mL of dichloromethane	18 mL of 5% PVA solution	Vortex and probe sonication	Freeze-dried with and without cryoprotection
Effect of emulsification procedures	None	8 mg of catalase in 300 µL of water	Only 3 mL of dichloromethane (No PLGA)	18 mL of 5% PVA solution	Vortex and probe sonication	No freeze-drying
Effect of dichloromethane (i.e., absence of dichloromethane)	None	8 mg of catalase in 300 µL of water	3 mL of water instead of dichloromethane (No PLGA)	18 mL of 5% PVA solution	Vortex and probe sonication	No freeze-drying
Effect of probe sonication (i.e., absence of probe sonication)	None	8 mg of catalase in 300 µL of water	Only 3 mL of dichloromethane (No PLGA)	18 mL of 5% PVA solution	Only vortex	No freeze-drying
Effect of trehalose	Trehalose 10, 50, 100 & 200 mg/mL	8 mg of catalase in 300 µL of trehalose solutions	Only 3 mL of dichloromethane (No PLGA)	18 mL of 5% PVA solution	Vortex and probe sonication	No freeze-drying
Effect of bovine serum albumin (BSA)	BSA 1, 10, 25 & 50 mg/mL	8 mg of catalase in 300 µL of BSA solutions	Only 3 mL of dichloromethane (No PLGA)	18 mL of 5% PVA solution	Vortex and probe sonication	No freeze-drying

2.2.2.2.2.B Encapsulation of catalase with trehalose

This experiment was performed to fabricate trehalose-stabilized catalase-loaded PLGA nanoparticles. PLGA and PVA solutions were prepared as mentioned in section 2.2.2.2.2.A. Trehalose solution was made in water at the concentration of 50 mg/mL. A solution of bovine liver catalase (8 mg) in 300 µL of trehalose solution was prepared. The final nanosuspension was then formulated in the same way as mentioned in section 2.2.2.2.2.A and freeze-dried.

2.2.2.2.2.C Encapsulation of catalase with bovine serum albumin

This experiment was conducted to fabricate bovine serum albumin-stabilized catalase-loaded PLGA nanoparticles. PLGA and PVA solutions were prepared in the same way as mentioned in section 2.2.2.2.2.A. Bovine serum albumin (BSA) solution was made in water at the concentration of 25 mg/mL. A solution of bovine liver catalase (8 mg) in 300 µL of BSA solution was prepared. The final nanosuspension was then formulated in the same way as mentioned in section 2.2.2.2.2.A and freeze-dried. For cryoprotected samples, trehalose was added at different ratios to the final nanosuspension, mixed by vortexing and then freeze-dried.

2.2.2.2.2.D Simulation of nanoparticle formulation procedure without PLGA to investigate the effects of formulation parameters

2.2.2.2.2.D.i Effect of emulsification procedures

Catalase and PVA solutions were prepared in the same manner as mentioned in section 2.2.2.2.2.A. The protein solution was added to 3 mL of dichloromethane and emulsified in the same way as mentioned in section 2.2.2.2.2.A to form a secondary emulsion. The emulsion was then kept stirring in a fume hood overnight for evaporation of the entire dichloromethane after which the liquid was collected and its volume was measured. Catalase activity of the initial protein solution and the final liquid phase were determined.

2.2.2.2.2.D.ii Effect of dichloromethane (i.e., absence of dichloromethane)

Catalase and PVA solutions were prepared in the same way as mentioned in section 2.2.2.2.2.A. Then the protein solution was added to 3 mL of water instead of dichloromethane or PLGA polymer solution and vortexed for 30 seconds, followed by probe sonication for 1 minute on an ice bath as mentioned in section 2.2.2.2.2.A. This liquid mixture was added to 18 mL solution of PVA, vortexed for 30 seconds followed by probe sonication in the same way as mentioned above. Like the nanoparticle formulation procedure, the resultant liquid was kept stirring in a fume hood overnight although there was no organic solvent at all. Thereafter the liquid was collected, its volume was measured and catalase activity of the initial protein solution and the final liquid phase were determined.

2.2.2.2.2.D.iii Effect of probe sonication (i.e., absence of probe sonication)

Catalase and PVA solutions were prepared in the same manner as mentioned in section 2.2.2.2.2.A. The protein solution was added to 3 mL of dichloromethane and vortexed for 30 seconds, followed by vortexing again for 1 minute instead of the probe sonication for 1 minute. This liquid phase was then added to 18 mL solution of PVA, vortexed for 30 seconds, followed by vortexing again for 1 minute instead of probe sonication for 1 minute. Catalase activity of the initial protein solution and the final liquid phase were determined in the same way as mentioned in section 2.2.2.2.2.D.i after evaporation of the entire dichloromethane.

2.2.2.2.2.E Simulation of nanoparticle formulation procedure without PLGA to investigate the protective effects of trehalose and bovine serum albumin on catalase activity during encapsulation of the protein

2.2.2.2.2.E.i Effect of trehalose on catalase activity during encapsulation

This experiment was performed to evaluate any protective effect of trehalose on the catalase activity, when trehalose was added as a stabilizer to the emulsification process. PLGA and PVA solutions were prepared in the same way as mentioned in section 2.2.2.2.2.A. Four strengths of trehalose solutions were made in water as 10, 50, 100 and 200 mg/mL. Solutions of bovine liver catalase (8 mg) in 300 µL of trehalose solutions of the four strengths were prepared. The protein solution was added to 3 mL of dichloromethane instead of the 3 mL of polymer solution, and

emulsified in the same way as mentioned in section 2.2.2.2.2.A to form a secondary emulsion. The secondary emulsion was kept stirring in a fume hood overnight for evaporation of the entire dichloromethane after which the liquid was collected, its volume was measured and catalase activity of the initial protein solution and the final liquid phase were determined.

2.2.2.2.2.E.ii Effect of bovine serum albumin on catalase activity during encapsulation

This experiment was accomplished to assess any protective effect of bovine serum albumin on the catalase activity, when bovine serum albumin was added as a stabilizer to the emulsification process. PLGA and PVA solutions were prepared in the same way as mentioned in section 2.2.2.2.2.A. Four strengths of bovine serum albumin solutions were made in water as 1, 10, 25 and 50 mg/mL. Solutions of bovine liver catalase (8 mg) in 300 µL of BSA solutions of the four strengths were prepared. Following the same procedure as mentioned in section 2.2.2.2.2.E.i, catalase activity of the initial protein solution and the final liquid phase were determined after emulsification and evaporation of the entire dichloromethane.

2.2.3 Freeze-drying

The final nanosuspensions including the trehalose-mixed nanosuspensions were frozen in liquid nitrogen and then immediately placed in the lyophilization chamber

of a Benchtop Pro freeze dryer (Biopharma, UK) and lyophilized at a condenser temperature of -60°C and pressure of 18-20 millitorr for at least 48 hours.

2.2.4 Analysis of catalase activity

To analyse the enzymatic activity of catalase of catalase-loaded PLGA nanoparticles, the enzyme was extracted from the matrix of PLGA. 4 mL of PBS of and 4 mL of dichloromethane were added to a glass vial containing 6.5±0.4 mg of lyophilized nanoparticles and stirred for 30 minutes on a magnetic stir plate. To rule out the possible effect of trehalose on the extraction procedure, an equivalent amount of trehalose was added to each vial containing 6.5±0.4 mg of lyophilized nanoparticles before adding PBS and dichloromethane. After stirring for 30 minutes, the vial was left undisturbed for 3 hours. After 3 hours, the supernatant was collected from the top one of the two layers, transferred to an eppendorf, centrifuged at 4ºC for 10 minutes using an eppendorf centrifuge (Eppendorf Centrifuge 5417R, Eppendorf UK Limited, UK) at a speed of 10,000 rpm. Thereafter, the supernatant was taken out followed by filtration through a syringe filter of 0.2 μm size (Minisart single use filter unit, Sartorius Stedim Biotech, Germany). The filtrate was analysed for catalase activity.

Enzymatic activity of the enzyme, catalase, was determined by a modified standard catalase assay method[281-285] with the following formulae:

$$\text{Units/mL} = \frac{[\Delta A/\text{min(Sample)} - \Delta A/\text{min(Blank)}] \times \text{Reaction volume in mL} \times \text{df}}{\varepsilon^{mM} \times \text{Sample volume in mL}}$$

Where,

df = dilution factor and

ε^{mM} = Millimolar extinction coefficient of hydrogen peroxide at 240 nm

Briefly, 10 µL of catalase solution was mixed with 990 µL of PBS or 100 µL of catalase solution extracted from NPs was mixed with 900 µL of PBS in a quartz cuvette. Then, 1 mL of 20mM of H_2O_2 solution prepared in PBS was added to the cuvette, mixed rapidly by inversion and immediately placed in the chamber of a Beckman DU 800 UV/Vis Spectrophotometer (Beckman Coulter Inc., USA). The decrease of absorbance of 20mM H_2O_2 at 240 nm was monitored for 120 seconds with 5 seconds interval using the kinetic program of the spectrophotometer.

2.2.5 Reconstitution and analysis of particle size and zeta potential of the nanoparticles

Dynamic light scattering (DLS) is a technique that is utilized to characterize the particle size of a colloidal suspension by measuring time-dependent variations in the intensity of the scattered light that arise from diffusion of the particles due to

Brownian motion. The rate of diffusion due to Brownian motion is more rapid for smaller particles.[286] The relationship between the diffusion coefficient, i.e., the speed of a particle and its size can be defined in the Stokes-Einstein equation.

Stokes-Einstein equation:

$$D = \frac{k_B T}{6\pi\eta r}$$

Where, D is the diffusion coefficient, k_B is the Boltzmann constant, T is the temperature, η is the dispersant viscosity and r is the hydrodynamic radius of the particle.[286,287]

Dynamic light scattering technique was used to measure hydrodynamic diameter and zeta potential of catalase-loaded and plain PLGA nanoparticles with a Zetasizer Nano ZS instrument (Malvern Instruments, UK). Polydispersity index (PDI), an indicator of particle size distribution, represents the width of particle size distribution. PDI is dimensionless and scaled from 0 to 1, where 0 is monodisperse and 1 is polydisperse.[288,289] In this study, the DLS measurements were carried out at 25°C and at a measuring angle of 173° to the incident beam.

Freeze-dried catalase-loaded nanoparticles were reconstituted (1 mg/mL) in diluted PBS. After gently adding the vehicle in the inside wall of the vials, the vials were left undisturbed for one hour for wetting of the nanoparticles. This mixture was then sonicated on an ice bath for 30 seconds with a microtip probe sonicator. The nanosuspension thus prepared was further diluted and mixed well. This diluted

nanosuspension was used for measuring hydrodynamic diameter and zeta potential by DLS.

Plain PLGA nanoparticles were reconstituted (1 mg/mL) in diluted PBS in the same way as mentioned above except that vortexing was applied after one hour of wetting of the nanoparticles followed by keeping the vials undisturbed for one more hour before sonication. Also, ice bath was not used in the sonication process of plain PLGA nanoparticles. The reconstituted nanosuspension was further diluted and mixed well. Finally, the diluted nanosuspension was used for measuring hydrodynamic diameter and zeta potential by DLS.

2.2.6 Transmission electron microscopy

Lyophilized catalase-loaded PLGA nanoparticles which were cryoprotected by trehalose at a weight ratio of nanoparticles to trehalose of 1:60 were reconstituted in water (0.5 mg/mL) by sonicating on an ice bath for 30 seconds with a microtip probe sonicator. Plain PLGA nanoparticles lyophilized with 10 mg/mL of trehalose were reconstituted (0.5 mg/mL) in water.

Then, both of the nanosuspensions were diluted 10 times with water and used for characterization by transmission electron microscopy. 10 µL of the diluted nanosuspension was applied to TEM copper grid (TAAB Laboratories Equipment Ltd, Berks, UK). After 10 minutes, the liquid was removed by touching the edge of the grid with filter paper. 10 µL of filtered (0.2 µm syringe filter (Minisart single use filter unit, Sartorius Stedim Biotech, Germany) 2% (w/v) uranyl acetate solution

was placed onto the grid and left for 1 minute. Thereafter, uranyl acetate solution was removed by touching the edge of the grid with filter paper. After one hour, nanoparticles were imaged by a TEM (Tecnai G^2 BioTwin, FEI, Oregon, USA).

2.2.7 Statistical analysis

All the experiments were performed at least three times. Results are expressed as mean ± SD. Statistical analysis was performed by Student's *t*-test and one-way ANOVA followed by Tukey's multiple comparison tests using GraphPad Prism 6 software (GraphPad, San Diego, CA, USA). The results were considered significant at a *p* value of less than 0.05.

2.3 Results

2.3.1 Plain PLGA nanoparticles by nanoprecipitation method

2.3.1.1 Effect of lyophilization on plain PLGA nanoparticles

After vortexing, it was noticed that the plain PLGA nanoparticles which were cryoprotected with trehalose readily mixed with the vehicle without leaving any floating particles (B of Figure 14). On the contrary, clumps of particles were floating in the vial where trehalose was not added before freeze-drying (A of Figure 14).

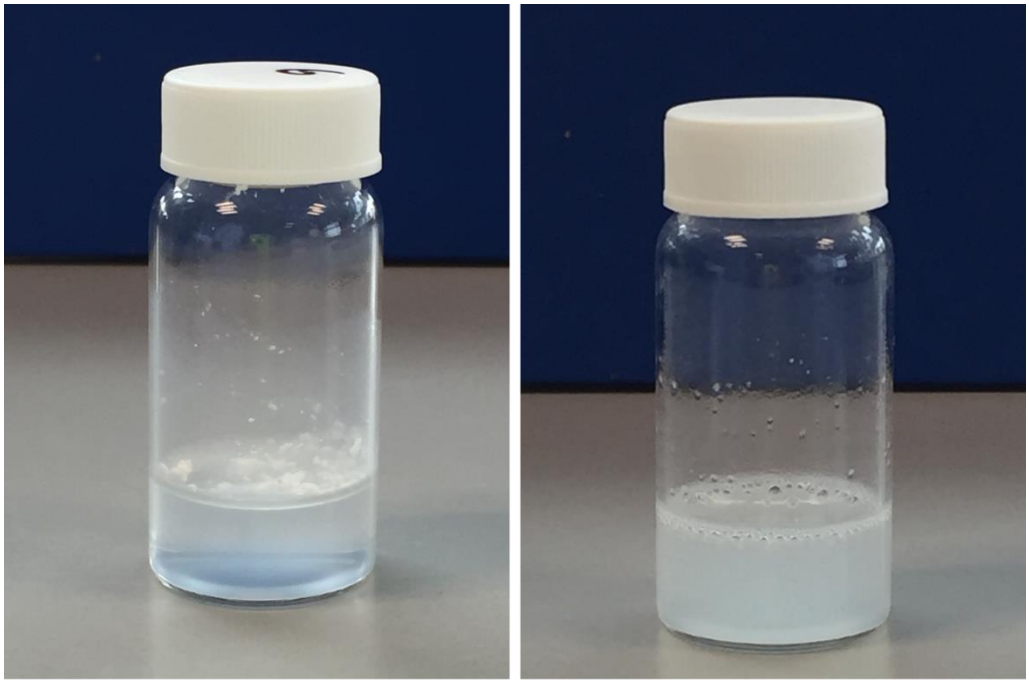

Figure 14: Representative photographs of reconstituted plain PLGA NPs after mixing by vortex. (A) Not cryoprotected by trehalose & (B) Cryoprotected by trehalose.

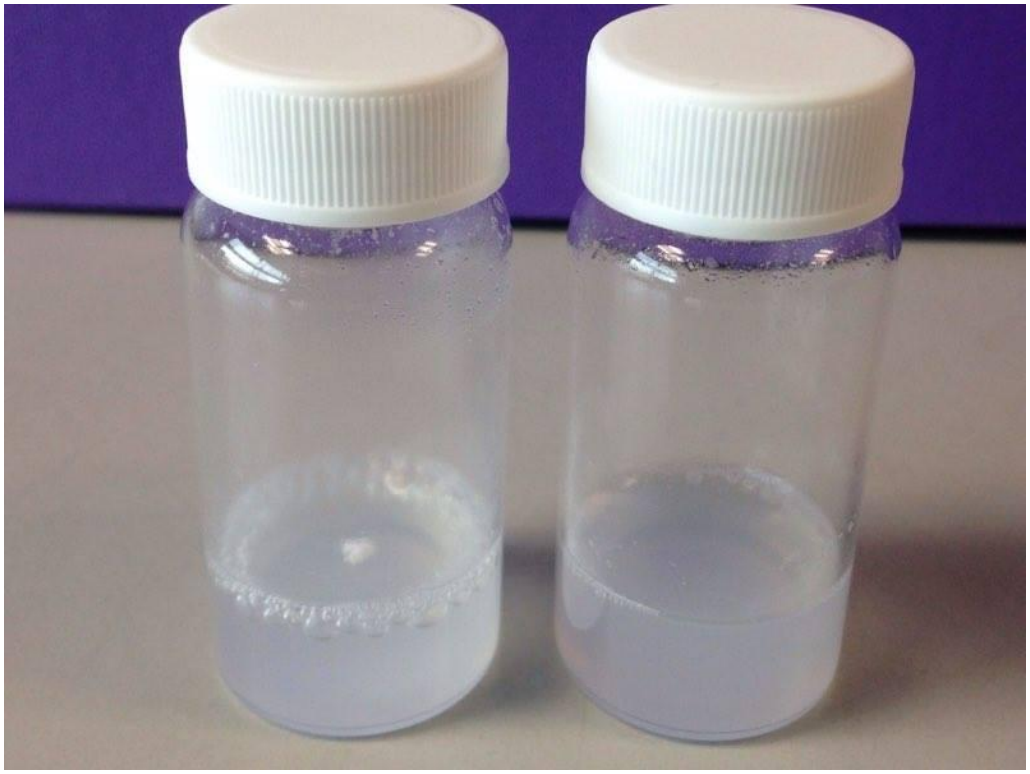

Figure 15: Comparison of non-cryoprotected and cryoprotected of plain PLGA NPs after reconstitution by vortex & probe sonication. NPs of left vial - not cryoprotected & NPs of right vial - cryoprotected by trehalose.

Clumps of particles were still floating after one hour of vortexing in the vials of the plain PLGA nanoparticles which were not freeze-dried with trehalose. Then, the vials were probe sonicated for 30 seconds, but there were still lumps of particles although probe sonication reduced floating of the particles and helped the particles in going into the suspension (left vial of Figure 15). In contrast, the physical appearance of the nanosuspensions of trehalose-protected nanoparticles did not change after the probe sonication (right vial of Figure 15).

2.3.1.2 Effect of trehalose on lyophilization-induced change of plain PLGA nanoparticles

The effect of freeze-drying on the hydrodynamic diameter of the plain PLGA nanoparticles is presented in Table 4. It was observed that hydrodynamic diameter of the freshly prepared nanoparticles slightly increased with an increasing concentration of trehalose added to the nanoparticulate suspension before freeze-drying.

Table 4: Action of trehalose in resisting aggregation of NPs upon lyophilization (FD is freeze-drying and HD is hydrodynamic diameter)

Condition	No Trehalose		10 mg/mL Trehalose		100 mg/mL Trehalose		200 mg/mL Trehalose	
	HD	PDI	HD	PDI	HD	PDI	HD	PDI
Fresh NPs	116.7±4.1 nm	0.087±0.010	118.3±3.8 nm	0.095±0.033	142.3±6.7 nm	0.102±0.014	174.2±14.1 nm	0.100±0.012
Reconstituted NPs after FD	Aggregation of NPs (1993.3±1547.3 nm)	0.840±0.105 (Range: 0.727 - 1)	139.5±2.7 nm	0.138±0.011	162.5±13.1 nm	0.162±0.021	212.5±12.8 nm	0.184±0.028

Reconstitution of freeze-dried nanoparticles where trehalose was not added as a cryoprotectant to protect from the damage induced by freeze-drying produced aggregation of nanoparticles. High PDI value indicated aggregation of nanoparticles in the absence of cryoprotection (Table 4). Three concentrations of trehalose were employed as cryoprotectant of plain PLGA nanoparticles in this study. All three concentrations reduced aggregation of the nanoparticles upon lyophilization and could preserve the initial hydrodynamic diameter of the nanoparticles with a high efficiency although the hydrodynamic diameters for all of the three formulations of trehalose-protected nanoparticles increased a little compared to the hydrodynamic diameters of the respective freshly prepared nanosuspensions. It was also observed that PDI values increased very slightly in

reconstituted cryoprotected nanoparticles (Table 4). In contrast, the PDI values rose tremendously after freeze-drying of nanoparticles without cryoprotection of trehalose and even reached the maximum value of 1 (Table 4).

2.3.1.3 Effect of trehalose on zeta-potential of lyophilized plain PLGA nanoparticles

The effect of adding trehalose as a cryoprotectant in the suspensions of plain PLGA nanoparticles is shown in Table 5.

Table 5: Effect of cryoprotection on zeta potential of NPs

Condition	No Trehalose	10 mg/mL Trehalose	100 mg/mL Trehalose	200 mg/mL Trehalose
Zeta Potential of Fresh NPs	-52.6±3.1 mV	-51.3±2.7 mV	-40.0±1.8 mV	-29.5±2.4 mV
Zeta Potential of Reconstituted NPs after FD	-51.4±1.4 mV	-49.9±2.1 mV	-43.9±2.2 mV	-32.7±2.3 mV

Freeze-drying itself did not change zeta potential of the nanoparticles. However, trehalose was observed to reduce the negative charge of the plain PLGA nanoparticles. This reduction of negative charge by trehalose was concentration dependent and increased with raising concentration of trehalose. This effect was noticed in both freshly prepared suspension of nanoparticles and reconstituted suspension of lyophilized nanoparticles.

2.3.1.4 TEM image of plain PLGA nanoparticles

TEM images of freshly prepared plain PLGA nanoparticles (Figure 16) and cryoprotected plain PLGA nanoparticles (Figure 17) showed that the nanoparticles were spherical in shape and were in the size range of 50 – 200 nm.

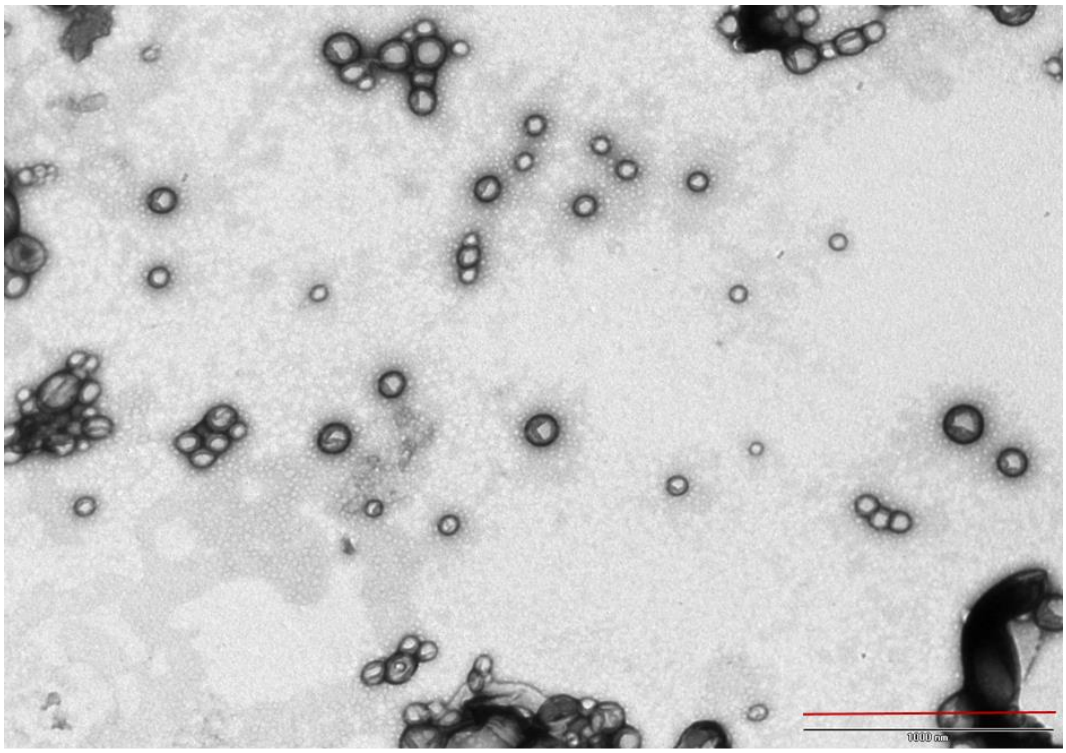

Figure 16: Representative TEM image of freshly prepared plain PLGA NPs.

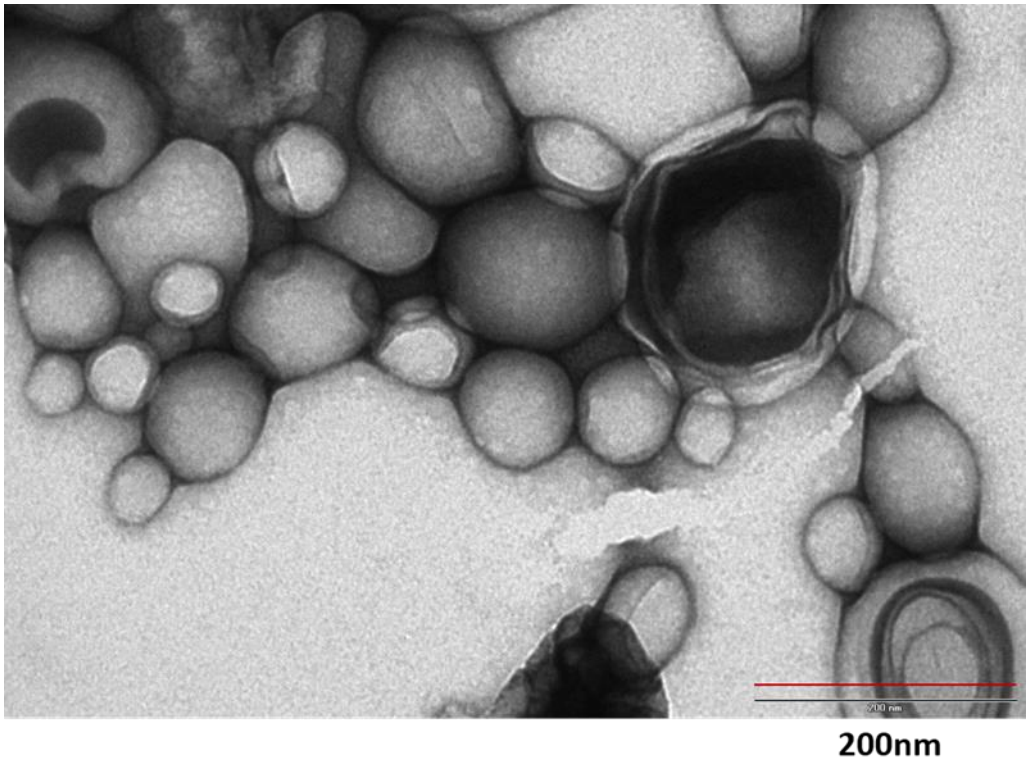

Figure 17: Representative TEM image of reconstituted plain PLGA NPs cryoprotected by trehalose.

2.3.2 Catalase-loaded PLGA nanoparticles

2.3.2.1 Catalase-loaded PLGA nanoparticles by nanoprecipitation method

It had not been possible to prepare catalase-loaded PLGA nanoparticles following the two-step nanoprecipitation method developed by Cruz *et al.*[279] Formulation of lysozyme-loaded PLGA nanoparticles were also attempted following the method as the authors demonstrated preparation of protein-loaded PLGA nanoparticles using lysozyme. But, similar with catalase-loaded PLGA nanoparticles, lysozyme-

loaded PLGA nanoparticles had also not been possible to formulate following this two-step nanoprecipitation method.

2.3.2.2 Catalase-loaded PLGA nanoparticles by double emulsion method

Most widely used technique for encapsulating protein into PLGA is the double emulsion method (w/o/w).[198] As it has been shown in section 2.3.1 that trehalose could minimize lyophilization-induced aggregation of plain PLGA nanoparticles prepared by the nanoprecipitation method, plain PLGA nanoparticles were not fabricated further using the double emulsion method to demonstrate the cryoprotection ability of trehalose in reducing aggregation of plain PLGA nanoparticles.

2.3.2.2.1 Stabilizers in encapsulation of catalase

Following the double emulsion method, unstabilized catalase-loaded PLGA nanoparticles were produced without cryoprotection. Astonishingly, it was found that the enzyme activity became just 1.47±0.29% (204±41 units) of the activity (13,861±476 units) of the enzyme initially added to the formulation procedure. The results are presented in Figure 18.

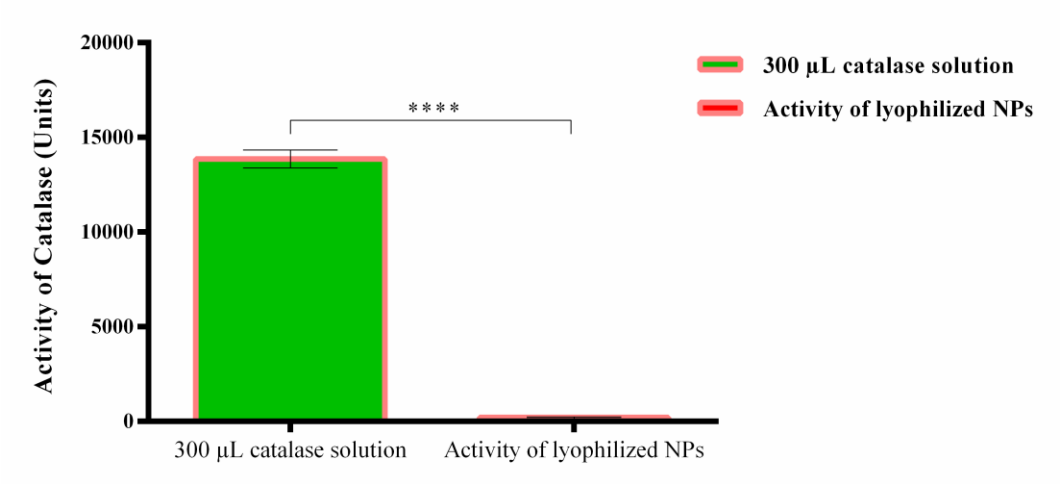

Figure 18: Activity of catalase retained in the nanoparticles after formulation without stabilizer and cryoprotection (n=5; ****P ≤ 0.0001).

The investigation was performed by completing the two steps of emulsification without PLGA. It has been observed that the procedure of the double emulsion method significantly reduced the catalase activity to 71.32±4.77% of the initial activity, i.e., the activity of 300 µL of catalase solution. The initial catalase activity was 14,003±383 units which was reduced to 9,987±668 units after emulsification procedures. The result is shown in Figure 19.

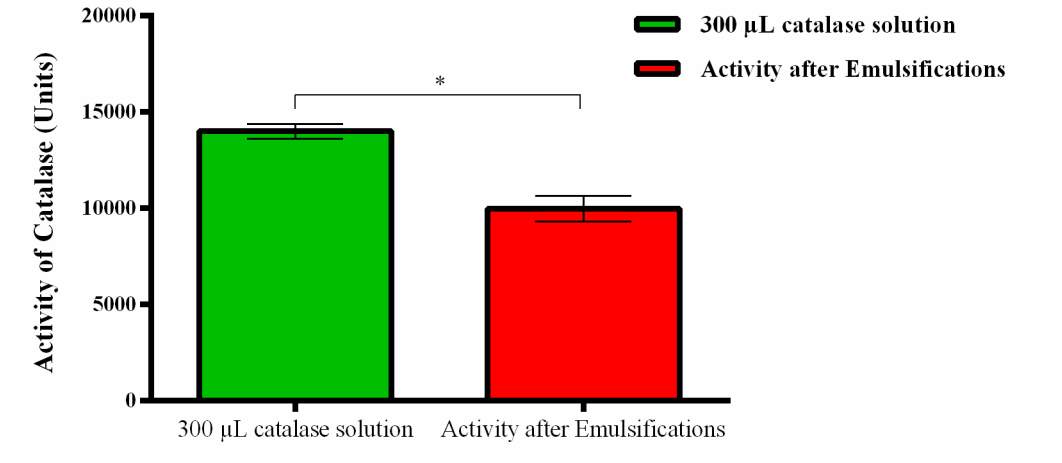

Figure 19: Effect of the emulsification procedure (n=3; *P ≤ 0.05).

Then, the investigation was proceeded to find out the effect of dichloromethane, the organic solvent, used in this encapsulation procedure. It has been accomplished by simulating the two emulsification steps using the same amount of water instead of dichloromethane in the first step. The result is presented in Figure 20 and it indicated that the activity of the enzyme was not significantly affected in the absence of a water/organic solvent interface although there was a little drop in the catalase activity, which was not statistically significant as compared to the initial activity. Initial catalase activity was 13,917±316 units which was reduced to 12,784±691 units after the simulated encapsulation procedure.

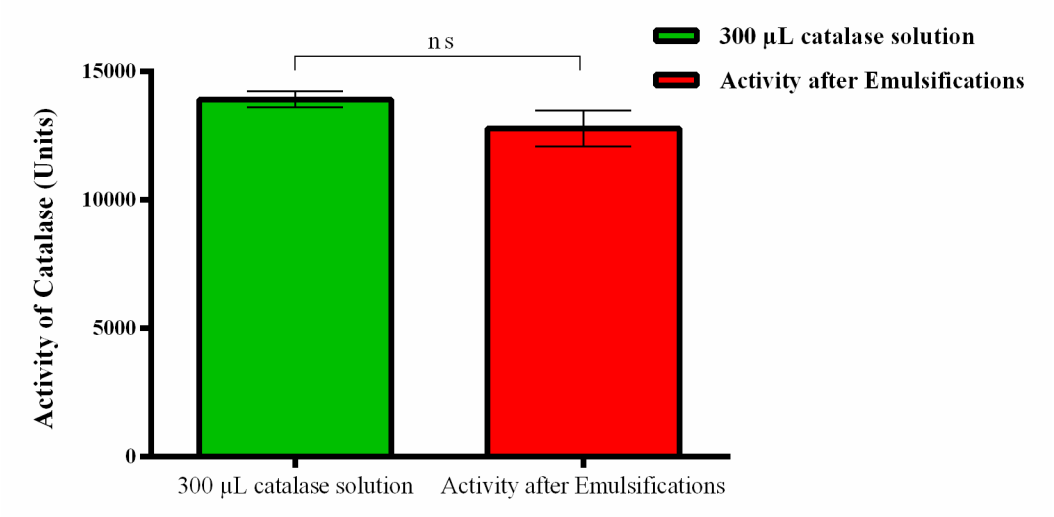

Figure 20: Effect of the absence of dichloromethane (n=4; ns, not significant).

The effect of ultrasonication on catalase activity was also evaluated by performing the encapsulation procedure without ultrasonication. Vortexing was applied instead of ultrasonication. In the presence of an interface of water/organic solvent, vortexing reduced the enzyme activity to 83.59±3.52% which was statistically significant as compared to the initial catalase activity of the protein solution used

in the emulsification process (Figure 21). Initial catalase activity, 13,903±360 units was reduced to 11,621±490 units due to the detrimental effect of vortexing in the presence of an aqueous/organic interface.

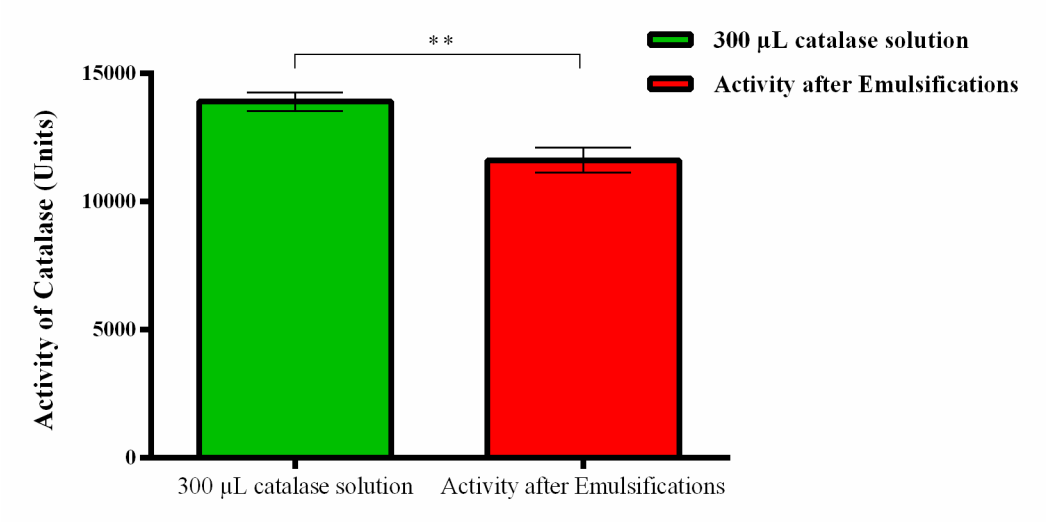

Figure 21: Effect of the absence of ultrasonication (n=3; **P ≤ 0.01).

In the presence of water/dichloromethane interface, ultrasonication after vortexing, caused more damage to the activity of catalase than only vortexing did. Vortexing followed by ultrasonication resulted in retention of 71.32±4.77% of initial activity. In contrast, only vortexing reduced the catalase activity to 83.59±3.52% of the initial activity. The difference was statistically significant. The comparison is shown in Figure 22 .

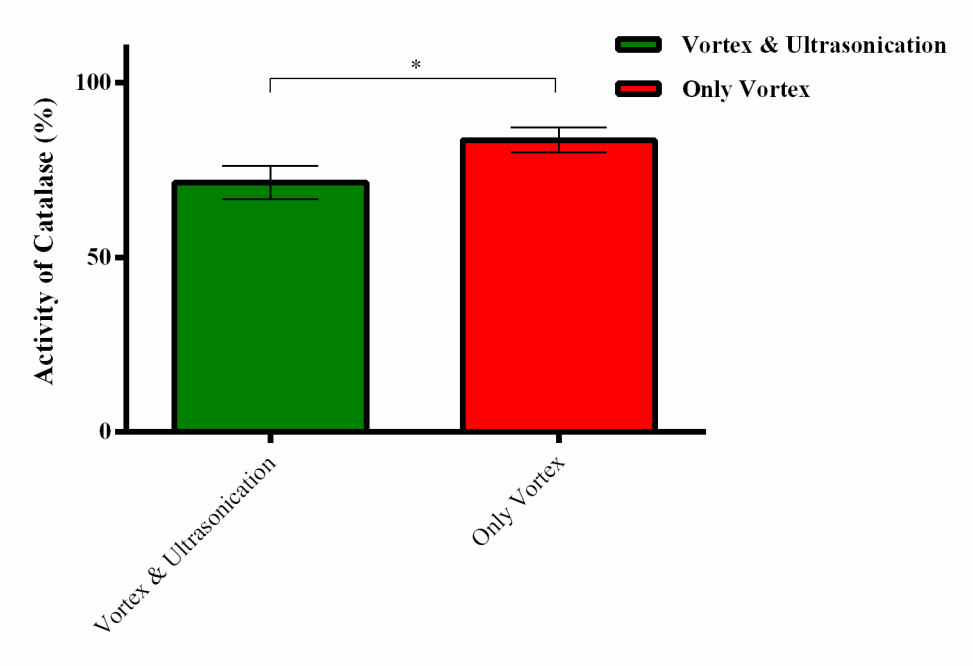

Figure 22: Comparative detrimental effects of vortex followed by ultrasonication and only vortex (n=3; *P ≤ 0.05).

Trehalose was added to the initial aqueous phase and it showed protective action in preserving the activity of catalase. The results of adding trehalose to the initial aqueous phase is presented in Figure 23.

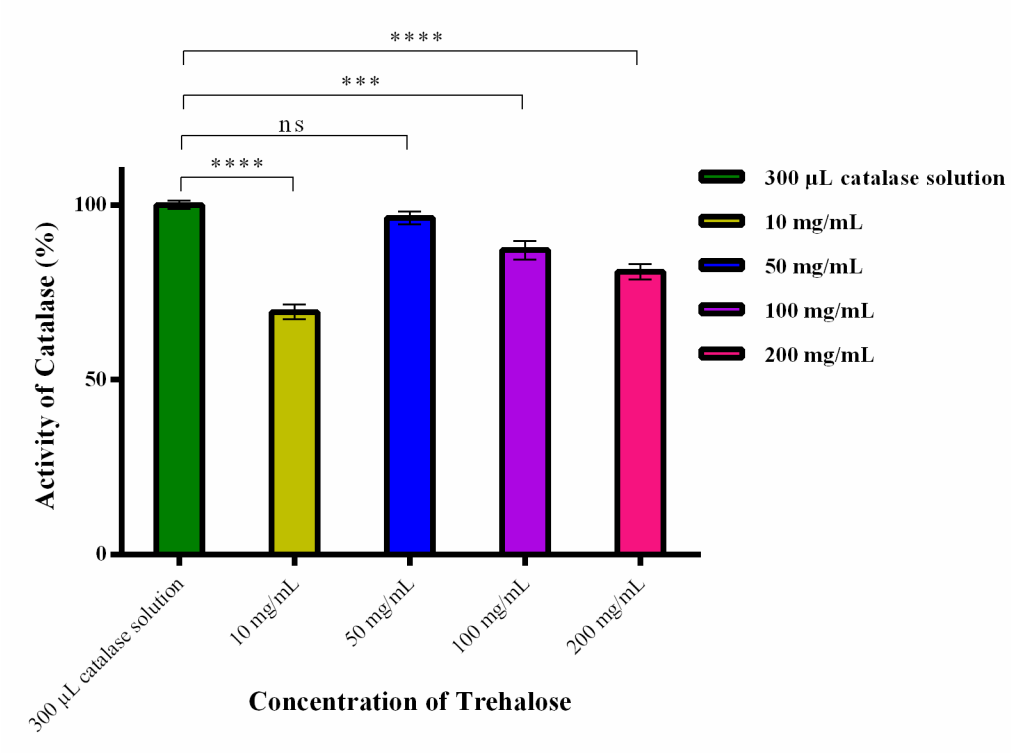

Figure 23: Effect of trehalose added to the initial aqueous phase (n=5; ns, not significant; ***P ≤ 0.001; ****P ≤ 0.0001).

Among the four concentrations of trehalose used in this study, 50 mg/mL was found to be the best protectant of the enzyme activity in the emulsification process. The activity retained by this concentration was significantly higher than those produced by the other three concentrations of trehalose, 10, 100 and 200 mg/mL. It has been observed in this study that there was no significant difference between the initial activity and the post-procedure activity of the enzyme when trehalose was added to the initial aqueous phase at 50 mg/mL concentration. This 50 mg/mL concentration of trehalose added to the initial aqueous phase could retain 96.19±1.85% of the initial activity.

In this study, bovine serum albumin was also found to retain catalase activity against emulsification-induced loss of activity. The result of stabilizing effect of bovine serum albumin is presented in Figure 24.

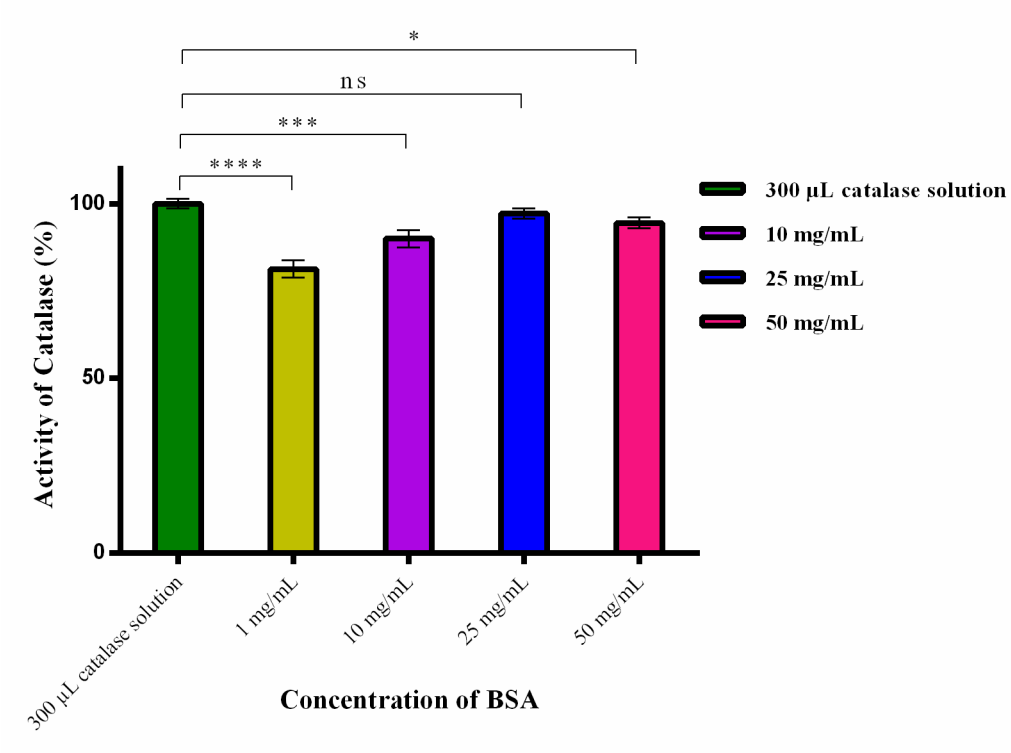

Figure 24: Effect of BSA added to the initial aqueous phase (n=5; ns, not significant; *P ≤ 0.05; ***P ≤ 0.001; ****P ≤ 0.0001).

At a concentration of 25 mg/mL, bovine serum albumin showed the best protective action in retaining the enzyme activity among the four concentrations used in this study. Only this concentration of bovine serum albumin showed no significant difference compared to the initial activity, i.e., activity of 300 µL of catalase solution. The activity retaining capacity of this concentration is significantly higher than those of the 1 and 10 mg/mL concentrations, but not significantly higher than that of the 50 mg/mL concentration. Addition of the BSA to the initial aqueous

phase at the concentration of 25 mg/mL could retain 97.13±1.45% of the initial activity.

Catalase-loaded PLGA nanoparticles were formulated with the most protective concentrations of the two stabilizers observed in this study; for trehalose, it was 50 mg/mL and for bovine serum albumin, it was 25 mg/mL. Activities of the freeze-dried nanoparticles prepared with the most protective concentrations of the two stabilizers were measured and compared. The results are shown in Figure 25.

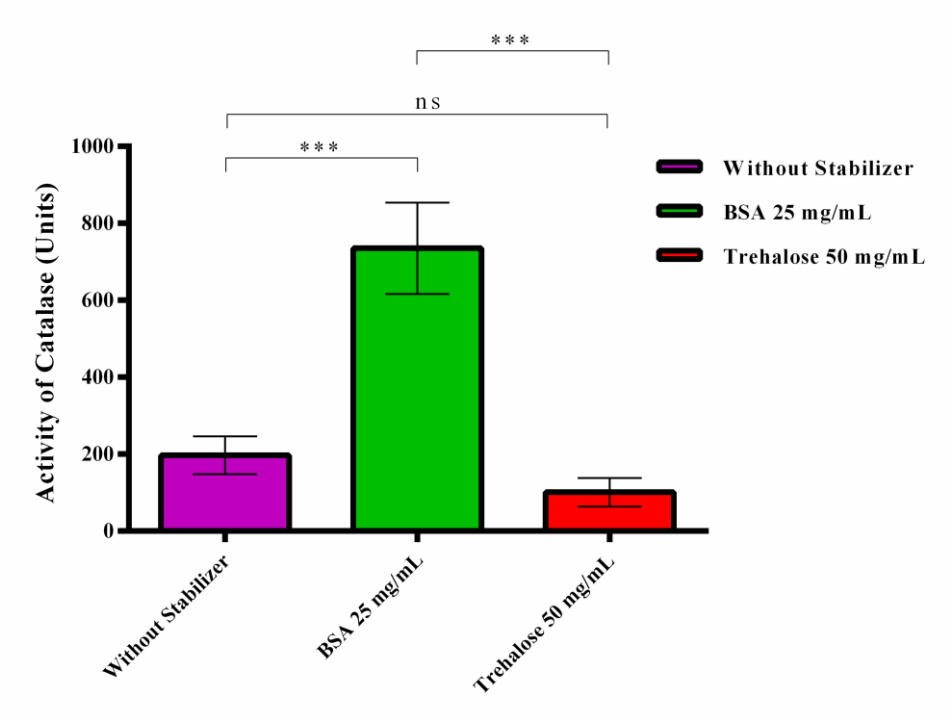

Figure 25: Comparison of the activities of stabilized and unstabilized nanoparticles (n=3; ns, not significant; ***P ≤ 0.001).

Nanoparticles prepared without any stabilizer produced catalase activity of 197±49 units. Activity in the 25 mg/mL of bovine serum albumin-stabilized nanoparticles was found to be 735±119 units which was about 3.7 times higher than that of the unstabilized nanoparticles. Surprisingly, trehalose showed the opposite effect of

bovine serum albumin. The activity of the trehalose-stabilized nanoparticles was even less than the unstabilized nanoparticles which was 101±37 units although the difference was not statistically significant.

2.3.3 Role of trehalose on lyophilization of bovine serum albumin-stabilized catalase-loaded nanoparticles

To evaluate the prospective protective action of trehalose against lyophilization-induced damage of catalase activity of the BSA-stabilized catalase-loaded nanoparticles, trehalose was added at different weight ratios of nanoparticles to trehalose before lyophilization. The activities of catalase-loaded PLGA nanoparticles lyophilized with or without trehalose is presented in Figure 26.

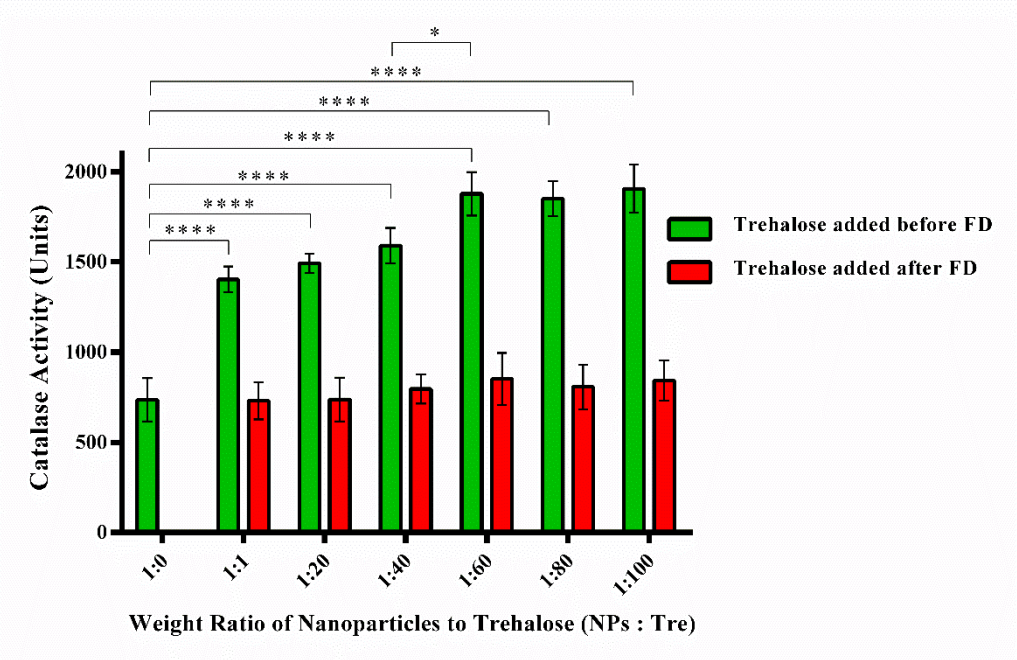

Figure 26: Role of trehalose in preserving catalase activity of BSA-stabilized catalase-loaded nanoparticles upon freeze-drying (n=3; *P ≤ 0.05; ****P ≤ 0.0001).

Trehalose was added at 1:1, 1:20, 1:40, 1:60, 1:80 and 1:100 weight ratios of nanoparticles to trehalose. To take into account any possible effect of trehalose during extraction procedure, equivalent amount of trehalose was added to each vial containing 6.5±0.4 mg of lyophilized nanoparticles just before extraction of catalase from the nanoparticles. The results showed a clear protective effect of trehalose in retaining enzymatic activity of catalase upon freeze-drying of catalase-loaded nanoparticles. All the ratios of trehalose applied in this study protected the activity of catalase significantly in comparison to the sample containing only nanoparticles and no trehalose. There was no significant difference observed among the formulation 1:0 and the formulations where trehalose was added after freeze-drying just before extracting the catalase from the nanoparticles. The activity of trehalose-protected nanoparticles became nearly double even with the ratios of 1:1.

The average catalase activity increased with increasing the ratios of trehalose to NPs although the increment among the ratios of 1:1, 1:20 & 1:40 were not statistically significant. Then the protective efficacy again appeared to rise significantly at the ratios of 1:60 as compared to 1:1, 1:20 and 1:40. There was no significant difference observed in the protective efficacy among the 1:60, 1:80 and 1:100 formulations. Addition of trehalose to protect the enzymatic activity upon freeze-drying of catalase-loaded PLGA nanoparticles could retain nearly 13.5% of the initial activity of the catalase added in the primary emulsification process.

2.3.4 Particle size, zeta potential and morphology of reconstituted BSA-stabilized catalase-loaded nanoparticles

The average sizes of the freeze-dried BSA-stabilized catalase-loaded PLGA nanoparticles observed by DLS were 189.2±4.1nm and 240.6±4.9nm for unprotected and trehalose protected nanoparticles upon lyophilization, respectively. TEM image of cryoprotected sample showed that the nanoparticles were spherical in shape and they were of diameters in the range of 56 – 155 nm which was less than that observed by DLS.

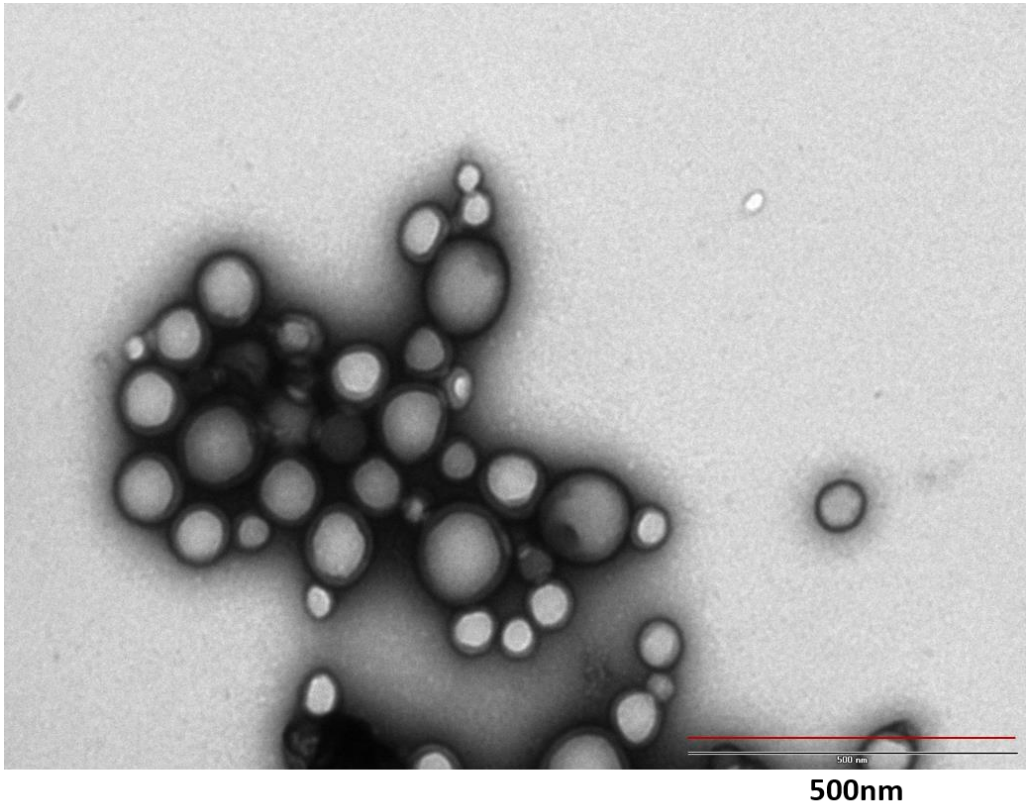

Figure 27: Representative TEM image of cryoprotected BSA-stabilized catalase-loaded PLGA NPs after reconstitution.

The mean zeta potential of the freeze-dried bovine serum albumin-stabilized catalase-loaded PLGA nanoparticles which were not cryoprotected were -32.03±1.04mv. On the contrary, the mean zeta potential for the cryoprotected nanoparticles (1:60) was -11.60±0.83mv.

2.4 Discussion

This study first demonstrated that trehalose could minimize loss of catalase activity induced by freeze-drying of catalase-loaded PLGA nanoparticles and this protective action observed was concentration-dependent. The present study also showed that processing parameters in the encapsulation process by double emulsion method could exert a detrimental effect on catalase activity, but this harmful effect could be reduced by adding a stabilizer to the catalase solution, i.e., the inner aqueous phase before primary emulsification in the double emulsion method.

Before making catalase-loaded PLGA nanoparticles to evaluate the potential protective action of trehalose in minimizing the damage induced by lyophilization, plain PLGA nanoparticles were prepared by the nanoprecipitation method and it was observed that trehalose could protect the plain PLGA nanoparticles from lyophilization-induced aggregation. A very small increment in hydrodynamic diameter of the nanoparticles was observed with increasing concentration of trehalose added as a cryoprotectant, and this increment might be due to a slow diffusion of the particles because of an enhanced viscosity of the dispersant medium brought about by trehalose. The PDI values also remained almost unchanged by freeze-drying when trehalose was added to the nanosuspensions before freeze-drying of the nanoparticles. Comparison of PDI values obtained for pre- and post-lyophilization gave an idea about conserving the nanoparticles size distribution.[228]

The formulation of catalase-loaded PLGA nanoparticles was attempted following a two-step nanoprecipitation method developed by Cruz *et al.*[279] However, this method did not produce any nanoparticles. As they demonstrated their method

using lysozyme, it was also attempted to adopt this nanoprecipitation method to encapsulate lysozyme into the PLGA nanoparticles and eventually the method was failed. There might be some parameters which were not explicit in the article. Then, the formulation of catalase-loaded PLGA nanoparticles was proceeded with the double emulsion method.

Catalase-loaded PLGA nanoparticles formulated without any stabilizer showed very low activity of catalase. This too low activity of catalase-loaded nanoparticles demanded investigation of the formulation procedure.

In the double emulsion method, compared to secondary emulsification step, primary emulsification is the step when most protein denaturation tends to occur.[210] Zhang *et al.* reported that most of the activity of glucose oxidase was lost during the first emulsification step which was 28% and, 20% lost in the second emulsification step.[211] So, investigation was concentrated on the first emulsification step.

The water/organic solvent interface formed in the emulsification process is a major factor that destabilizes the protein causing its denaturation and aggregation. When proteins migrate and adsorb at the water/organic solvent interface their tendency to aggregate develops. They become unfolded by exposing their hydrophobic region to the organic solvent.[210,212]

Proteins also degrade when exposed to ultrasound.[210,213] Zambaux *et al.* showed that the effect of vortexing on protein C activity was less than that of sonication.[193] This study also confirmed that probe sonication was more harmful than vortexing for catalase activity in presence of a water/organic solvent interface. It was observed

that only vortexing could also damage catalase activity when there was an interface formed between water and dichloromethane. Interface formation is usually more detrimental to proteins than sonication.[213] This study's findings also supported this observation. Sonication produces cavitation stress resulting in local temperature rising and free radical formation that ultimately degrades protein.[214,215] Stanwick *et al.* reported that the activity of neurotrophin-3 was reduced by sonication.[215] However, sonication is suitable to formulate small nanoparticles.[290]

Using additives in the encapsulation process to stabilize protein drugs is the most commonly used technique.[216] It was reported that trehalose could improve L-asparaginase activity during encapsulation procedure.[217] Cleland *et al.* showed that trehalose stabilized recombinant human growth hormone when aqueous solution of this hormone was emulsified with dichloromethane.[218] It has been suggested that trehalose protects the protein against organic solvents by preferential hydration, and hence hinders its contact with the organic solvent.[217,218]

Like the trehalose-stabilized emulsification process of this study, no significant difference was noticed between the initial activity and the post-emulsification activity of catalase, when bovine serum albumin was added as a stabilizer to the emulsification process of catalase. The stabilization capability of bovine serum albumin was shown to protect the parathyroid hormone from unfolding and aggregation during formulation of PLGA nanoparticles.[219] It has also been observed that BSA added to the inner aqueous phase could preserve more than 80% of the integrity of insulin-like growth factor-I (IGF-I) from the emulsification and ultrasonication-induced damage of the protein. Albumins used in the initial aqueous phase in the first emulsification step of multiple emulsifications process

significantly protected proteins. Albumins were assumed to protect the proteins from contact with the organic solvents and hydrophobic surfaces by occupying the water/organic solvents interface.[220]

Both trehalose and bovine serum albumin in this study protected the enzymatic activity during the emulsification procedure in a concentration dependent manner. With increasing concentration, the growing tendency of the protective effect of trehalose was observed until a certain point after that its protective efficacy declined with enhancing concentration. In case of bovine serum albumin, the upward tendency of the protective effect was also detected until a certain limit after that it seemed that it plateaued where only one concentration was studied in this study after the peak protective concentration.

Concentration-dependent stabilizing outcome of bovine serum albumin helped to assume that the rate of migration and adsorption of the bovine serum albumin molecules onto the water/organic solvent interface was linked to a concentration gradient. It was suggested that increasing the number of bovine serum albumin molecules in the protein solution, the flux of the molecules escalated to the degree that the interface site was preferentially occupied by them.[291] So, it can be inferred that once the occupation of the water/organic solvent interface by bovine serum molecules becomes complete and reaches at a saturation level, no more protection cannot be achieved by additional protein molecules. First upward trend until the peak followed by downward trend of the protective effect of trehalose was not reported yet. Further investigations are warranted to explain this behaviour of trehalose in protecting catalase in emulsification procedure.

After identifying the most effective concentration of trehalose and bovine serum albumin in protecting catalase during emulsification, catalase-loaded PLGA nanoparticles were prepared with that concentration of the two stabilizers of this study; for trehalose, it was 50 mg/mL and for bovine serum albumin, it was 25 mg/mL. Addition of BSA to the inner aqueous phase helped in protecting the catalase in the formulation process and showed an increased catalase activity which was about 3.7 times higher than that of unstabilized catalase-loaded nanoparticles. Surprisingly, trehalose could not provide any such protective effect in formulation of catalase-loaded nanoparticles. Instead it produced nanoparticles which showed even lower catalase activity than the unstabilized ones though the difference was not statistically significant. The same observation was reported in another study by Sturesson *et al.*, where presence of sucrose and trehalose reduced the bioactivity of urease.[292] In contrast to the findings of this study, trehalose present in the inner aqueous phase, produced nanospheres retaining the biological activity of L-asparaginase.[217]

Trehalose could stabilize proteins in the emulsification process and this was also observed in the present study.[217,218] Besides stabilizing proteins, trehalose is a cryoprotectant of proteins.[199,229,292] In addition to stabilizing therapeutic proteins in the emulsification procedure, bovine serum albumin also provided cryoprotection of the protein-loaded nanoparticles.[217,219,220] So, it can be speculated that a certain degree of cryoprotection was achieved in both cases of freeze drying of trehalose- and bovine serum albumin-stabilized catalase-loaded PLGA nanoparticles when they were added to the inner aqueous phases. Also, it can be assumed that these two stabilizers might help to protect the enzymatic activity against the

water/dichloromethane interface formed during the extraction procedure of this enzyme from the nanoparticles during analysis of catalase activity. On the contrary, no stabilization in either the emulsification or extraction procedures and no cryoprotection in the lyophilization of nanoparticles were obtained in this case of unstabilized catalase-loaded PLGA nanoparticles to protect the enzyme activity. But, this study found that the enzymatic activity of trehalose-stabilized nanoparticles is even less than that of unstabilized nanoparticles though the difference was not statistically significant. The findings of other studies and this work indicate that the protection brought about by trehalose during formulation of PLGA nanoparticles varies with the individual protein to be encapsulated. Further investigations are required to find out the reason of the inability of trehalose to protect the enzymatic activity of catalase-loaded PLGA nanoparticles as a stabilizer added to the inner aqueous phase.

Freeze-drying creates stresses of freezing and dehydration that can destabilize a colloidal suspension of nanoparticles. There occurs a phase separation while freezing a sample. Cryo-concentrated solution and ice are phase separated. In nanoparticulate suspensions, the cryo-concentrated part contains nanoparticles and the other ingredients of the system.[293] This elevated concentration may cause aggregation. Even in some cases, this elevated concentration may induce fusion of nanoparticles that are irreversible. Moreover, nanoparticles could be destabilized due to a mechanical stress on the nanoparticles exerted by crystallization of ice. Before freezing, special excipients are usually incorporated to the nanoparticulate suspensions as protectants to defend these delicate systems of nanosuspensions.[294] These special excipients are cryoprotectants and lyoprotectants. Cryoprotectant

protects the sample from freezing-induced stress and lyoprotectant from drying-induced stress. Sugars like trehalose, sucrose, glucose and mannitol are commonly used in freeze-drying of nanoparticles to protect them from lyophilization-induced damage.[228,295,296] Sugars function as both cryoprotectant and lyoprotectant. Trehalose is a very good protectant of labile proteins upon their freeze-drying of biomolecules. It has been shown that it is very effective in stabilizing labile proteins during lyophilisation.[228,229]

Upon freeze-drying of catalase-loaded PLGA nanoparticles, trehalose added to the nanosuspension before freeze-drying, could conserve nearly 13.5% of the initial activity of catalase that was employed in the primary emulsification step. Wolf *et al.* reported that trehalose could reduce the activity loss of L-asparaginase upon lyophilization of L-asparaginase-loaded PLGA nanoparticles.[217] The cryoprotection provided by trehalose in this study was concentration-dependent. The best cryoprotection was achieved with the weight ratio of nanoparticles to trehalose of 1:60 after which increasing trehalose did not improve catalase activity. Carpenter *et al.* reported that trehalose protected the activity of phosphofructokinase from freeze-drying induced-damage in a concentration-dependent manner. But, after a certain limit, further increasing of trehalose concentration gradually decreased the phosphofructokinase activity. The authors suggested that trehalose might crystallize and lose hydrogen bonding at its very high concentrations.[297]

A mechanism reported by Abdelwahed *et al.* can be attributed to trehalose in protecting both the plain PLGA nanoparticles and the catalase-loaded nanoparticles from the freezing stress of lyophilization. During freezing of the freeze-drying

process, cryo-concentrated part from separated phases of ice and cryo-concentrated liquid may be vitrified. Nanoparticles can be contained and immobilized within this vitrified glassy matrix of cryoprotectants. This immobilization of nanoparticles can inhibit aggregation and guard the nanoparticles against ice crystals-exerted mechanical stress.[293]

Nanoparticle stabilization by trehalose during the step of freezing in the freeze-drying process can also be explained by the particle isolation hypothesis. This hypothesis suggests that sugars used in the lyophilization process separate the nanoparticles in the unfrozen portion, and this spatial separation of the nanoparticles resists aggregation of particles during freezing of the sample.[298] Prevention of aggregation of nanoparticles could help to maintain the native structure of encapsulated catalase.

The water replacement hypothesis may explain the mechanism of stabilizing nanoparticles by trehalose during drying step of lyophilization. The mechanism assumes that at the end of the drying stage, hydrogen bonds are formed between trehalose and polar groups OH of polyvinyl alcohol adsorbed onto nanoparticle surface and free carboxylic end groups of the PLGA located on nanoparticle surface. These hydrogen bonds can keep the nanoparticles in pseudo-hydrated state. Acing as water substitute, trehalose protects the native structures of the nanoparticles and thus may help in retaining the native structure of catalase inside the PLGA matrix.[293]

The bigger size of the cryoprotected sample might be due to the effect of trehalose added to protect from the damage induced by freeze-drying. Singhal *et al.* reported

the average size of catalase-loaded PLGA nanoparticles obtained by DLS was 280nm.[277] This nanoparticle was not cryoprotected and bigger than the nanoparticles prepared in this work. This can be attributed to the addition of more bovine serum albumin in the primary emulsification step compared to that added to this work's primary emulsification step.

Zeta potential is a useful way to estimate the condition of the surface of nanoparticles, and to identify any change after lyophilization. It can also be utilized to study any interaction of the surface of nanoparticles with the protectant molecule added for minimizing lyophilization-induced damage. The negative charge of the reconstituted catalase-loaded PLGA nanoparticles which were not freeze-dried with trehalose was -32.03±1.04mv. This indicated the existence of the PLGA polymer's free carboxylic end groups on surface of the nanoparticles. When they were freeze-dried with trehalose at a weight ratio of nanoparticles to trehalose of 1:60, the mean zeta potential changed to -11.60±0.83mv. This reduced negativity of the zeta potential upon lyophilization with trehalose suggested that the number of free carboxylic end groups had been reduced because of forming hydrogen bond between trehalose and some of the free carboxylic end groups. Swed *et al.* observed the mean zeta potential of -29.0±2.6 mv for their lysozyme-loaded PLGA nanoparticles which were not cryoprotected and this is close to the zeta potential of the catalase-loaded PLGA nanoparticles prepared in this study.[276]

2.5 Conclusion

The most common technique of encapsulating a protein into PLGA, a biodegradable polymer, is the double emulsion method (w/o/w). However, protein becomes easily denatured and degraded when it comes in contact with the interface of water and organic solvent formed during emulsification procedure of the double emulsion method. Catalase-loaded PLGA nanoparticles were produced following a modified double emulsion method. The enzymatic activity of the nanoparticles was found to be 1.47% of the protein initially added to the initial aqueous phase. Trehalose and bovine serum albumin were reported that they could protect proteins from emulsification-induced damage. In accordance, it has been observed in this study that trehalose and BSA added to the initial aqueous phase could protect catalase from the emulsification-induced degradation of catalase. Astonishingly, trehalose-stabilized emulsification produced nanoparticles whose activity was even worse than that fabricated by the unstabilized emulsification process. In contrast, activity of the nanoparticles produced by bovine serum albumin-stabilized emulsification process was about 3.7 times higher than that of the unstabilized emulsification.

In order to stabilize the PLGA nanoparticles from hydrolytic degradation and to reduce the instability of loaded protein, lyophilization is commonly used to remove water. But, freeze-drying itself affects stability of both the polymeric nanoparticles and the encapsulated protein. This study showed that trehalose could minimize aggregation of plain PLGA nanoparticles induced by freeze-drying. Trehalose is a very good protectant not only for nanoparticles but also for protein as well to shield them from lyophilization-induced stress. This study found that trehalose could

minimize the activity loss of catalase-loaded PLGA nanoparticles upon freeze-drying and this protective action was concentration-dependent. In the presence of trehalose, freeze-drying of catalase-loaded PLGA nanoparticles has been demonstrated to be a suitable method for conservation of enzymatic activity of the encapsulated catalase.

3 Evaluation of Potential Therapeutic Use of Cryoprotected BSA-Stabilized Catalase-Loaded PLGA Nanoparticles in Myocardial Ischemia/Reperfusion Injury

3.1 Introduction

Acute myocardial infarction (MI) is an emergency condition and needs immediate hospitalization. This is the most critical consequence of ischemic heart diseases.[3] In patients of acute myocardial infarction, the size of the myocardial infarct is the main determining factor for prognosis of the disease, and acute MI is the major cause of chronic heart failure.[42,101] Reduction of the myocardial infarct size can be partially attained by promptly initiating reperfusion therapy with thrombolytics and/or percutaneous coronary intervention (PCI) in those patients. But, reperfusion, i.e., restoration of blood supply to the ischemic area of the myocardium, itself induces ischemia/reperfusion injury (I/R injury), which elicits a localized oxidative burst and regional inflammatory responses causing injury and even death of the cardiac myocytes that ultimately results in significant myocardial damage. This I/R injury may cause arrhythmias, myocardial stunning, microvascular injury and inflammatory response.[105-112]

Endogenous antioxidant defence systems normally regulate reactive oxygen species (ROS). Oxidative stress occurs when the rate of ROS formation exceeds the rate of ROS removal by the endogenous antioxidant defence systems.[76] This resultant oxidative stress due to the imbalance between the production and removal of ROS,

is related with the cell death in cardiac pathologies of ischemia/reperfusion injury and heart failure.[90,91] Oxidative stress is an important factor for expansion of the myocardial damage during reperfusion following myocardial ischemia, and determines the ultimate size of the myocardial infarct. This stress induces death of cardiomyocytes through apoptosis and necrosis.[92-96]

In the brain, oxygen delivery is about three times of its oxygen consumption. In the heart muscle, oxygen delivery is 1.5 to 1.6 times of its oxygen consumption which reflects the scenario of skeletal muscle in moderate exercise. This indicates that the myocardium consumes an excess amount of oxygen.[82] Accepting electron, molecular oxygen will form the superoxide anion ($O_2^{\bullet -}$) and this formation of superoxide anion can be mediated either by enzymatic process where it is performed by NADPH oxidase and xanthine oxidases or by non-enzymatic reactions where it occurs with the redox active compounds such as semiubiquinone of mitochondrial electron transport chain.[299,300] The cardiomyocytes respond to low-level of the superoxide anion generation and convert it to H_2O_2 by the enzymatic action of superoxide dismutase in cytoplasm or mitochondria. This H_2O_2 formed from the superoxide anion is detoxified to water either by catalase or by the glutathione peroxidase (GPx) system.[83] H_2O_2 more likely interacts with iron cations (Fe^{2+}) via the Fenton reaction to form a highly toxic and the most damaging radical species, the hydroxyl radical ($^{\bullet}OH$), instead of being detoxified by catalase or glutathione peroxidase. This hydroxyl radical is excessively formed during ischemia-reperfusion. It rapidly reacts with nucleic acids, lipids and proteins.[84]

Using reduced glutathione (GSH), GPx catalyses H_2O_2 and eliminates it. Reduced glutathione (GSH), an antioxidant utilized by GPx to remove H_2O_2, are abundant

in organisms that counteract ROS by enzymatic or non-enzymatic way. On the contrary, the heart's low activities of catalase and GPx, and lesser content of the reduced glutathione (GSH) than other tissues indicate that the heart is more susceptible to oxidative stress-induced cellular damage.[86] It has been shown that catalase activity of the heart cells is as little as 2% of the activity that exists in liver cells.[87,88]

Although both the superoxide and H_2O_2 are elevated following myocardial infarction, the levels of their endogenous scavengers, superoxide dismutase and catalase, even more decrease.[97,98] Catalase is not only the system that controls the level of H_2O_2 in the myocardium, but it is also the major mechanism of the peroxidase activities in the heart cells in spite of its low content.[89]

Offsetting the oxidative stress with antioxidants reduced injury and showed recovery from ischemia/reperfusion injury in different studies.[149] Earlier studies showed that catalase overexpressed in transgenic mice could provide protection against hypoxia-reoxygenation cardiotoxicity, functional alterations induced by ischemia/reperfusion, and even against doxorubicin-induced toxicity of cardiomyocytes.[154-157] This proof of principle of the protective action of catalase in transgenic mice indicates the potential therapeutic value of catalase in ischemia/reperfusion injury. But, this is not a mode of therapy that can be realistic for therapeutic application. To achieve a therapeutic outcome in the ischemia/reperfusion injury, it would be the most appropriate approach to develop a delivery system for catalase that can deliver the antioxidant protein to the affected cardiomyocytes immediately prior to the oxidative stress elicited by the ischemia/reperfusion injury. A recent study showed that pitavastatin-loaded PLGA

nanoparticles reduced myocardial infarct size and improved LV dysfunction and cardiac remodelling after I/R injury. On the contrary, free pitavastatin administered intravenously failed to show any therapeutic effect in such condition, and this supports the possibility of nanoparticle-mediated therapy in I/R injury.[169]

In the previous study of chapter 2, catalase-loaded PLGA nanoparticles were fabricated using bovine serum albumin (BSA) as a stabilizer in the encapsulation process and cryoprotected by employing trehalose as a cryoprotectant, and finally the nanoparticles were characterized. No studies have been addressed yet with regard to investigation of the protective effect of catalase-loaded PLGA nanoparticles in preserving any type of cardiomyocytes from injury induced by oxidative stress. HL-1 cardiomyocytes have been shown to be a useful model for studying various features of cardiac physiology and pathophysiology due to their demonstration of the same characteristics of differentiated cardiomyocytes while maintaining proliferation in the culture.[301] The goal of this study was to explore the ability of the cryoprotected BSA-stabilized catalase-loaded PLGA nanoparticles to protect the HL-1 cardiomyocytes from H_2O_2-mediated oxidative stress.

3.2 Materials and methods

3.2.1 Materials

Penicillin-Streptomycin (10,000 units/mL of penicillin and 10,000 µg/mL of streptomycin) from Invitrogen, Thermo Fisher Scientific, UK. Hydrogen peroxide solution 30% (w/w) in water, Accutase solution, L-Glutamine solution (200mM), Fibronectin solution (0.1%), Gelatin from bovine skin, Foetal bovine serum, Trypsin-EDTA solution (0.05% trypsin, 0.02% EDTA), (±)-Norepinephrine (+)-bitartrate salt, Ascorbic acid, Claycomb medium from Sigma-Aldrich (Poole, UK). Caspase-3/7 Green Flow Cytometry Assay Kit (Invitrogen, Thermo Fisher Scientific, UK), Alexa Fluor 488 Annexin V/Dead Cell Apoptosis Kit (Invitrogen, Thermo Fisher Scientific, UK), PrestoBlue cell viability reagent (Invitrogen, Thermo Fisher Scientific, UK), Bovine serum albumin conjugated Alexa Fluor 488 (Invitrogen, Thermo Fisher Scientific, UK), Hoechst 33342 (Invitrogen, Thermo Fisher Scientific, UK), FM4-64FX (Invitrogen, Thermo Fisher Scientific, UK).

3.2.2 Cell culture

HL-1 mouse cardiomyocytes were grown in Claycomb medium supplemented with 10% foetal bovine serum, 100 units/mL of penicillin, 100 µg/mL of streptomycin, 2mM L-glutamine and 0.1mM norepinephrine dissolved in 0.3mM ascorbic acid. All the culture flasks and well plates were pre-coated with fibronectin prepared in 0.02% gelatin solution.[301,302] Cells were maintained at 37°C and 5% CO_2.

3.2.3 Reconstitution of freeze-dried nanoparticles

Freeze-dried catalase-loaded nanoparticles were reconstituted in supplemented calycomb medium without addition of the norepinephrine solution. The dispersion was sonicated using a microtip probe sonicator (SONOPULS HD 2070, BANDELIN electronic, Berlin, Germany) on an ice bath for 30 seconds.

3.2.4 Induction and treatment of oxidative stress

3.2.4.1 Induction of oxidative stress

Oxidative stress was induced by exposing the HL-1 cardiomyocytes to H_2O_2.[303,304] The cells were exposed to H_2O_2 for 24 and 3 hours. Unexposed cardiomyocytes served as controls. Briefly, the cells were seeded onto 24-well plates at a density of 50,000 cells/well. After 24 hours of seeding, the medium was aspirated and the cells were washed with PBS devoid of calcium and magnesium. Then, the cells were incubated for 24 and 3 hours with different concentrations of H_2O_2 prepared in claycomb medium in the absence of norepinephrine. Cell viability was checked after 24 and 3 hours of H_2O_2 incubation.

3.2.4.2 Treatment of oxidative stress with nanoparticles

The Hl-1 cells were undergone of both pre- and post-injury treatment by the cryoprotected BSA-stabilized catalase-loaded PLGA nanoparticles for oxidative stress induced by the selected sub-lethal concentration of H_2O_2. The

cardiomyocytes were seeded onto 24-well plates at a density of 50,000 cells/well. After 24 hours of seeding, the medium was aspirated and the cells were washed with PBS devoid of calcium and magnesium. The cells were then incubated with either the H_2O_2 or the reconstituted nanoparticle suspensions.

In case of pre-injury treatment of the cells with the catalase-loaded nanoparticles, cells were first exposed to different doses of the suspensions of nanoparticles for 3 hours. Cardiomyocytes which were incubated with only claycomb media for 3 hours instead of nanoparticulate suspensions served as control. After exposing the cells to the nanosuspensions or media for 3 hours, the suspensions and media were aspirated and the cells were washed with PBS devoid of calcium and magnesium. Then, the cells were incubated for 24 hours with the selected sub-lethal concentration of H_2O_2. The viability of the cardiomyocytes was checked after H_2O_2 incubation for 24 hours by Prestoblue assay. Following this pre-injury treatment protocol, the efficacies of the three formulations of catalase-loaded nanoparticles which were freeze-dried with trehalose at 1:60, 1:80 and 1:100 weight ratios of nanoparticles to trehalose were evaluated by applying the most optimum dose of the nanoparticles as observed in the previous pre-injury experiment before injuring the cells with the selected sub-lethal concentration of H_2O_2.

In case of post-injury treatment with the catalase-loaded nanoparticles, the cardiomyocytes were first exposed to the selected sub-lethal concentration of H_2O_2 for 3 hours. After exposing the cells to the H_2O_2 for 3 hours, the H_2O_2 was aspirated and the cells were washed with PBS devoid of calcium and magnesium. The cells were then incubated for 24 hours with different doses of the nanoparticulate suspensions. Cardiomyocytes which were incubated with only claycomb media for

24 hours instead of the nanoparticulate suspensions followed by H_2O_2 treatment served as control. The viability of the cardiomyocytes was checked after incubation with the nanoparticles for 24 hours by Prestoblue assay.

3.2.4.3 Cell viability

The effect of only H_2O_2, H_2O_2 & cryoprotected BSA-stabilized catalase-loaded nanoparticles and only cryoprotected BSA-stabilized catalase-loaded nanoparticles, were evaluated by Prestoblue cell viability assay. Briefly, the cardiomyocytes were washed with PBS devoid of calcium and magnesium after H_2O_2 or medium or nanoparticles had been aspirated. The cells were then incubated in 1:10 diluted Prestoblue reagent in HBSS supplemented with calcium and magnesium for one hour.[305] After one hour incubation with Prestoblue reagent, the fluorescence was read by an Infinite M200 microplate reader (Tecan AG, Switzerland) using 96-well plates following excitation at 560 nm and emission at 590 nm.

3.2.5 Induction and treatment of apoptosis

3.2.5.1 Caspase-3/7 assay

Hydrogen peroxide-induced apoptosis and treatment of this apoptosis with the cryoprotected BSA-stabilized catalase-loaded nanoparticles (cryoprotected by trehalose at a weight ratio of NPs to trehalose of 1:60) were assessed by flow cytometric determination of caspase activity using the cellevent caspase-3/7 green

flow cytometry kit to distinguish viable and apoptotic HL-1 cells. When caspase-3 or caspase-7 in apoptotic cells is activated, this cell-permeant and intrinsically non-fluorescent substrate cleaves and binds to DNA to produce a bright, green fluorescence signal.

Briefly, the cells were seeded onto 6-well pre-coated culture plates at a density of 200,000 cells/well. After 24 hours of seeding, the medium was aspirated and catalase-loaded nanoparticulate suspensions prepared in the same way as mentioned in section 3.2.3 were added at a selected dose (800 µg/well) to the NPs-treatment group wells. For the control groups, the medium was replaced with the claycomb medium devoid of norepinephrine after 24 hours of seeding the cells. The cells were then incubated for 3 hours. After 3 hours of incubation, all the wells were washed with serum-free DMEM, and 2 mL of 200µM of H_2O_2 prepared in serum-free DMEM was added to each well of both the treatment and positive control groups, and 2 mL of serum-free DMEM was added to each well of the negative control group. Then, the cells were incubated for 1 hour. After incubation of 1 hour, all the wells were washed with the claycomb medium devoid of norepinephrine, and 2 mL of the claycomb medium devoid of norepinephrine was added to each well. The cells were then incubated for 6 hours. After 6 hours of incubation, the cells were collected with accutase solution, labelled with the CellEvent Caspase-3/7 Green Detection Reagent according to the manufacturer's protocol and analysis of 10,000 cells per sample was performed by a flow cytometer (Beckman Coulter FC500, Beckman Coulter Inc. CA, USA). The percentages of viable and apoptotic cells were determined using the Kaluza 1.5a software (Beckman Coulter Inc. CA, USA).

3.2.5.2 Annexin V and propidium iodide assay

Hydrogen peroxide-induced apoptosis and treatment of this apoptosis with the cryoprotected BSA-stabilized catalase-loaded nanoparticles (cryoprotected by trehalose at a weight ratio of NPs to trehalose of 1:60) were also evaluated by performing a dual-colour analysis of alexa fluor 488 annexin V binding and propidium iodide uptake by flow cytometry analysis using the alexa fluor 488 annexin V/dead cell apoptosis kit according to the manufacturer's instructions. Annexin V is a protein and it specifically binds to phosphatidylserine residues, which are exposed on the outer surface of apoptotic cells.[306,307] Because of the loss of membrane integrity, necrotic cells also expose phosphatidylserine to which annexin V binds. So, only staining with annexin V can't differentiate between apoptotic and necrotic cells. Propidium iodide is used for this differentiation between apoptotic and necrotic cells. Propidium iodide is impermeant to both live and apoptotic cells, but binds tightly to the nucleic acids of the leaky necrotic cells and stains them.[308] After staining with annexin V and propidium iodide, the apoptotic cells show green fluorescence, the dead cells show red and green fluorescence, and the live cells show little or no fluorescence.

Briefly, the cells were seeded, washed, treated with catalase-loaded nanoparticles and 200μM of H_2O_2, and incubated for 1 hour in the same way as mentioned in section 3.2.5.1. After incubation of 1 hour, all the wells were washed with the claycomb medium devoid of norepinephrine, followed by addition of 2 mL of the claycomb medium devoid of norepinephrine to each well. One group of the cells was then incubated for 6 and the other group was for 24 hours. After incubation of 6 and 24 hours, the cells were collected using accutase solution, labelled with

annexin V and propidium iodide following the manufacturer's protocol, and analysis of 10,000 cells per sample was performed by a flow cytometer (Beckman Coulter FC500, Beckman Coulter Inc. CA, USA). The percentages of viable, apoptotic and necrotic cells were determined with the Kaluza 1.5a software (Beckman Coulter Inc. CA, USA).

3.2.6 Cytotoxicity of nanoparticles

The cardiomyocytes were seeded onto 24-well plates at a density of 50,000 cells/well. After 24 hours of seeding, the medium was aspirated and the cells were washed with PBS devoid of calcium and magnesium. Then, the cells were incubated for 24 hours with different doses of the cryoprotected BSA-stabilized catalase-loaded nanoparticles (cryoprotected by trehalose at a weight ratio of NPs to trehalose of 1:60) prepared in claycomb medium without the norepinephrine. For the untreated group that served as control, cardiomyocytes were incubated with only claycomb medium for the next 24 hours. To determine cytotoxicity of the nanoparticles on cardiomyocytes, cell viability was measured by Prestoblue assay after incubation with the nanoparticulate suspensions or claycomb medium for 24 hours.

3.2.7 Co-exposure of cardiomyocytes with 1000µM of H_2O_2 and 200 µg/well of nanoparticles

The cardiomyocytes were simultaneously injured and treated with H_2O_2 and the cryoprotected BSA-stabilized catalase-loaded nanoparticles (cryoprotected by trehalose at a weight ratio of NPs to trehalose of 1:60), respectively. For this co-exposure of H_2O_2 and nanoparticles, the cells were seeded onto 24-well plates at a density of 50,000 cells/well. After 24 hours of seeding, the medium was aspirated and the cells were washed with PBS devoid of calcium and magnesium. Cardiomyocytes which were incubated with only claycomb medium for next 24 hours served as control, i.e., untreated. Another group of cardiomyocytes were incubated with only 1000µM of H_2O_2 for 24 hours and the co-exposure group of the cardiomyocytes incubated with both of the 1000µM of H_2O_2 and 200 µg/well of nanoparticles where the both were added to each well simultaneously and mixed by gentle pipetting. After 24 hours of incubation, the claycomb medium, H_2O_2 and nanoparticles were aspirated and the cells were washed with PBS devoid of calcium and magnesium. Then, the cell viability was determined by Prestoblue assay.

3.2.8 Cellular uptake of nanoparticles

3.2.8.1 Alexa Fluor 488-stained BSA-stabilized catalase-loaded PLGA nanoparticles

3.2.8.1.1 Encapsulation of catalase with BSA conjugated Alexa Fluor 488

In order to fabricate the Alexa Fluor 488-stained BSA-stabilized catalase-loaded PLGA nanoparticles, the polymer solution was prepared by dissolving 81 mg of PLGA polymer in 3 mL of dichloromethane. To prepare polyvinyl alcohol solution, 5 gm of PVA was added to 100 mL of water with magnetic stirring on a hot plate and 70–80ºC heat was applied to dissolve it completely in the water. After preparation of the solution of polyvinyl alcohol, it was kept in the room temperature to cool down to room temperature. The solution of PVA was then passed through a syringe filter of 0.2 µm size (Minisart single use filter unit, Sartorius Stedim Biotech, Germany). BSA conjugated Alexa Fluor 488 solution was made in water at a concentration of 2 mg/mL. Bovine serum albumin solution was made at the concentration of 25 mg/mL with this BSA conjugated Alexa Fluor 488 solution. A solution of bovine liver catalase (8 mg) in 300 µL of this mixed solution of BSA and BSA conjugated Alexa Fluor 488 was prepared. The protein solution was then added to the polymer solution and vortexed for 30 seconds. After vortexing for 30 seconds, the mixture was sonicated for 1 minute on an ice bath with a probe sonicator (SONOPULS HD 2070, BANDELIN electronic, Germany) and a primary emulsion was formed. This primary emulsion was added to 18 mL solution of PVA, vortexed for 30 seconds followed by sonication in the same way as mentioned above to form the secondary emulsion. The resultant emulsion was kept stirring in

a fume hood overnight for evaporation of the entire dichloromethane. The nanoparticles were recovered by centrifuging the dispersion at 39,800 x g for 30 minutes at 4ºC (Rotor JA-17, Beckman J2-21 centrifuge, Beckman Coulter Inc., CA, USA). After centrifugation, the supernatant was removed and the pellet was resuspended in water followed by vortexing and sonication in the same way as mentioned above. The suspension was then centrifuged again at 39,800 x g for 30 minutes at 4ºC (Rotor JA-17, Beckman J2-21 centrifuge, Beckman Coulter Inc., CA, USA). This washing step was repeated two times. Finally, the pellet was redispersed in water, vortexed and sonicated on an ice bath in the same way as mentioned above. The final nanosuspension was then freeze-dried. For samples protected from lyophilization-induced damage, trehalose was added to the final nanosuspension at a ratio of the nanoparticles to trehalose of 1:60, mixed by vortexing and then freeze-dried.

3.2.8.1.2 Analysis of catalase activity of Alexa Fluor 488-stained BSA-stabilized catalase-loaded PLGA nanoparticles

To analyse enzymatic activity of the encapsulated catalase of Alexa Fluor 488-stained BSA-stabilized catalase-loaded PLGA nanoparticles, the enzyme was extracted from the matrix of PLGA. 4 mL of PBS of and 4 mL of dichloromethane were added to a glass vial containing 6.5±0.4 mg of the lyophilized nanoparticles and stirred for 30 minutes on a magnetic stir plate. After stirring for 30 minutes, the vial was left undisturbed for 3 hours. After 3 hours, the supernatant was collected from the top one of the two layers, transferred to an eppendorf, centrifuged at 4ºC

for 10 minutes using an eppendorf centrifuge (Eppendorf Centrifuge 5417R, Eppendorf UK Limited, UK) at a speed of 10,000 rpm. Thereafter, the supernatant was taken out followed by filtration through a syringe filter of 0.2 µm size (Minisart single use filter unit, Sartorius Stedim Biotech, Germany). The filtrate was analysed for catalase activity.

Enzymatic activity of the enzyme, catalase, was determined by a modified standard catalase assay method[281-285] with the following formulae:

$$\text{Units/mL} = \frac{[\Delta A/\text{min(Sample)} - \Delta A/\text{min(Blank)}] \times \text{Reaction volume in mL} \times \text{df}}{\varepsilon^{mM} \times \text{Sample volume in mL}}$$

Where,

df = dilution factor and

ε^{mM} = Millimolar extinction coefficient of hydrogen peroxide at 240 nm

Briefly, 100 µL of catalase solution extracted from the NPs was mixed with 900 µL of PBS in a quartz cuvette. Then, 1 mL of 20mM of H_2O_2 solution prepared in PBS was added to the cuvette, mixed rapidly by inversion and immediately placed in the chamber of a Beckman DU 800 UV/Vis Spectrophotometer (Beckman Coulter Inc., USA). The decrease of absorbance of 20mM H_2O_2 at 240 nm was monitored for 120 seconds with 5 seconds interval using the kinetic program of the spectrophotometer.

3.2.8.2 Flow cytometry analysis

HL-1 cells were seeded onto 12-well pre-coated culture plates at a density of 100,000 cells/well. After 24 hours of seeding the cells, the medium was aspirated and 1.0 mL of the reconstituted nanosuspension containing 200 µg of the Alexa Fluor 488-stained BSA-stabilized catalase-loaded PLGA nanoparticles that were cryoprotected by trehalose at a weight ratio of NPs to trehalose of 1:60, was added to each well. The suspension was prepared by reconstituting the freeze-dried nanoparticles in the same way as mentioned in the section 3.2.3. For the control group, the medium was replaced with the claycomb medium devoid of norepinephrine after 24 hours of seeding the cells. The cells were then incubated for 3 hours. Next, all the wells were washed with PBS devoid of calcium and magnesium and the cells were collected with the help of accutase solution. Then, the cell suspensions were centrifuged, supernatants discarded and re-suspended in PBS devoid of calcium and magnesium. This procedure of centrifugation, discarding supernatants and re-suspending in PBS devoid of calcium and magnesium was repeated further for two times. Then, the cell suspensions were centrifuged and supernatants were discarded again, and the cell pellets were re-suspended in a solution of 2% (w/v) bovine serum albumin prepared in PBS devoid of calcium and magnesium. These cell suspensions were centrifuged again, supernatants discarded and lastly fixed by 3.7% of paraformaldehyde in PBS devoid of calcium and magnesium. The fixed samples were analysed by a flow cytometer (Beckman Coulter FC500, Beckman Coulter Inc. CA, USA) collecting data from

10,000 cells per sample. Analysis of uptake of the nanoparticles by HL-1 cells were calculated using the Kaluza 1.5a software (Beckman Coulter Inc. CA, USA).

3.2.8.3 Super resolution microscopy

The cellular uptake of catalase-loaded PLGA nanoparticles by HL-1 cells was further confirmed by super resolution microscopy (3D SIM) with an Elyra PS1, super resolution microscope (Carl Zeiss, Oberkochen, Germany) using 63x Glycerol Immersion Lens (LCI Plan-Neofluar 63x/1.3 Imm Korr DIC M27) (Carl Zeiss).

HL-1 cells were grown on gelatin and fibronectin-coated ZEISS High precision Cover Glasses (Carl Zeiss) (18 mm x 18 mm) with a thickness of 170 ± 5 μm for 24 hours using 6-well culture plates at a density of 200,000 cells/well. After 24 hours of seeding the cells, the medium was aspirated and 2.0 mL of the reconstituted 400 μg/mL of the Alexa Fluor 488-stained BSA-stabilized catalase-loaded PLGA nanoparticles that were cryoprotected by trehalose at a weight ratio of NPs to trehalose of 1:60, was added to each well. The suspension was prepared by reconstituting the freeze-dried nanoparticles in the same way as mentioned in the section 3.2.3. Then, the cells were incubated for 3 hours. After incubation of 3 hours with the Alexa Fluor 488-labelled nanoparticles, the cover glasses were washed with PBS containing calcium and magnesium to remove the nanoparticles not uptaken by the cells. The cells were then incubated with the fluorescent nuclear dye Hoechst 33342 (working solution concentration 1.0 μL/mL) for 10 minutes at 37 °C. After removing the Hoechst 33342 staining solution, the HL-1 cells were

washed again with PBS containing calcium and magnesium, and stained with the membrane dye FM4-64FX. The working solution of the dye FM4-64FX was prepared in ice-cold HBSS at a concentration of 5 µg/mL. This working solution of the dye was applied on the cells on ice for 1 minute. Immediately after staining for 1 minute, this staining of the cells was fixed with ice-cold 3.7% paraformaldehyde solution placed on ice for 10 minutes. The cover glasses were rinsed with HBSS for three times and mounted using Vectashield H-1000 (Vector Laboratories, CA, USA), sealed and imaged. The images were obtained with z-stacks and computationally reconstructed for 3D-SIM images using Zeiss Zen2 software (Carl Zeiss).

3.2.9 Statistical analysis

All experiments were performed at least three times. Results are expressed as mean ± SD. Statistical analysis was performed by Student's *t*-test and one-way ANOVA followed by Tukey's multiple comparison tests using GraphPad Prism 6 software (GraphPad, San Diego, CA, USA). The results were considered significant at a p value of less than 0.05.

3.3 Results

3.3.1 Cytotoxicity upon exposure to hydrogen peroxide

The potential sub-lethal dose of hydrogen peroxide at which cytotoxicity was observed was determined first and cytotoxicity was initially quantified by metabolic activity assay after exposing the cells to hydrogen peroxide for 3 and 24 hours.

When the cells were exposed to increasing concentration of hydrogen peroxide for 3 hours, no significant differences were observed among the control, 100µM, 250µM and 500µM of hydrogen peroxide. The results are shown in Figure 28.

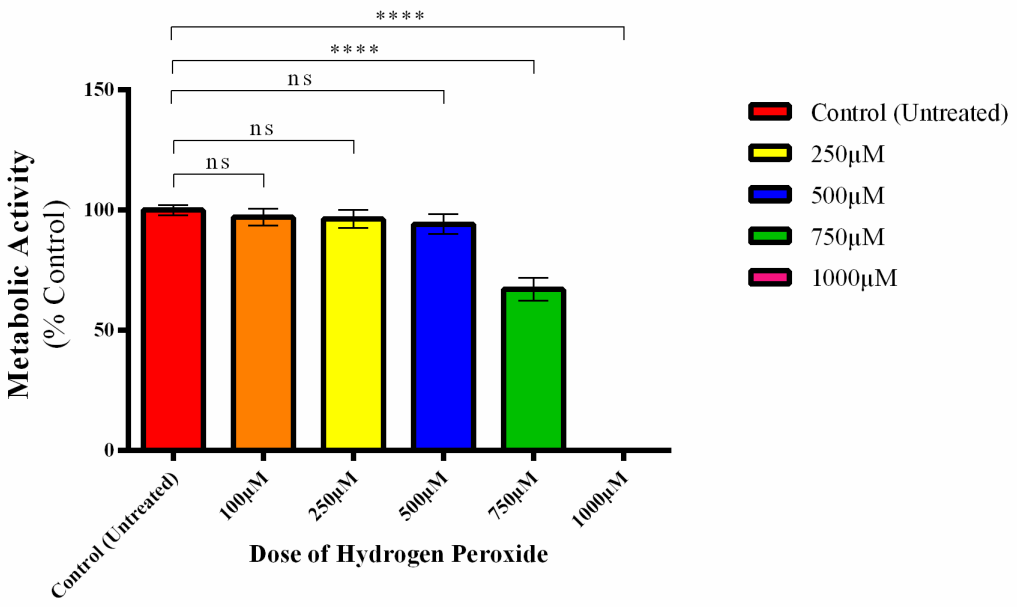

Figure 28: Effect of H_2O_2 on HL-1 cell viability upon exposure for 3 hours (n=5; ns, not significant; ****P ≤ 0.0001).

The loss of cell viability was found to be dose-dependent. Statistically significant decrease was observed when 750µM of hydrogen peroxide was applied beyond 500µM. Only 67.1±4.8% cells remained viable after injuring them with 750µM of

H_2O_2 for 3 hours. On the contrary, no cells were found viable when the cells had been incubated with 1000µM of H_2O_2 for 3 hours. As there was no viable cell for subsequent treatment with catalase-loaded nanoparticles after injuring them with 1000µM of H_2O_2 and no significant differences were observed among the control, 100µM, 250µM and 500µM H_2O_2, 750µM of H_2O_2 was selected for further experiments to evaluate the potential post-injury treatment efficacy of the catalase-loaded nanoparticles where the cardiomyocytes were first exposed to the 750µM of H_2O_2 for 3 hours before treating them with catalase-loaded nanoparticles.

Similar findings were observed when the cells were incubated with hydrogen peroxide for 24 hours. There was no significant difference noticed among the control, 100µM, 250µM and 500µM of hydrogen peroxide. The results are shown in Figure 29.

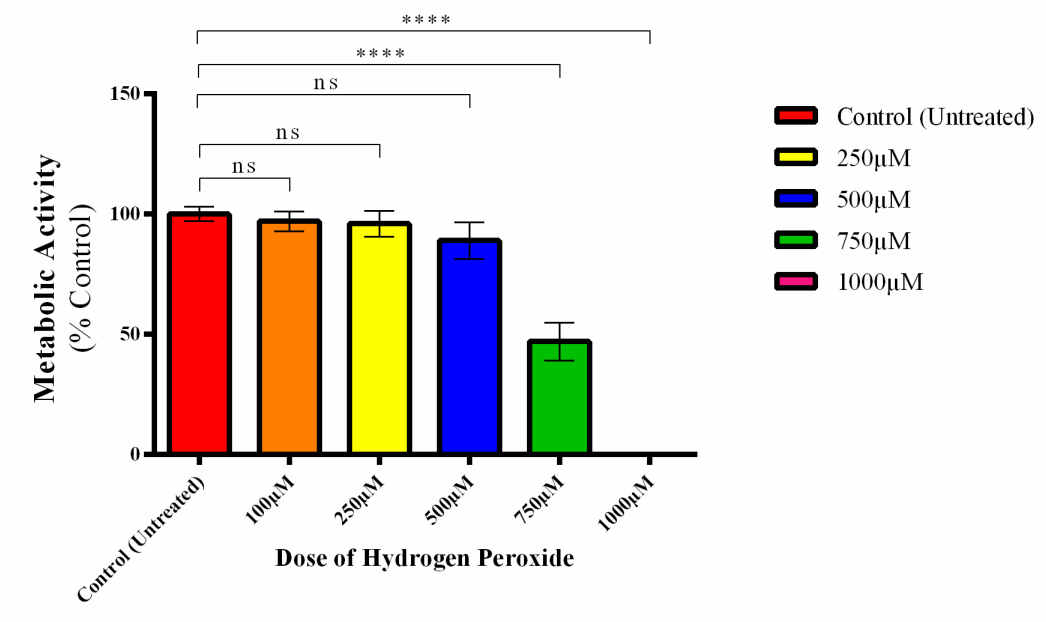

Figure 29: Effect of H_2O_2 on HL-1 cell viability upon exposure for 24 hours (n=4; ns, not significant; ****P ≤ 0.0001).

The only significant difference of the cell viability with the control was observed when the cells were incubated with 750µM and 1000µM of hydrogen peroxide. Incubation with 750µM of H_2O_2 for 24 hours left only 47.0±7.9% cells viable, compared to the control. Likewise the 3 hours treatment of 1000µM of H_2O_2, no viable cells were left when they had been injured with 1000µM of H_2O_2 for 24 hours. Cell viability was lost in a dose-dependent manner alike the treatment of H_2O_2 for 3 hours. Likewise for the experiments to determine the post-injury treatment efficacy of catalase-loaded nanoparticles, 750µM of H_2O_2 was selected for future experiments to evaluate the potential pre-injury treatment efficacy of the nanoparticles because there was no cells found viable after injuring them with 1000µM of H_2O_2 and no significant difference was noticed among the control, 100µM, 250µM and 500µM of H_2O_2.

3.3.2 Cryoprotected BSA-stabilized catalase-loaded nanoparticles protected cardiomyocytes from hydrogen peroxide-induced cytotoxicity

To determine the potential ability of catalase-loaded nanoparticles in protecting the HL-1 cardiomyocytes from oxidative stress in pre-injury treatment of the cells with the nanoparticles, the cells were incubated with an increasing dose of the BSA-stabilized catalase-loaded PLGA nanoparticles that were cryoprotected by trehalose at a weight ratio of NPs to trehalose of 1:60, for 3 hours before injuring them with 750µM of H_2O_2 for the next 24 hours. After 24 hours of injury by H_2O_2, viability of the cells was measured by Prestoblue assay. The results are presented in Figure 30.

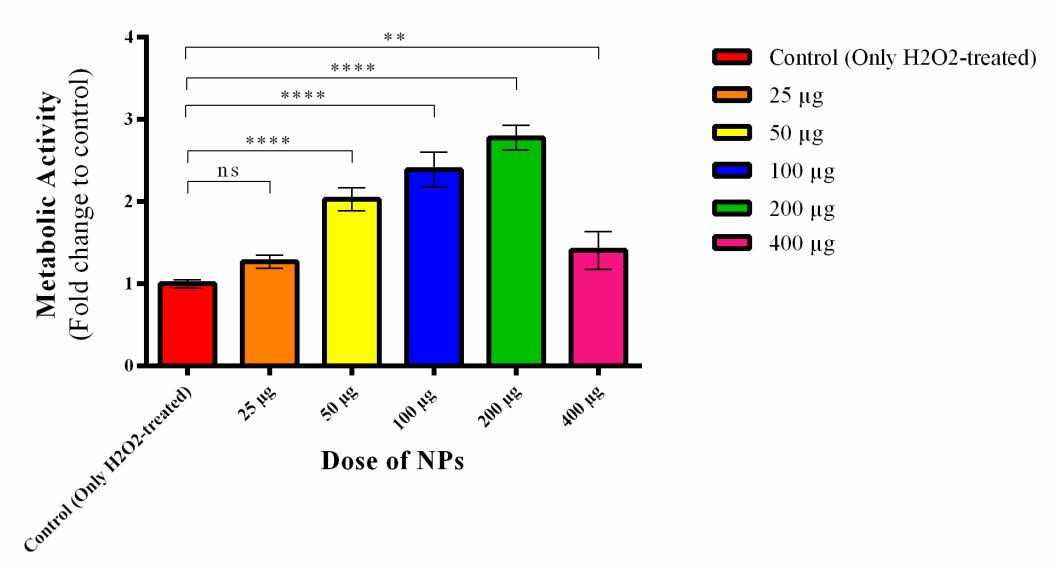

Figure 30: Effect of catalase-loaded nanoparticles in protecting the cardiomyocytes from oxidative stress induced by H_2O_2 when the cells were incubated for 3 hours with the BSA-stabilized catalase-loaded PLGA nanoparticles that were cryoprotected by trehalose at a weight ratio of NPs to trehalose of 1:60, before injuring them with H_2O_2 (n=5; ns, not significant; **P ≤ 0.01; ****P ≤ 0.0001).

There was a little difference noticed in the protective action of the nanoparticles produced by the dose of 25 µg of nanoparticles/well, compared to the control which was treated by only 750µM of H_2O_2. But, the difference was not statistically significant. Only significant protection from the oxidative stress started to appear from the dose of 50 µg/well, for which the cell viability was 2.03±0.14 times of that of the control. The nanoparticles preserved the cell viability in a dose-dependent manner. Likewise, doses of 100 µg/well & 200 µg/well significantly preserved the viability of cells by 2.39±0.21 and 2.78±0.15 times of the control, respectively. Surprisingly, a sudden drop was detected after the dose of 200 µg/well in preserving viability of the cells. In comparison to the control, this high dose of 400 µg/well showed significant protective action where cell viability was 1.41±0.23 times of that the control. Among the five doses of the nanoparticles employed in this study,

200 µg/well produced the maximum protective action and this was statistically different from the actions generated by all other doses of the nanoparticles.

Another set of experiment was designed to compare the protective efficacies of the three formulations of nanoparticles in preserving the cell viability upon exposure to hydrogen peroxide. Before freeze-drying, trehalose was added to the nanosuspensions at 1:60, 1:80 and 1:100 weight ratios of nanoparticles to trehalose in order to reduce the loss of catalase activity upon freeze-drying. As there was no significant difference noticed among the catalase activity of the three formulations, they were investigated further in this cellular oxidative stress model to find out the formulation which would be the best to provide the maximum protective action in oxidative stress-induced by hydrogen peroxide. The optimum dose of the nanoparticles observed in the previous experiment was 200 µg/well, and accordingly this dose was employed here to compare the efficacies of the three formulations. The results are presented in Figure 31.

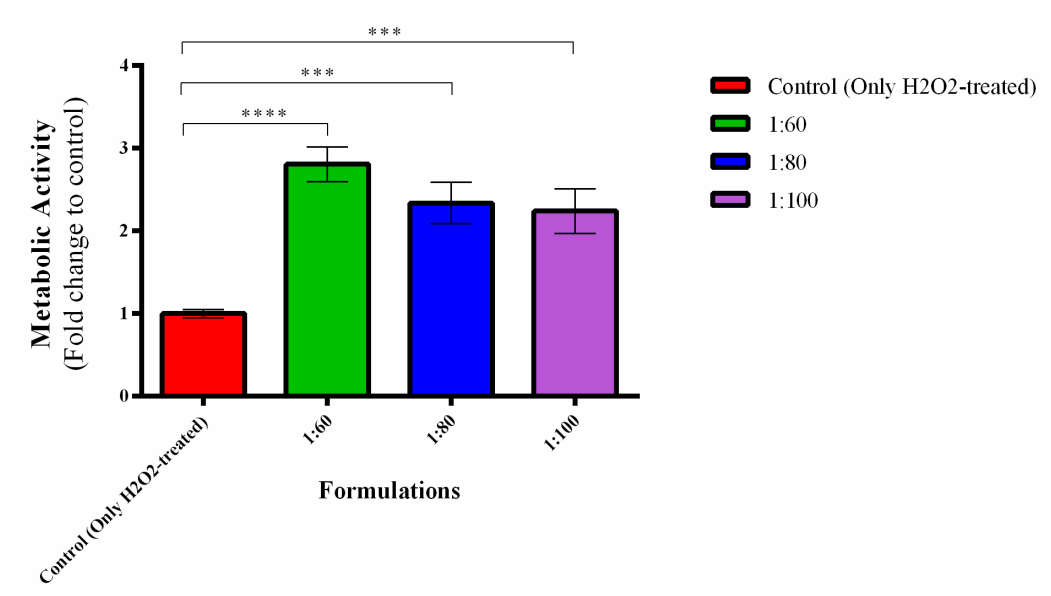

Figure 31: Comparison of the protective effects provided by the three formulations of the cryoprotected BSA-stabilized catalase-loaded nanoparticles, where the cells were incubated with the nanoparticles for 3 hours before injuring them with H_2O_2 for the next 24 hours (n=3; ***P ≤ 0.001; ****P ≤ 0.0001).

All of the three formulations of catalase-loaded nanoparticles showed protective efficacy in oxidative stress induced by hydrogen peroxide, and these actions are statistically significant as compared to the control. Compared to the control, these formulations of 1:60, 1:80 and 1:100 preserved the cell viability by 2.81±0.21, 2.34±0.25 and 2.24±0.27 times of that of the control, respectively. The difference between the protective actions produced by the 1:60 and 1:80 formulations was not statistically significant. Similarly, there was no statistically significant difference observed between the efficacies of 1:80 and 1:100. But, the protective effect of 1:60 was higher than that of 1:100, which was statistically significant.

For evaluation of the ability of the BSA-stabilized catalase-loaded PLGA nanoparticles cryoprotected by trehalose at a weight ratio of NPs to trehalose of 1:60, in protecting the HL-1 cardiomyocytes from the oxidative stress in post-injury

treatment with the nanoparticles, the cells were incubated with 750µM of H_2O_2 for 3 hours followed by treating them with an increasing dose of nanoparticles for the next 24 hours. After 24 hours of incubation with the nanoparticles, cell viability was determined by Prestoblue assay. The results are mentioned in Figure 32.

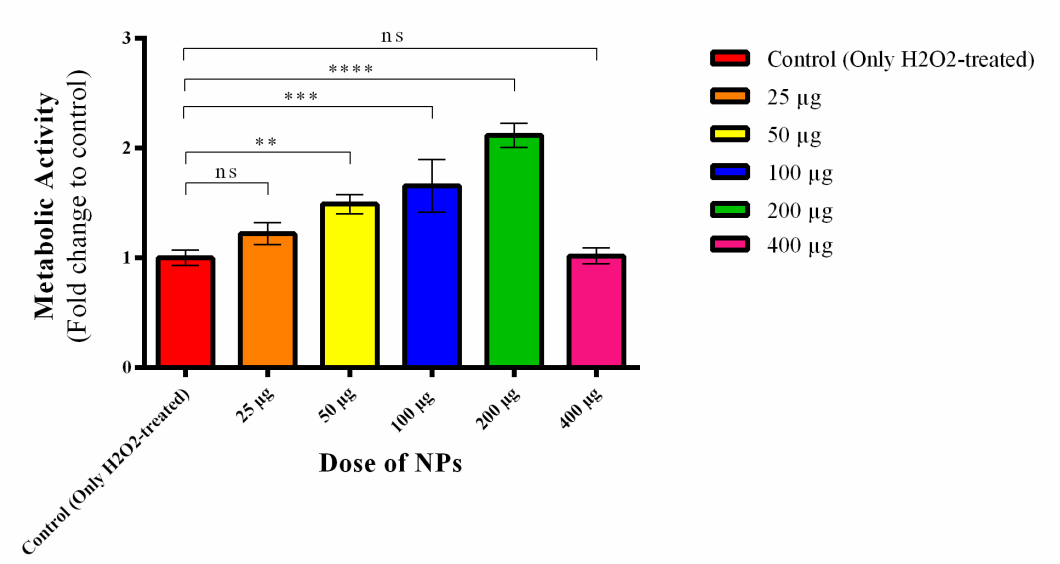

Figure 32: Protective effect of catalase-loaded nanoparticles in oxidative stress of cardiomyocytes induced by H_2O_2 for 3 hours followed by treating them with the BSA-stabilized catalase-loaded PLGA nanoparticles that were cryoprotected by trehalose at a weight ratio of NPs to trehalose of 1:60, for the next 24 hours (n=3; ns, not significant; **P ≤ 0.01; ***P ≤ 0.001; ****P ≤ 0.0001).

Like the pre-injury treatment experiment, a small difference was also observed in the protective action of the nanoparticles generated by the dose of 25 µg of nanoparticles/well as compared to the control, but the difference was not statistically significant. Statistically significant protective action started to appear from the dose of 50 µg/well, for which the cell viability was 1.49±0.09 times of the control. Like the protective action in pre-injury treatment, the nanoparticles protected the cells in a dose-dependent manner in this post-injury treatment study.

Doses of 100 µg/well & 200 µg/well significantly preserved the cell viability by 1.66±0.24 and 2.12±0.11 times of the control, respectively. Astonishingly, the protective action of the nanoparticles disappeared when the dose was shifted to 400 µg/well from the dose of 200 µg/well. This high dose of 400 µg/well unexpectedly produced no significant protective action in comparison to the control. The dose of 200 µg/well was found to be the most effective in preserving the cells upon exposure to hydrogen peroxide and its protective efficacy was significantly higher than those of other doses.

3.3.3 Cryoprotected BSA-stabilized catalase-loaded nanoparticles protected cardiomyocytes from hydrogen peroxide-induced apoptosis

Apoptosis was induced in the HL-1 cardiomyocytes by exposing them to hydrogen peroxide and the potential capability of the cryoprotected BSA-stabilized catalase-loaded PLGA nanoparticles (cryoprotected by trehalose at a weight ratio of NPs to trehalose of 1:60) in alleviating this induced apoptosis was evaluated by flow cytometric determination of the activities of executioner caspases, caspase-3 and -7. The results of the caspase activities are shown in Figure 33 and Figure 34.

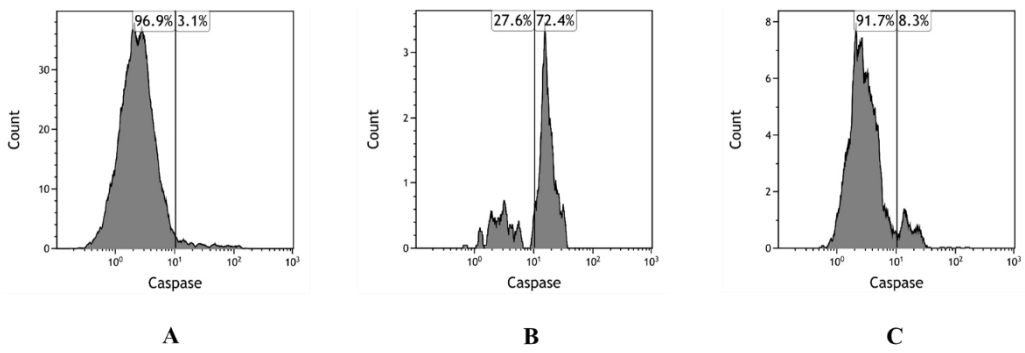

Figure 33: Representative flow cytometric analysis showing protective effect of the nanoparticles in reducing caspase-positive apoptotic HL-1 cells upon exposure to H_2O_2. (A) Negative Control: Untreated. (B) Positive Control: H_2O_2-treated. (C) Treated: NPs & H_2O_2-treated.

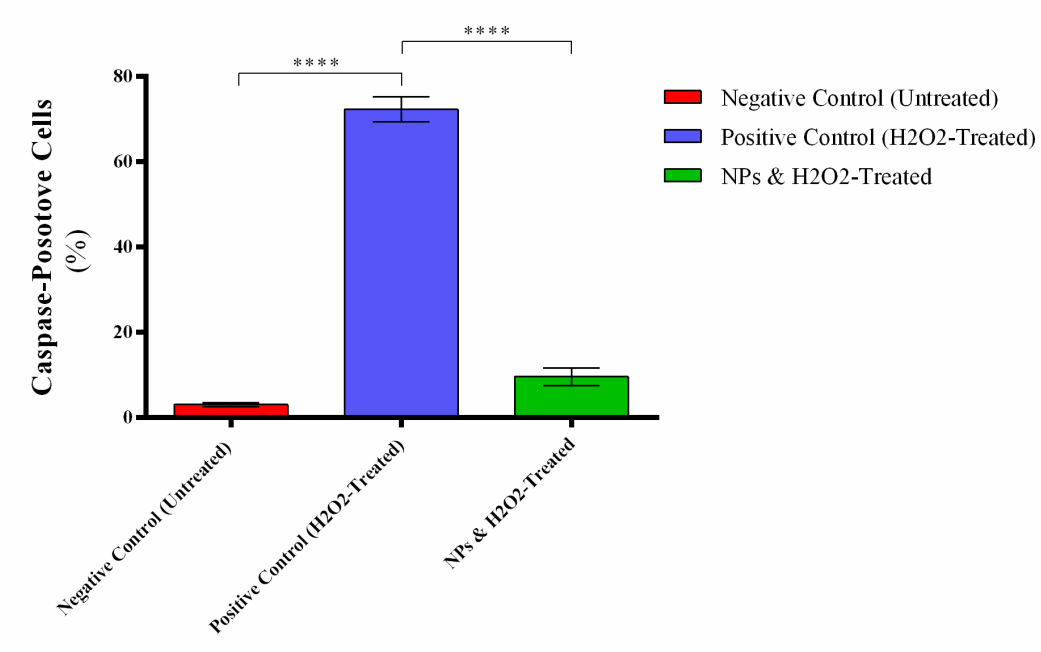

Figure 34: Summary of changes in the percentages of caspase-positive apoptotic HL-1 cells as evaluated in the experiments shown in Figure 33 (n=3; ****P ≤ 0.0001).

Upon exposure to hydrogen peroxide, caspase-3 and -7 activities were increased in the HL-1 cells which were represented here as the positive control group, and caspase-positive cells were 72.3±2.9% of the live population. Pre-treatment of the cells with the nanoparticles before exposing them to H_2O_2 reduced the incidence of apoptosis in the cardiomyocytes along with increasing the number of live cells which declined after an assault with H_2O_2. Nanoparticle-treated cells showed a big drop in the caspase-positive population to 9.6±2.1% of live cells and this difference is statistically significant.

The potential ability of the cryoprotected BSA-stabilized catalase-loaded nanoparticles (cryoprotected by trehalose at a weight ratio of NPs to trehalose of 1:60) in alleviating hydrogen peroxide-induced apoptosis was also evaluated by bi-colour flow cytometry analysis of alexa fluor 488 annexin V binding and propidium iodide uptake. Analysis was performed at two different time periods – the first one at 6 hours and the second one at 24 hours after exposing the cells to hydrogen peroxide. The results of 6 hours are shown in Figure 35 & Figure 36 and those of 24 hours in Figure 37 & Figure 38.

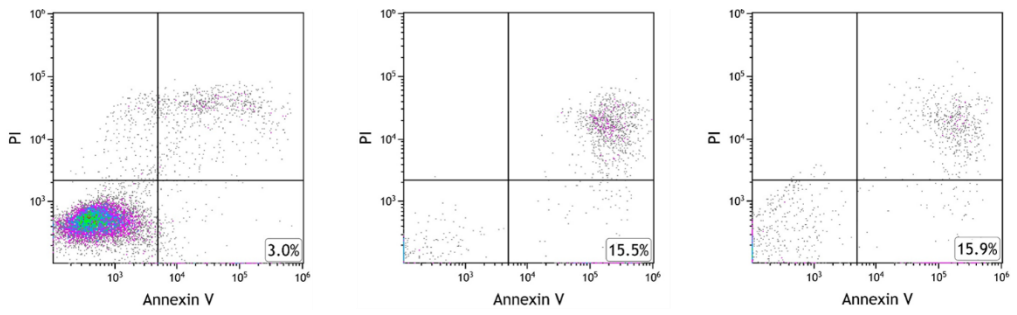

A **B** **C**

Figure 35: Representative flow cytometric analysis showing no visible protective effect of the nanoparticles in reducing apoptosis of HL-1 cells observed after 6 hours of exposure to H_2O_2. (A) Negative Control: Untreated. (B) Positive Control: H_2O_2-treated. (C) Treated: NPs & H_2O_2-treated.

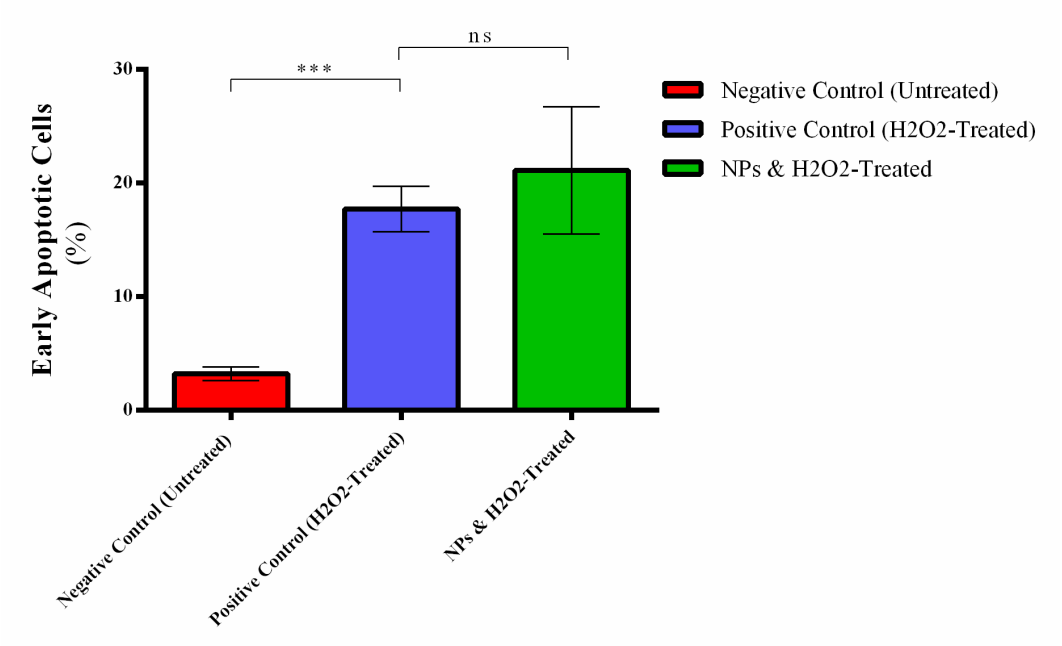

Figure 36: Summary of the percentages of apoptotic cells observed after 6 hours of exposure to H_2O_2 as evaluated in the experiments shown in Figure 35 (n=3; ns, not significant; ***$P \leq 0.001$).

Cell populations of the lower right quadrants of the dot plots of Figure 35 and Figure 37 represented early apoptotic cells and showed staining by annexin V-alexa fluor 488, but remained unstained by propidium iodide. The study of 6 hours readings exhibited that the cells of the positive control group resulted in increased percentages of early apoptotic cells among the live cells after stressed with H_2O_2. 17.7±2.0% of the cell population was found early apoptotic in the positive control group and this difference was statistically significant in comparison to the negative

control group where the cells were not exposed to hydrogen peroxide (Figure 36). 21.0±5.6% of the cell population was found early apoptotic in the nanoparticles-treated group and this was not statistically significant in comparison to the positive control group where the cells were exposed to hydrogen peroxide (Figure 36). Similar with the caspase study, it was also found that treatment with nanoparticles could preserve the number of live cells which was reduced by H_2O_2 assault in the positive control group.

Likewise the study of 6 hours, the population of early apoptotic cells in the positive control group of the 24 hours study was also increased significantly as compared to the negative control (Figure 38) and it was 74.3±2.4%. Unlike the 6 hours study, a reduction in the early apoptotic cells appeared in the nanoparticle-treated group of the 24 hours study, and this difference was statistically significant. Treatment with the nanoparticles reduced the percentages of the early apoptotic cells from 74.3±2.4% to 56.0±6.6% (Figure 38).

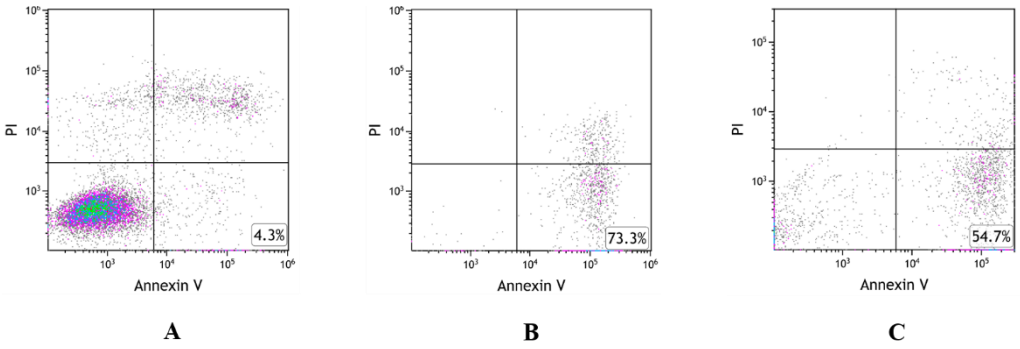

Figure 37: Representative flow cytometric analysis showing protective effect of the nanoparticles in reducing apoptosis of HL-1 cells observed after 24 hours of exposure to H_2O_2. (A) Negative Control: Untreated. (B) Positive Control: H_2O_2-treated. (C) Treated: NPs & H_2O_2-treated.

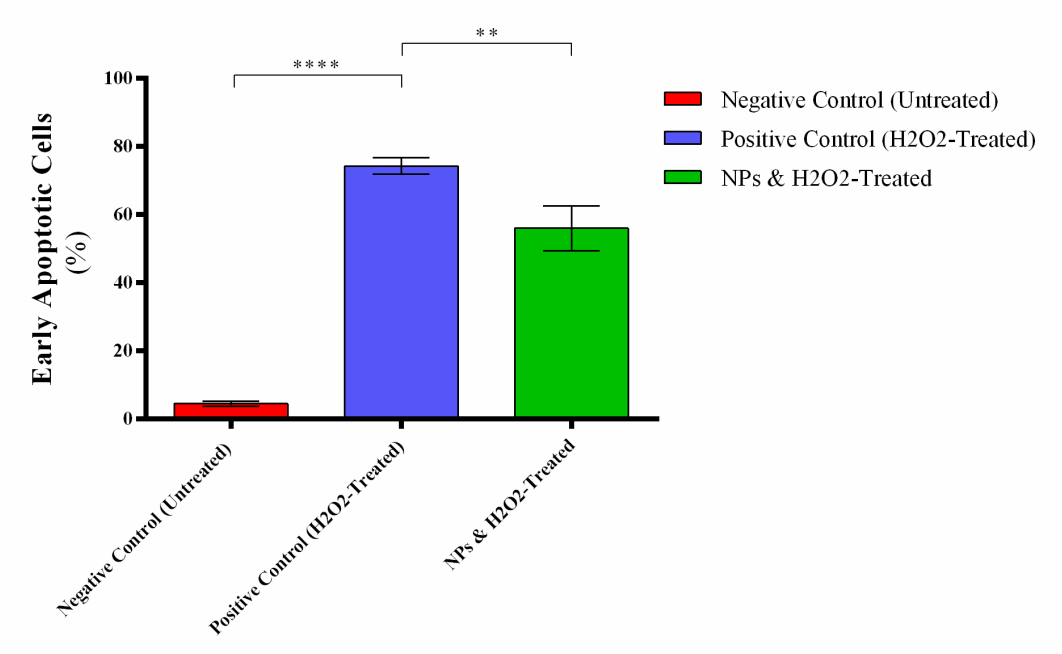

Figure 38: Summary of changes in the percentages of the apoptotic cells observed after 24 hours of exposure to H_2O_2 as evaluated in the experiments shown in Figure 37 (n=3; **P ≤ 0.01; ****P ≤ 0.0001).

3.3.4 Cytotoxicity of the cryoprotected BSA-stabilized catalase-loaded nanoparticles

The cryoprotected BSA-stabilized catalase-loaded nanoparticles (cryoprotected by trehalose at a weight ratio of NPs to trehalose of 1:60) were evaluated for any possible cytotoxicity caused by the nanoparticles themselves in the experiments. Doses of 25, 50, 100, 200 and 400 µg/well were investigated in this cytotoxicity study. The results are shown in Figure 39.

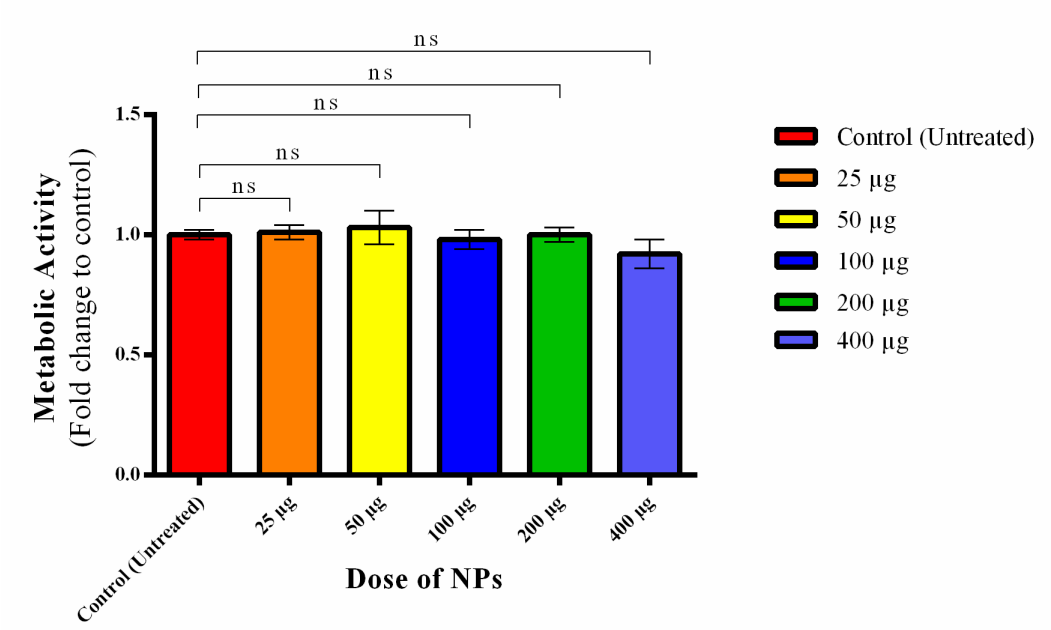

Figure 39: Effect of the cryoprotected BSA-stabilized catalase-loaded nanoparticles on cell viability of the HL-1 cardiomyocytes upon incubating them with the nanoparticles for 24 hours (n=3; ns, not significant).

In comparison to the control, none of the five doses of 25 µg/well, 50 µg/well, 100 µg/well, 200 µg/well and 400 µg/well of catalase-loaded nanoparticles produced any toxicity to the cardiomyocytes that could be statistically significant. After 24 hours treatment with the nanoparticles in case of the dose of 400 µg/well, a little depression was observed in the cell viability as compared to the other doses. This dose of 400 µg/well resulted in a change of the cell viability of 0.92±0.06 fold to the control, but this change was not statistically significant.

3.3.5 Presence of the cryoprotected BSA-stabilized catalase-loaded nanoparticles neutralized H_2O_2 of higher strength in contact with the cardiomyocytes

Ability of the cryoprotected BSA-stabilized catalase-loaded nanoparticles (cryoprotected by trehalose at a weight ratio of NPs to trehalose of 1:60) to preserve the cardiomyocytes in the presence of hydrogen peroxide was investigated. In the co-exposure group, 1000µM of H_2O_2 and 200 µg of nanoparticles were simultaneously added to the wells and mixed gently. The results of this co-treatment experiment are shown in Figure 40.

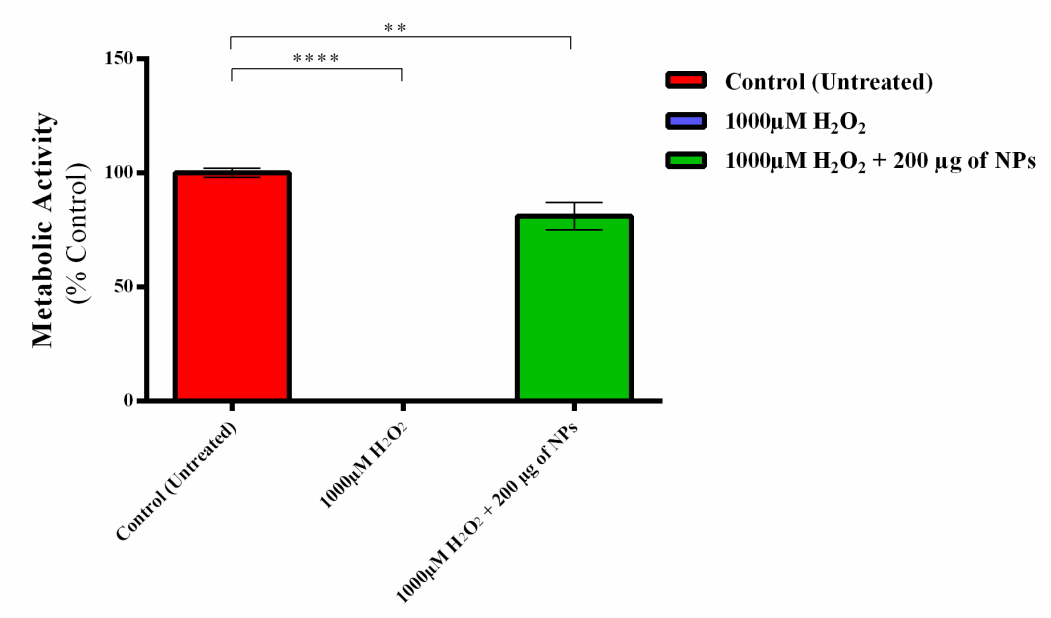

Figure 40: Effect of the co-treatment of the cryoprotected BSA-stabilized catalase-loaded nanoparticles and H_2O_2 on cell viability of the HL-1 cardiomyocytes (n=3; **P ≤ 0.01; ****P ≤ 0.0001).

Exposure of the cells to 1000µM of H_2O_2 for 24 hours showed a devastating effect on the cells and left no cells viable at all. But, the devastating effect of this high strength of 1000µM of H_2O_2 was dramatically neutralized by the nanoparticles incorporated simultaneously into the wells with 1000µM of H_2O_2. 81±6% of the cells remained viable in presence of 1000µM of H_2O_2 and the reason of this high percentage of viable cells was attributable to the neutralization of H_2O_2 by the catalase-loaded nanoparticles. Due this high neutralizing capacity of the catalase-loaded nanoparticles, only around 19% of the cells were lost in spite of the presence of a lethal concentration of H_2O_2.

3.3.6 Alexa Fluor 488-stained BSA-stabilized catalase-loaded PLGA nanoparticles

3.3.6.1 Effect of trehalose on lyophilization of Alexa Fluor 488-stained BSA-stabilized catalase-loaded PLGA nanoparticles

Trehalose was observed to be effective in minimizing lyophilization-induced damage to the BSA-stabilized catalase-loaded PLGA nanoparticles containing BSA conjugated Alexa Fluor 488, where trehalose was added at a weight ratio of NPs to trehalose of 1:60. As it was observed that trehalose was not significantly affecting the analytical procedure of determining the enzymatic activity (Figure 26, Chapter 2), trehalose was not added to the analytical process as a control. The result is shown in Figure 41. Catalase activity of the nanoparticles (1:0), which were not freeze-dried with trehalose was 721±101 units. In contrast, catalase activity was 1834±116 units for the freeze-dried nanoparticles (1:60), where trehalose was added at 1:60

weight ratio of nanoparticles to trehalose. The difference in the catalase activity between these two formulations of 1:0 and 1:60 was statistically significant.

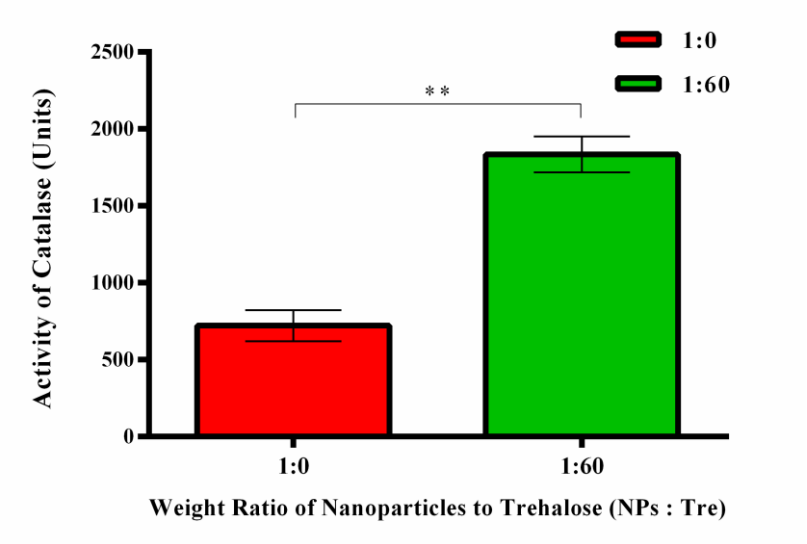

Figure 41: Role of trehalose in preserving catalase activity of BSA-stabilized catalase-loaded nanoparticles containing Alexa Fluor 488 upon freeze-drying (n=3; **P ≤ 0.01).

3.3.6.2 Flow cytometry and super resolution microscopy

After incubation of the cardiomyocytes with the dose of 200 µg/well of the cryoprotected BSA-stabilized catalase-loaded PLGA nanoparticles labelled with Alexa Fluor 488 (cryoprotected by trehalose at a weight ratio of NPs to trehalose of 1:60), uptake of the nanoparticles by the cells were analysed by flow cytometry. The representative histograms are shown in Figure 42. The uptake study showed that the Alexa Fluor 488-labelled catalase-loaded nanoparticles were uptaken by HL-1 cells.

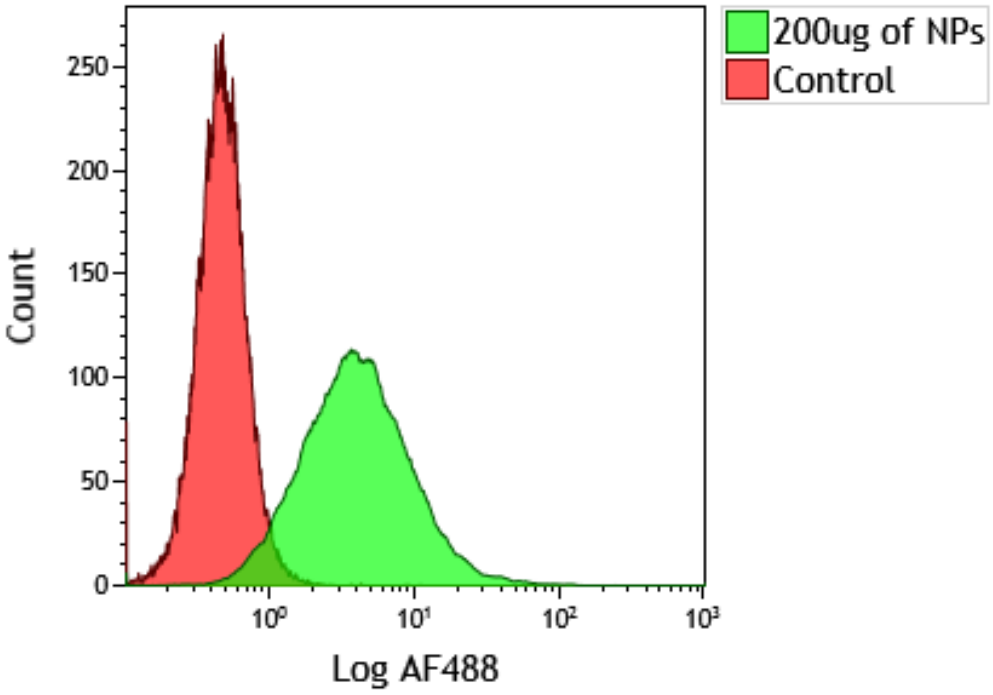

Figure 42: Representative flow cytometric histograms showing uptake of the cryoprotected BSA-stabilized catalase-loaded PLGA nanoparticles labelled with Alexa Fluor 488 by HL-1 cells (n=3).

Internalization of the cryoprotected Alexa Fluor 488-labelled nanoparticles into the HL-1 cells was also investigated by imaging with super resolution microscopy (3D SIM) in order to find out the location of the nanoparticles whether they were remained on the cell membranes or they were inside the cells. The images are presented in Figure 43 and Figure 44 .

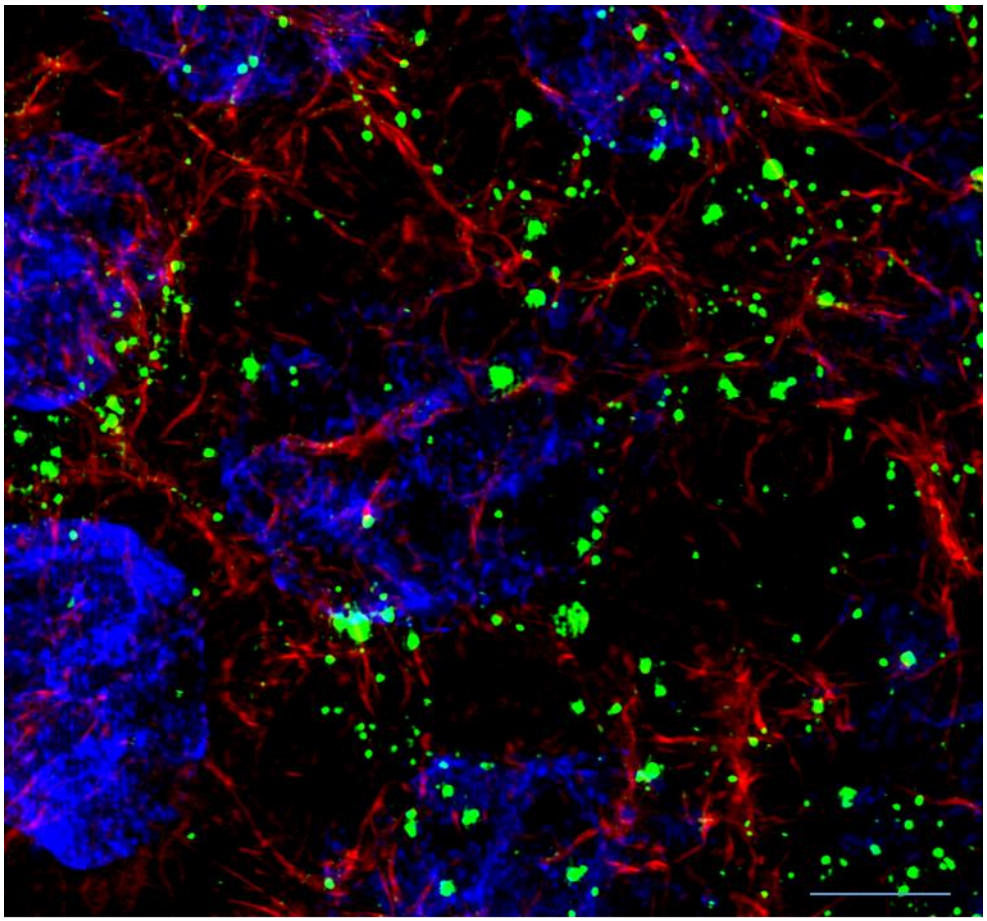

Figure 43: Representative super-resolution microscopy (3D SIM) image of HL-1 cardiomyocytes showing adsorption of the Alexa Fluor 488-labelled catalase-loaded PLGA nanoparticles on the cell membranes. Staining: Blue-Nucleus, Green-NPs, Red-Plasma membrane.

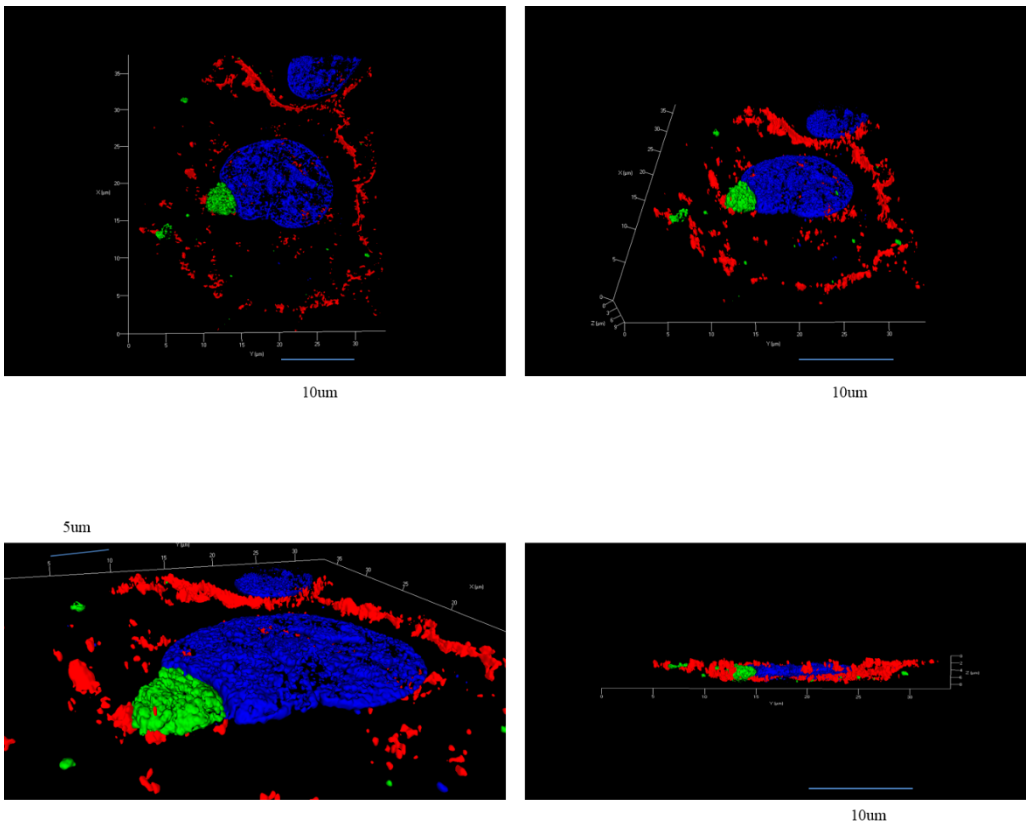

Figure 44: Representative super-resolution microscopy (3D SIM) reconstructed images of HL-1 cells showing with orthogonal sections that cluster of Alexa Fluor 488-labelled nanoparticles were in the focal plane of nucleus indicating internalization of particles. Staining: Blue-Nucleus, Green-NPs, Red-Plasma membrane.

Although flow cytometry study indicated that the nanoparticles were successfully internalized into the HL-1 cells, the real scenario was completely different. The images obtained by super-resolution microscopy showed that most of the nanoparticles remained adsorbed onto the cell membrane instead of internalization and very small amount of the nanoparticles were internalized.

3.4 Discussion

The present study demonstrated for the first time that catalase-loaded PLGA nanoparticles protected HL-1 cardiomyocytes from oxidative stress and could be a promising approach in treating oxidative stress-induced cell damage that occurs in myocardial ischemia-reperfusion injury.

The myocardium controls the contractile function of the heart by maintaining its demand and supply of oxygen in different physiological and pathological conditions. Myocardial infarction is a medical emergency and life-threating condition. During acute myocardial infarction, two processes are involved in inflicting damage to the myocardium – ischemia and successive reperfusion. Reperfusion induces overproduction of ROS those damage cardiomyocytes through formation of DNA adduct, peroxidation of lipids, oxidation of proteins and cellular machinery. The cardiomyocytes constitute a major bulk of the myocardium. Any kind of stress seriously affects cardiomyocytes and different signalling cascades, leading to myocardial dysfunction. It has been suggested from animal studies that reperfusion injury may account for up to 50% of the final myocardial infarct size. The resultant size of the myocardial infarct is highly linked with developing heart failure. Myocardial reperfusion process has continued to improve with more effective and appropriately timed reperfusion. But, developing therapies to decrease reperfusion injury has not been progressed at all.[9,309-312]

A number of studies reported that antioxidants or scavengers like catalase and superoxide dismutase decreased size of the myocardial infarct,[313-316] whereas some studies reported no beneficial effect on infarct size.[317-322] A big number of clinical

trials failed to prove any beneficial effect shown in the basic laboratory settings. The causes of this failure in clinical trials can be attributed to improper design of the clinical trials, using inappropriate animal MI models, and testing of the therapies in clinical settings those failed to provide any conclusive cardioprotection.[323]

A recognized model of inducing oxidative stress in cells is exposing the cells to H_2O_2.[324-326] In the present study, H_2O_2 was used to induce oxidative stress in HL-1 cardiomyocytes. In comparison to the unexposed cells, a significant loss of cell viability was observed in the HL-1 cells exposed to H_2O_2. About 67% cells were found viable after an incubation of 3 hours with 750µM of H_2O_2. This loss of viability was close to the viability reported by Keene *et al.* where exposure of 4 hours with 750µM of H_2O_2 resulted in 35-45% cell death.[327] This sub-lethal concentration of H_2O_2 was employed to induce oxidative stress in the HL-1 cells for evaluating ability of the cryoprotected BSA-stabilized catalase-loaded PLGA nanoparticles in protecting the cardiomyocytes. Cells were incubated with the nanoparticles for 3 hours so that cells could uptake nanoparticles before injuring them with the sub-lethal concentration of H_2O_2. This experiment of pre-injury treatment showed that the catalase-loaded nanoparticles could successfully protect the cells from oxidative stress induced by H_2O_2. The ability of the nanoparticles to rescue the cells after injuring them with the sub-lethal concentration of H_2O_2 was also investigated. Surprisingly, the nanoparticles proved their efficacy in rescuing the cells even after injuring them with 3 hours exposure to this sub-lethal concentration of H_2O_2. In both cases, the protective action was dose-dependent. Expectedly more protective action was noticed in case of pre-injury treatment than that observed in post-injury treatment. Catalase-loaded nanoparticles, which were

already internalized before the onset of the assault by hydrogen peroxide, could neutralize the H_2O_2 that diffused into the cells from the medium before exerting its detrimental effect. Alternatively, the damage that had already started and possibly some irreversible damage had already been accomplished by the H_2O_2, was not possible to prevent to the same degree as in the case of pre-injury treatment. Additionally the nanoparticles adsorbed onto the cell membranes might help in reducing the H_2O_2-induced damage by contributing to the neutralization of H_2O_2. Ansley *et al.* suggested that the pre-existent antioxidants from both intra- and extracellular sources may withstand the free radicals acutely generated and can help in the functional recovery of the cardiomyocytes.[84] In both cases of pre- and post-injury treatments, the lowest dose of the nanoparticles applied in this study showed insufficiency to elicit any protective response. Interestingly, the highest dose employed in this study produced the least protective action among the effective doses in pre-injury treatment and showed no protection at all in post-injury treatment. In the former case, the protective action dramatically fell down when the dose was increased from the most optimum dose, 200 µg/well to the highest dose, 400 µg/well. It indicates that there could be a limit of nanoparticles for the cardiomyocytes up to which the cells can tolerate and maintain their ability to recover. Beyond the limit, the cells become more vulnerable in contact with the load of nanoparticles and become less able to recover metabolic activity. This assumption is strengthened by the findings observed in the post-injury treatment where the injured cells were treated with the nanoparticles. Because of exceeding the limit of nanoparticles, the highest dose could not produce more protective response in this case. Instead the highest dose failed here to show any protective

response, compared to the control. The reason may be attributable to the cellular damage already happened before initiating treatment with the nanoparticles.

After observation of the protective action of the cryoprotected catalase-loaded nanoparticles against oxidative stress and determining the most optimum dose of the nanoparticles, efficacies of the three nanoparticles formulations, 1:60, 1:80 and 1:100 were compared. The nanoparticles were freeze-dried with trehalose at 1:60, 1:80 and 1:100 weight ratios of nanoparticles to trehalose. Applying the most optimum dose observed in the pre-injury treatment protocol, this comparison was conducted to confirm that the formulation 1:60 was the right one to continue for further experiments as the activity of catalase among the three formulations were comparable. Cytocompatibility of the nanoparticles was also checked, and found all of the doses of the nanoparticles employed in the study were cytocompatible. Compared to the control, the highest dose showed a small loss of cell viability in the cytocompatibility study although it was not statistically significant. However, this observation of losing cell viability with the highest dose of the nanoparticles is assumed to support that the cardiomyocytes could tolerate a certain limit of nanoparticles beyond which they might face adverse condition and start to lose their ability to recover from the oxidative insult. From the findings of the above studies, it could be inferred that excess amount of nanoparticles and/or trehalose might adversely affect the cardiomyocytes, but it warranted further investigations.

Myocardial ischemia primarily produces cell death caused by necrosis.[117,328,329] Nevertheless, a number of observations in animal and human hearts strongly suggested that loss of cardiomyocyte due to apoptosis contributes to the total cell loss in ischemia/reperfusion.[20,328,330] Accumulating evidence has suggested that

apoptosis is mainly activated or augmented during reperfusion after an episode of ischemia.[331,332] Apoptosis is usually held to be accountable for the ongoing loss of myocardial myocytes following ischemia/reperfusion although a large variation in the apoptotic myocytes percentage (0.05 to 35%) was observed in rats.[46,333] It is stated that the development of myocardial infarction following ischaemia/reperfusion is closely linked with the apoptotic cells existing in peri-necrotic area.[334] Accordingly, an expansion of the infarction area was reported following reperfusion.[335] Apoptosis is mostly predominant in the first few hours of ischemia. Molecular MRI technique showed that the majority of the apoptotic cardiomyocytes existing mainly in the mid-myocardium still remained viable even in the 4 to 6 hours of ischemia-reperfusion.[336] This time window for therapeutic intervention is supported by the observation that erythropoietin administered even after 24 hours of I/R injury could protect the myocardium by reducing apoptosis of cardiomyocytes.[337]

Efficacy of the cryoprotected catalase-loaded nanoparticles was evaluated in reducing apoptosis of the HL-1 cardiomyocytes induced by oxidative stress. Apoptosis was induced in the cardiomyocytes by assaulting them with 200µM of H_2O_2 which was lower in strength compared to the strength that was used in the previous investigations to measure the protective efficacy of the nanoparticles. It has been reported that lower doses of hydrogen peroxide triggered apoptosis and higher doses preferentially caused necrosis of the cardiomyocytes although lower doses were also reported to cause necrotic cell death in the cardiomyocytes.[338-340] In this study, 200µM of H_2O_2 successfully induced apoptosis in the cardiomyocytes which was confirmed by determining the activities of the executioner caspases,

caspase-3 and -7 by flow cytometry. Treatment of the cells with the nanoparticles before inducing apoptosis by H_2O_2, resulted in a marked decrease in the caspase-positive population. Similarly, annexin V-PI dual-staining experiments performed by flow cytometry after 24 hours of H_2O_2 treatment showed a drop in the apoptosis rate. But, when the annexin V-PI flow cytometry analysis was performed after 6 hours of H_2O_2 exposure, no significant resistance against apoptosis was shown by the nanoparticles although a little significant apoptotic population was observed in both the nanoparticles+H_2O_2-treated and the only H_2O_2-treated cells, compared to the untreated cells. This difference in the percentages of apoptotic populations between the 6 hours and 24 hours groups of annexin V-PI experiments and detection of apoptosis by the activities of caspases at 6 hours, can be attributed to that phosphatidylserine exposure is a later event in HL-1 cells and activation of caspase-3 and -7 precedes to translocation of phosphatidylserine. HT1376 cells were reported to start annexin V staining after 48 hours upon treatment with docetaxel.[341] HL-1 cells showed 28.6% annexin V-positive cells after 24 hours of incubation with 175nM of staurosporine.[342] In contrast, Suzuki *et al.* reported that the number of annexin V-positive cells in rat cardiomyocytes increased significantly after 4 hours of H_2O_2 stimulation.[343] Bailey *et al.* observed that the earliest event in the process of apoptosis was activation of caspases and suggested that it might vary depending on cell type.[344] After ischemia-reperfusion, Seshadri *et al.* found very little apoptotic cells, only about 0.5%, which was reduced to about 0.1% by treatment with superoxide dismutase-loaded polyketal microparticles, and this small reduction resulted in a significant functional recovery of the rat myocardium.[345] The present study showed a big reduction in the percentages of apoptotic cells in HL-1 cardiomyocytes. So, it is expected that the cryoprotected BSA-stabilized catalase-

loaded PLGA nanoparticles prepared in this study could be an effective therapeutic approach in preserving the myocardial function because of having this high anti-apoptotic effect.

Ability of the cryoprotected BSA-stabilized catalase-loaded PLGA nanoparticles prepared in this study was also investigated to check their power of neutralizing H_2O_2 and of protecting the cells from the H_2O_2-induced damage in presence of the nanoparticles. Surprisingly, 1000µM of H_2O_2 exposure left around 81% cells viable in presence of the nanoparticles. In contrast, no viable cells were observed after insulting them with 1000µM of H_2O_2. It was speculated that most of the H_2O_2 became neutralized by the nanoparticles before exerting its damaging effect to the cells.

Cellular uptake study by super resolution microscopic images showed that most of the nanoparticles observed over the cells were not internalized. A small portion of the nanoparticles were internalized and others adsorbed and remained associated with the cell membrane. Lin *et al.* showed that endocytosis dependent on palmitoylation was vastly induced upon reoxygenation of hypoxic myocardium, which could suggest that nanoparticles could be internalized in the cardiomyocytes by enhanced endocytosis after reperfusion.[346] In cardiomyocytes, hydrogen peroxide induces conditions like reperfusion.[347,348] So, it is assumed that this enhanced endocytosis passively induced by hydrogen peroxide helped in the increased internalization of the nanoparticles than those seen in the microscopic images, and this was not reflected in the microscopic images as the cells were not treated at all by hydrogen peroxide before obtaining microscopic samples. This assumption is strengthened by the observation of Ikeda *et al.* who reported a very

poor internalization of PLGA nanoparticles in rat cardiomyocytes, possibly due to electrostatic repulsion between the negatively charged plasma membranes of the cardiomyocytes and the negatively charged PLGA nanoparticles, and showed that hydrogen peroxide treatment increased internalization of cyclosporine A-loaded PLGA nanoparticles into the rat cardiomyocytes.[165]

Although the nanoparticles adsorbed onto the cell surface might help to the neutralization of the hydrogen peroxide before diffusing into the cells, the protective efficacy of the nanoparticles could be confirmed by their post-injury treatment results, the internalized nanoparticles and the prospective increased uptake of the nanoparticles due to enhanced endocytosis. It warrants further imaging of the cells for uptake study after treating the cells with both hydrogen peroxide and nanoparticles.

Two major ROS, superoxide anion and H_2O_2 are elevated in ischemia-reperfusion and activities of the endogenous scavengers of these two ROS, superoxide dismutase and catalase progressively decline.[97,98] Treatment of cardiomyocytes with H_2O_2 induces generation and accumulation of superoxide anion and NO. After oxidizing, NO may also play the role of ROS by converting to reactive nitric oxide species. Reaction of the superoxide with the nitric oxide free radical can form peroxynitrite, a very detrimental oxidant to the cells.[309]

It was reported that H_2O_2 exposure reduced activities of the two principal endogenous antioxidant enzymes, catalase and superoxide dismutase in the cardiomyocytes.[349] It could be inferred that the cryoprotected nanoparticles after internalization into the cells neutralized the H_2O_2 that had already diffused inside

the cells from the medium, the H_2O_2 that was diffusing from the medium, the H_2O_2 that was generated inside the cells and tried to restore the normal level of catalase and superoxide dismutase enzymes those were declined upon exposure to H_2O_2.

Because of sensitivity and simplicity, the cell viability assay is a commonly used technique performed in monitoring cytotoxicity of every compound or material of interest.[350] As this study was the first step of evaluating the potential protective effect of the cryoprotected BSA-stabilized catalase-loaded PLGA nanoparticles in rescuing HL-1 cardiomyocytes from the oxidative stress induced by hydrogen peroxide, only the cell viability assay and apoptosis assay were applied in this work to investigate the protective effect of the nanoparticles. This work warrants further cellular experiments including determination of intracellular reactive oxygen species (ROS) using 2′,7′-dichlorofluorescin diacetate.[351]

A number of studies demonstrated superiority of the nanoparticle-based drug delivery systems over their free drug counterparts in myocardial ischemia-reperfusion injury.[165,168,352] Singhal *et al.* demonstrated that catalase-loaded nanoparticles were better in protecting human neurons than free catalase.[277] Catalase is an endogenous antioxidant enzyme. The promising protective effect shown by the cryoprotected BSA-stabilized catalase-loaded PLGA nanoparticles to rescue the cardiomyocytes from oxidative stress makes the nanoparticle a valuable candidate for further investigation including animal trials and mechanistic studies.

3.5 Conclusion

The present study showed that the cryoprotected BSA-stabilized catalase-loaded PLGA nanoparticles could protect the HL-1 cardiomyocytes from oxidative stress-induced damage. Oxidative stress was induced in the cells by hydrogen peroxide. The nanoparticles were effective in both pre- and post-injury treatment of the cells and could reduce apoptosis of the cardiomyocytes induced by oxidative stress. The protective response elicited by the nanoparticles was dose-dependent and this protective action was increased with increasing dose of the nanoparticles. The same dose was found to be optimum in both cases of pre- and post-injury treatments. After exceeding the optimum dose of this study, the protective response declined, even diminished in post-injury treatment. Cellular uptake study by flow cytometry demonstrated that the cells could uptake nanoparticles, but super resolution microscopic images suggested that most of the nanoparticles were adsorbed onto the cell membrane and remained associated with the cell membrane, and only a small portion of the nanoparticles were internalized. Cytotoxicity study indicated that the nanoparticles were cytocompatible. Further investigations including animal trials are warranted to explore the therapeutic potential of the nanoparticles in treating myocardial ischemia-reperfusion injury and other diseases where oxidative stress plays an important role.

4 Investigation of Structural Changes of Encapsulated Catalase upon Lyophilization and Cryoprotection of Unstabilized Catalase-Loaded PLGA Nanoparticles

4.1 Introduction

Infrared spectroscopy is a useful way of determining the secondary structure of a protein.[353,354] It has been used to investigate different stress-induced conformational changes in protein and, also to quantify secondary structural composition of protein.[199,245,246] Information of secondary structure is acquired by analysing the amide I band of protein's IR spectra. In the region of 1700 and 1600 cm^{-1} of the IR spectra, this band is observed and it is generated from the amide group's C=O stretching vibrations, coupled with the in-plane N—H bending and C—N stretching vibrations.[247,248] Rise to the frequencies of different C=O stretching vibrations caused by every form of secondary structures of proteins produce the characteristic band positons those are utilized in determining the secondary structures of proteins.[245] Nevertheless, it is possible to detect changes only in secondary structure with IR spectroscopy. Minute changes in tertiary structures of proteins those are not gone together with changes in the secondary structures may be happened during lyophilization of protein drugs. Small changes in tertiary structures with no noticeable alterations in secondary structure may affect a protein's conformational stability.[252-254]

Fluorescence spectroscopy is commonly employed in studying proteins. Fluorescence signals are highly sensitive to the surrounding microenvironment of

the fluorescence probe, and indicate the conformational state of a protein.[242,244] Most of the proteins contain tryptophan, tyrosine and phenylalanine amino acid residues. These are intrinsically fluorescent. Tryptophan is the most helpful fluorescent probe among the three amino acid residues for fluorescence study of proteins.[244] Intrinsic tryptophan fluorescence emission of a protein depends on its protein/solvent microenvironment and any change in the microenvironment of the tryptophan residue(s) can be observed in the tryptophan fluorescence emission. So, intrinsic tryptophan fluorescence is useful for studying alterations in the tertiary structure of proteins.[242,261-264] Among the fluorescence properties, fluorescence intensity and maximum emission wavelength are commonly used for studying proteins.[264-267] Upon unfolding, a multi-tryptophan protein may show an increased or decreased fluorescence intensity depending on the quenching or energy transfer processes.[268] Tryptophan maximum emission wavelength (λ_{max}) depends on the location of tryptophan residue(s) in proteins. Denaturation of proteins generally changes the microenvironment of the tryptophan(s) from a comparatively hydrophobic core to a relatively polar aqueous microenvironment and results in a red-shift of the tryptophan maximum emission wavelength (λ_{max}).[264]

The study of chapter 2 showed that enzymatic activity of the encapsulated catalase was lost during lyophilization of catalase-loaded PLGA nanoparticles and trehalose added as a cryoprotectant could minimize this activity loss of catalase loaded into the PLGA nanoparticles. In this study, the aim was to structurally characterize the encapsulated catalase of the unstabilized catalase-loaded PLGA nanoparticles upon lyophilization with and without cryoprotection.

4.2 Materials and methods

4.2.1 Unstabilized Catalase-loaded PLGA nanoparticles

4.2.1.1 Fabrication of unstabilized catalase-loaded PLGA nanoparticles

Catalase-loaded nanoparticles were formulated following a modified double emulsion method.[277,280] Briefly, the PLGA polymer solution was prepared by dissolving 81 mg of PLGA polymer in 3 mL of dichloromethane. To prepare polyvinyl alcohol solution, 5 gm of PVA was added to 100 mL of water with magnetic stirring on a hot plate and 70–80ºC heat was applied to dissolve it completely in the water. After preparation of the solution of polyvinyl alcohol, it was kept in the room temperature to cool down to room temperature. Then the solution of PVA was passed through a syringe filter of 0.2 μm size (Minisart single use filter unit, Sartorius Stedim Biotech, Germany). A solution of bovine liver catalase (8 mg) in 300 μL of water was prepared. The protein solution was then added to the polymer solution and vortexed for 30 seconds. After vortexing for 30 seconds, the mixture was sonicated for 1 minute on an ice bath with a probe sonicator (SONOPULS HD 2070, BANDELIN electronic, Germany) and a primary emulsion was formed. This primary emulsion was added to 18 mL solution of PVA, vortexed for 30 seconds followed by sonication in the same way as mentioned above to form the secondary emulsion. The resultant emulsion was kept stirring in a fume hood overnight for evaporation of the entire dichloromethane. The nanoparticles were recovered by centrifuging the dispersion at 39,800 x g for 30 minutes at 4ºC (Rotor JA-17, Beckman J2-21 centrifuge, Beckman Coulter Inc., CA, USA). After centrifugation, the supernatant was discarded and the pellet was

resuspended in water followed by vortexing and sonication in the same way as mentioned above. The suspension was then centrifuged again at 39,800 x g for 30 minutes at 4ºC (Rotor JA-17, Beckman J2-21 centrifuge, Beckman Coulter Inc., CA, USA). This washing step was repeated two times. Finally, the pellet was redispersed in water, vortexed and sonicated on an ice bath in the same way as mentioned above. For samples protected from lyophilization-induced damage, trehalose was added at different ratios to the final nanosuspension, mixed by vortexing and then freeze-dried.

4.2.1.2 Analysis of catalase activity of unstabilized catalase-loaded PLGA nanoparticles

To analyse enzymatic activity of the encapsulated catalase of catalase-loaded PLGA nanoparticles, the enzyme was extracted from the matrix of PLGA. 4 mL of PBS of and 4 mL of dichloromethane were added to a glass vial containing 5.9±0.5 mg of lyophilized nanoparticles and stirred for 30 minutes on a magnetic stir plate. After stirring for 30 minutes, the vial was left undisturbed for 3 hours. After 3 hours, the supernatant was collected from the top one of the two layers, transferred to an eppendorf, centrifuged at 4ºC for 10 minutes using an eppendorf centrifuge (Eppendorf Centrifuge 5417R, Eppendorf UK Limited, UK) at a speed of 10,000 rpm. Thereafter, the supernatant was taken out followed by filtration through a syringe filter of 0.2 µm size (Minisart single use filter unit, Sartorius Stedim Biotech, Germany). The filtrate was analysed for catalase activity.

Enzymatic activity of the enzyme, catalase, was determined by a modified standard catalase assay method[281-285] with the following formulae:

$$\text{Units/mL} = \frac{[\Delta A/\min(\text{Sample}) - \Delta A/\min(\text{Blank})] \times \text{Reaction volume in mL} \times \text{df}}{\varepsilon^{mM} \times \text{Sample volume in mL}}$$

Where,

df = dilution factor and

ε^{mM} = Millimolar extinction coefficient of hydrogen peroxide at 240 nm

Briefly, 100 µL of catalase solution extracted from the NPs was mixed with 900 µL of PBS in a quartz cuvette. Then, 1 mL of 20mM of H_2O_2 solution prepared in PBS was added to the cuvette, mixed rapidly by inversion and immediately placed in the chamber of a Beckman DU 800 UV/Vis Spectrophotometer (Beckman Coulter Inc., USA). The decrease of absorbance of 20mM H_2O_2 at 240 nm was monitored for 120 seconds with 5 seconds interval using the kinetic program of the spectrophotometer.

4.2.2 ATR-FTIR spectroscopy analysis

Secondary structure of unstabilized catalase-loaded into the PLGA nanoparticles was evaluated by ATR-FTIR spectroscopy. The changes in the secondary structure

of the encapsulated catalase of catalase-loaded unstabilized PLGA nanoparticles was analysed by an Agilent Cary 630 FTIR spectrometer (Agilent Technologies, Inc., CA, USA) equipped with a Diamond ATR Accessory. The IR spectra were collected in 4000 - 650 cm^{-1} region with 256 scans for each run at 4 cm^{-1} resolution. Each sample was measured at least three times. The measurements were averaged. The raw data was baseline corrected in the region of 1710 – 1610 cm^{-1} and area-normalized in this range. Peak-fitting of multiple lorentzians was then performed. This spectral processing was performed by Origin (Origin Software, Inc., CA, USA).

4.2.3 Fluorescence spectroscopy analysis

4.2.3.1 Unfolding of catalase by guanidine hydrochloride

A 6.0M guanidine hydrochloride solution in PBS and a catalase solution of 0.6 mg/mL in PBS were prepared as stock solutions. From the stock solutions, different strengths of GdnHCl and catalase solutions were prepared, and these solutions were mixed by vortexing in such a manner that every solution of the fluorescence measurements in unfolding study contained the defined concentration of GdnHCl and 0.15 mg/mL of catalase. The samples were kept overnight at room temperature for equilibration before fluorescence measurements.

Intrinsic tryptophan fluorescence on the unfolding of catalase by GdnHCl was measured with a fluorescence spectrophotometer (Varian Cary Eclipse Fluorescence Spectrophotometer, Agilent Technologies, USA) using the following

instrumental parameters: excitation wavelength 295 nm, excitation bandwidth 5 nm, emission bandwidth 5 nm, scan rate 600 nm/min. The emission was recorded in the range of 300 – 450 nm.

4.2.3.2 Fluorescence study of unstabilized catalase-loaded PLGA nanoparticles

To evaluate tertiary structural alterations of the encapsulated catalase of catalase-loaded PLGA nanoparticles, the enzyme was extracted from the matrix of PLGA. 1.5 mL of PBS of and 1.5 mL of dichloromethane were added to a glass vial containing 5.9±0.5 mg of lyophilized nanoparticles and stirred for 30 minutes on a magnetic stir plate. To rule out the possible effect of trehalose on the extraction procedure, an equivalent amount of trehalose was added to each vial containing 5.9±0.5 mg of lyophilized nanoparticles before adding PBS and dichloromethane. After stirring of 30 minutes, the vial was left undisturbed for 3 hours. After 3 hours, the supernatant was collected from the top one of the two layers, transferred to an eppendorf, centrifuged at 4ºC for 10 minutes using an eppendorf centrifuge (Eppendorf Centrifuge 5417R, Eppendorf UK Limited, UK) at a speed of 10,000 rpm. Thereafter, supernatant was taken out followed by filtration through a syringe filter of 0.2 μm size (Minisart single use filter unit, Sartorius Stedim Biotech, Germany). The filtrate was then used for fluorescence measurement with the same fluorimeter following the same instrumental parameters as mentioned above.

4.3 Results

4.3.1 Effect of trehalose on lyophilization of unstabilized catalase-loaded PLGA nanoparticles

In order to study the potential structural changes of catalase associated with lyophilization of catalase-loaded PLGA nanoparticles and potential protection of trehalose by reducing this structural alteration of catalase encapsulated into the PLGA nanoparticles, the catalase-loaded PLGA nanoparticles were fabricated without using bovine serum albumin as a stabilizer in the formulation process. Catalase activity of this unstabilized nanoparticles were measured after extraction from the nanoparticles and the result is presented in Figure 45.

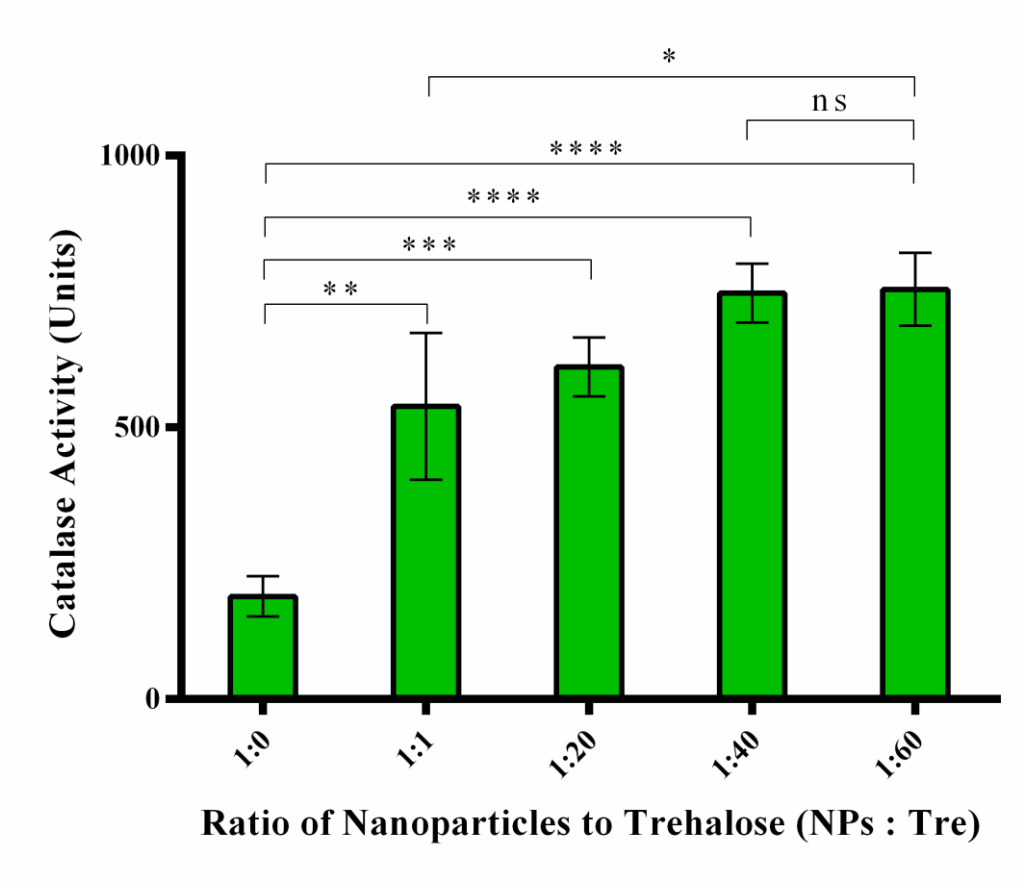

Figure 45: Role of trehalose in lyophilization of unstabilized catalase-loaded PLGA nanoparticles (n=3; ns, not significant; *P ≤ 0.05; **P ≤ 0.01; ***P ≤ 0.001; ****P ≤ 0.0001).

Catalase activity was found to be 189±37 units when the unstabilized nanoparticles were freeze-dried without trehalose. Likewise the BSA-stabilized nanoparticles, trehalose successfully reduced the loss of catalase activity of these unstabilized nanoparticles upon lyophilization. All the four ratios of trehalose applied in the study protected enzymatic activity of the encapsulated catalase significantly in comparison to the sample containing only unstabilized nanoparticles and no trehalose as a cryoprotectant. When trehalose was added as a cryoprotectant at weight ratios of nanoparticles to trehalose of 1:1, the activity of trehalose-protected nanoparticles became about 2.85 times of that of the nanoparticles which were not

cryoprotected. Although the average catalase activity increased when trehalose content was raised by 20 times from 1:1 to 1:20, the difference in catalase activity between the formulations of 1:1 and 1:20 was not statistically significant. But, the increments of 1:1 vs 1:40 and 1:1 vs 1:60 were statistically significant. Catalase activity of the formulations of 1:40 and 1:60 were very close and the difference was not statistically significant. 747±54 and 754±67 units of catalase activity were observed for the unstabilized formulations of 1:40 and 1:60, respectively.

4.3.2 ATR-FTIR spectroscopic study

The amide I spectra were checked for changes in secondary structure of the catalase loaded into the PLGA nanoparticles. The baseline corrected and area-normalized spectra in the amide I region is presented in Figure 46.

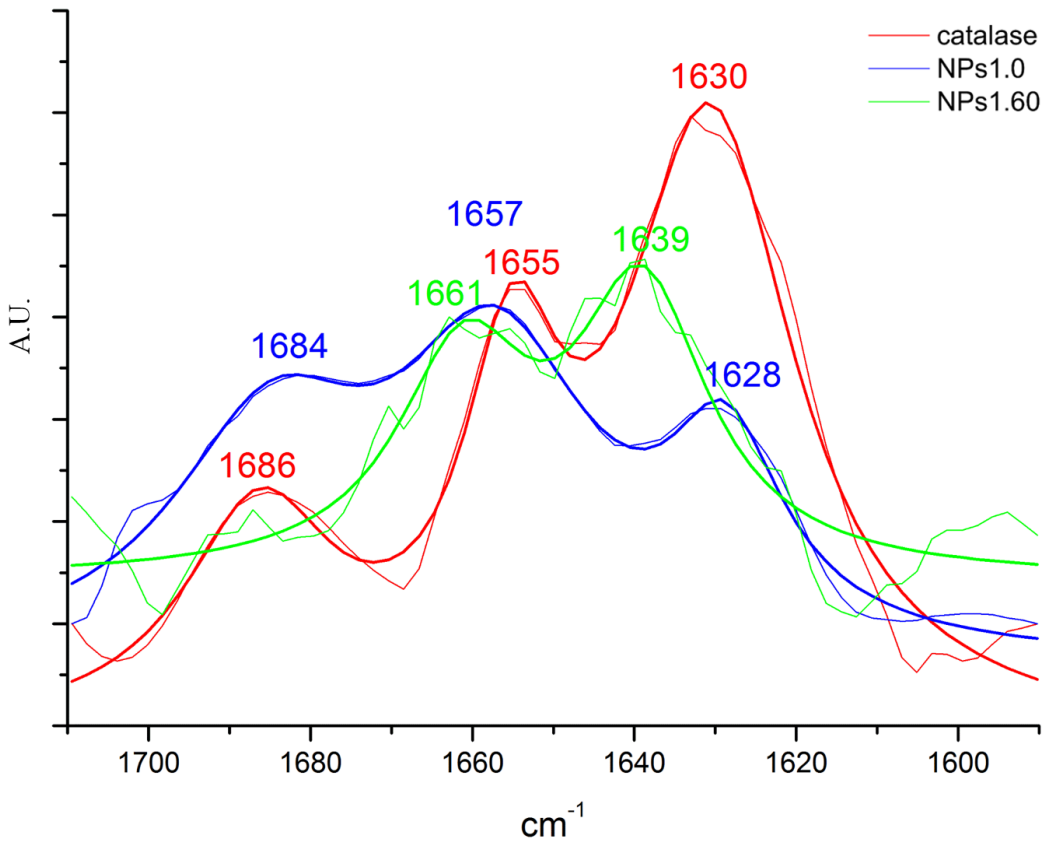

Figure 46: Baseline-corrected and area-normalized amide I spectra of native catalase, non-cryoprotected (1.0) and cryoprotected (1.60) unstabilized catalase-loaded nanoparticles.

The analysis was mainly focused on the regions of 1660 - 1650 cm^{-1} for α-helix, 1690 - 1680 cm^{-1} for intermolecular β-sheet and 1644 - 1620 cm^{-1} for intramolecular β-sheet content.[355,356] The spectra of native catalase and the nanoparticles of 1:0 formulation showed that the α-helix band of the native catalase was at 1655cm^{-1} which was reduced and slightly shifted to 1657 cm^{-1} in the nanoparticles after lyophilization without trehalose. The intermolecular β-sheet band appeared at 1686 cm^{-1} in case of native catalase and the band slightly shifted to 1684 cm^{-1} with an increased content in case of 1:0 nanoparticles. The band observed at 1630 cm^{-1} for native catalase and that observed at 1628 cm^{-1} for 1:0 nanoparticles could be ascribed to intramolecular β-sheet. The intramolecular β-sheet band was drastically

reduced from native catalase to 1:0 nanoparticles, and slightly shifted to lower frequency. In the case of 1:60 nanoparticles which were cryoprotected by trehalose, two absorption bands appeared at 1639 cm^{-1} and at 1661 cm^{-1} which were outside of the above mentioned regions. Then, we compared the spectra of freeze-dried trehalose and that of 1:60 nanoparticles, and observed that the spectra were almost similar and overlapping each other (Figure 47).

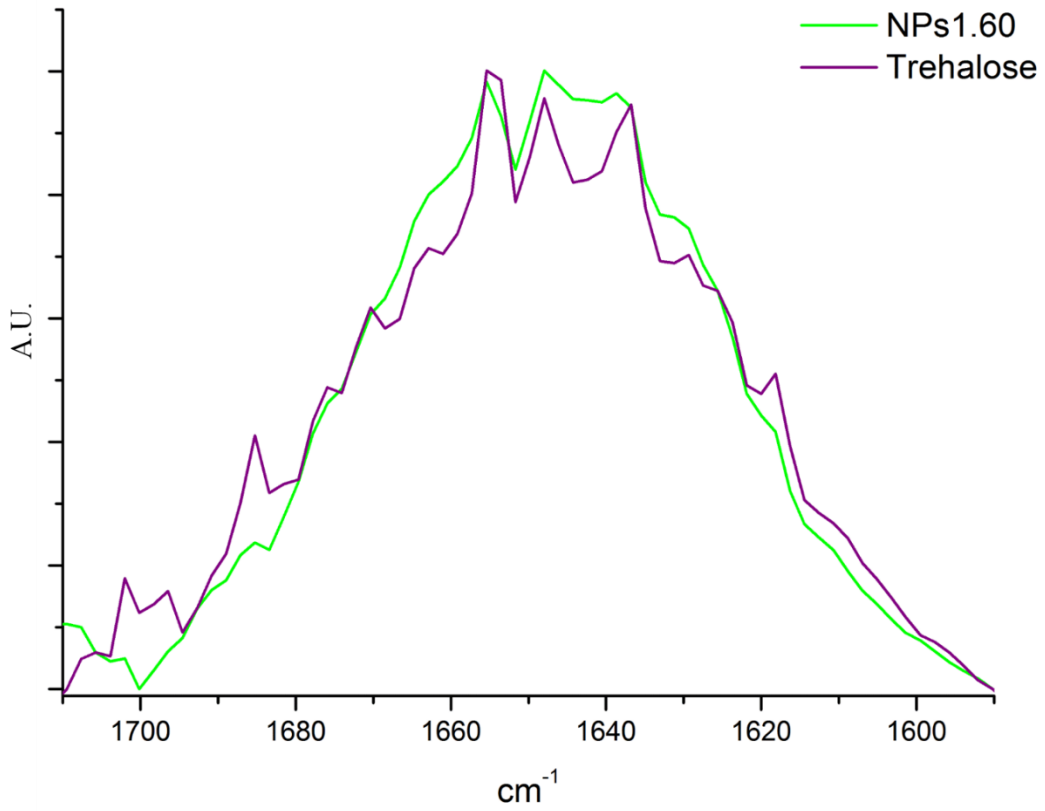

Figure 47: Comparison of the spectra of freeze-dried trehalose and cryoprotected nanoparticles (1.60).

This similarity in the spectra of freeze-dried trehalose and that of 1:60 nanoparticles indicated that these two bands at 1639 cm^{-1} and at 1661 cm^{-1} were coming from the trehalose that was added as a cryoprotectant, not from the 1:60 nanoparticles.

4.3.3 Fluorescence spectroscopic study

4.3.3.1 Fluorescence intensity of catalase and unstabilized catalase-loaded PLGA nanoparticles

Tryptophan emission was monitored in an unfolding study of catalase in the presence of guanidine hydrochloride. In the absence of GdnHCl, fluorescence maximum emission wavelength (λ_{max}) of catalase solution observed was 334.7±0.6 nm. Effect of GdnHCl on tryptophan fluorescence intensity of catalase solution at 335 nm is shown in Figure 48.

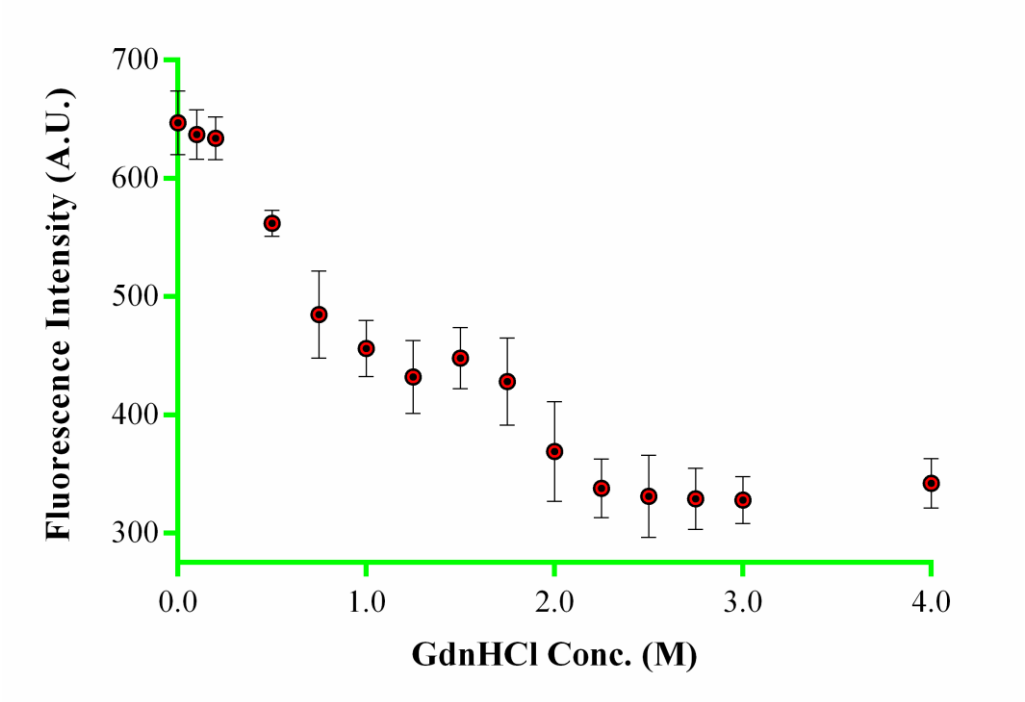

Figure 48: Effect of GdnHCl on tryptophan fluorescence intensity of catalase solution observed at 335 nm.

Fluorescence intensity reduction with increasing concentration of GdnHCl was also observed at 328 nm and this effect is presented in Figure 49.

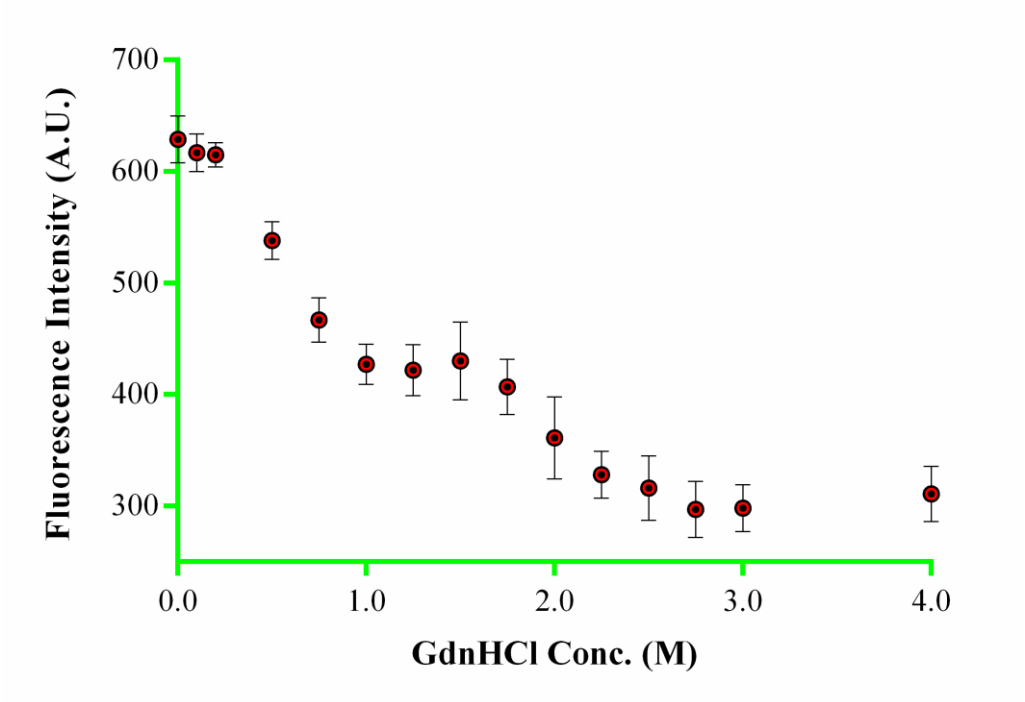

Figure 49: Effect of GdnHCl on tryptophan fluorescence intensity of catalase solution observed at 328 nm.

The spectra observed at both 328 and 335 nm showed similar pattern of reduction in tryptophan fluorescence intensity with gradual increasing of GdnHCl concentration in the protein solution. Fluorescence intensity was found to start to decline from 0.1M GdnHCl, starting concentration of GdnHCl of this study. Thereafter, the intensity reduction seemed to be slow until the next concentration of this study, 0.2M GdnHCl. Then, the intensity sharply fell over increasing concentration of GdnHCl until getting near 1.0M GdnHCl. The intensity changed a

little from 1.25M to 1.75M of GdnHCl, and finally it reached a plateau at 2.75M GdnHCl.

Tryptophan fluorescence intensities of catalase solutions extracted from both the formulations of 1:0 and 1:60 of unstabilized catalase-loaded nanoparticles were also measured and compared. Comparison of their intensities at 328 nm is presented in Figure 50.

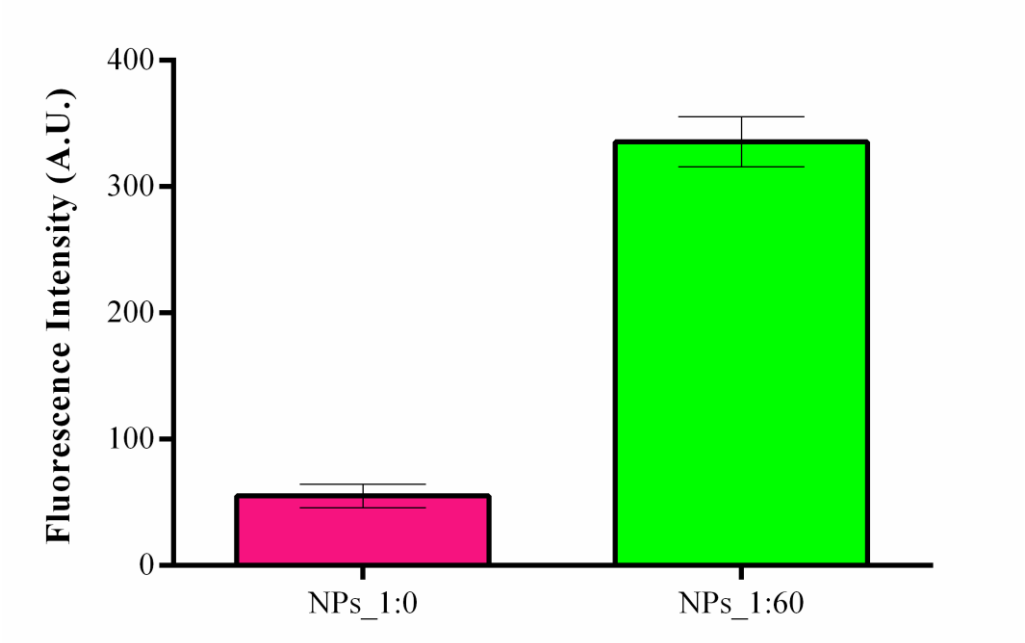

Figure 50: Comparison of tryptophan fluorescence intensities of 1:0 and 1:60 formulations of NPs.

The catalase solution extracted from the 1:0 formulation of nanoparticles that was not cryoprotected by trehalose, produced intensity of 55±9 a.u., but the protein solution extracted from the cryoprotected 1:60 formulation produced intensity of 336±20 a.u. The intensity of the nanoparticles cryoprotected by trehalose at a

weight ratio of nanoparticles to trehalose of 1:60, is about six times of that of the nanoparticles those were not cryoprotected by trehalose.

4.3.3.2 Tryptophan maximum emission wavelength of catalase and unstabilized catalase-loaded PLGA nanoparticles

The tryptophan emission maximum of catalase solution was changed with the concentration of guanidine hydrochloride added for unfolding of the protein. The changes in Trp λ_{max} is presented in Figure 51.

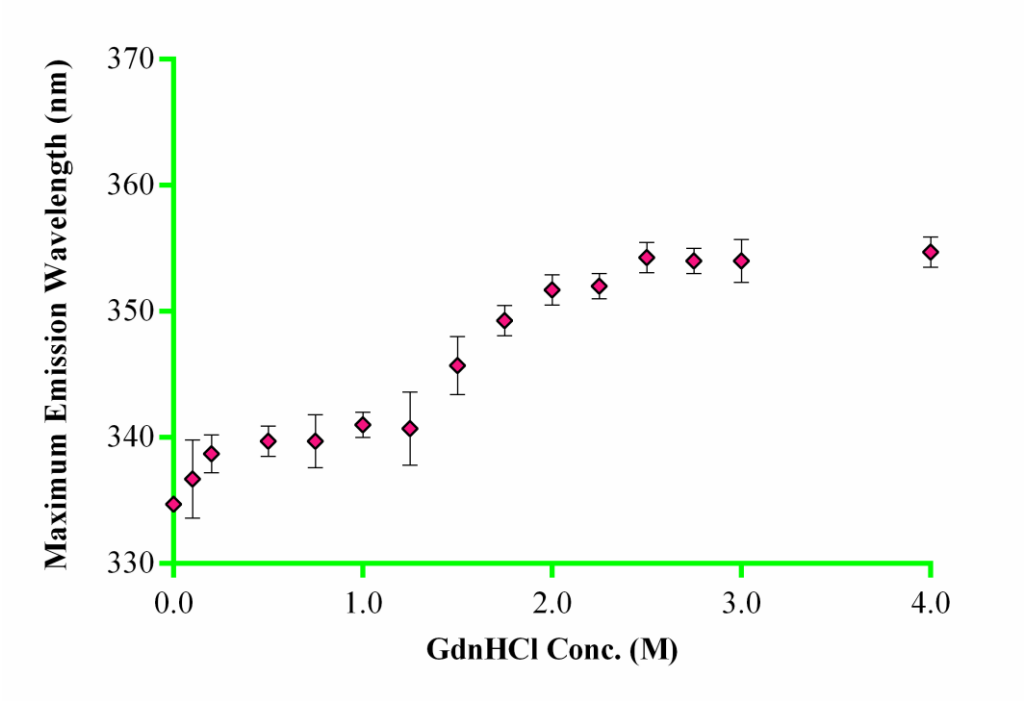

Figure 51: Changes in tryptophan maximum emission wavelength of catalase with raising concentration of GdnHCl.

The tryptophan emission maximum was red-shifted with gradual denaturation of the enzyme, catalase. In the absence of the denaturing agent, Trp λ_{max} was 334.7±0.6 nm. At the highest concentration of GdnHCl of this study, 4.0M, the Trp λ_{max} was found to be 354.7±1.2 nm, and this was very similar to that observed for the 3.0M GdnHCl, which was 354.0±1.7 nm.

Tryptophan emission maximum was also monitored for the solutions extracted from both the formulations of 1:0 and 1:60 of the unstabilized catalase-loaded nanoparticles and Trp λ_{max} was compared. The comparison is presented in Figure 52.

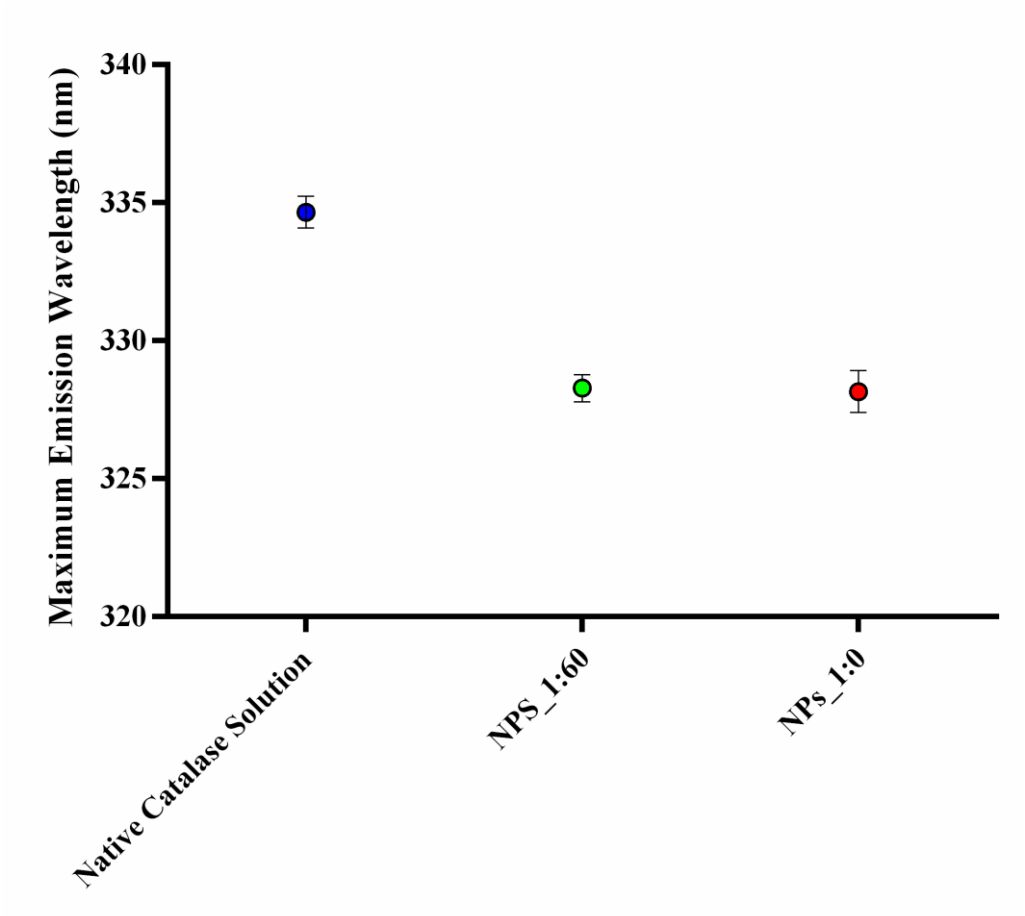

Figure 52: Comparison of the tryptophan maximum emission wavelengths of the native catalase solution and solutions extracted from NPs.

Tryptophan emission maximum was blue- shifted for NPs-extracted solutions in presence of trehalose. The Trp λ_{max} was found very similar for both types of nanoparticles and it was 328.2±0.8 nm and 328.3±0.5 nm for 1:0 and 1:60 nanoparticles, respectively.

4.4 Discussion

This study demonstrated that lyophilization caused structural alterations of catalase encapsulated into the PLGA nanoparticles and cryoprotection by trehalose could minimize these structural alterations.

The study of chapter 2 showed that lyophilization induced a loss of catalase activity of catalase-loaded PLGA nanoparticles which were stabilized with another protein bovine serum albumin. The best cryoprotection was achieved with the addition of trehalose at a weight ratio of 1:60 of nanoparticles to trehalose. These nanoparticles were found to be effective in reducing oxidative stress-induced damage to cardiomyocytes in a cell culture model of oxidative stress and were more effective than other two formulations, 1:80 and 1:100. As the BSA added as a stabilizer to the primary emulsification step of the encapsulation process may interfere with structural characterization of the encapsulated catalase by infrared and fluorescence spectroscopy, catalase-loaded PLGA nanoparticles were formulated without BSA for investigation of structural changes in the encapsulated catalase upon lyophilization of the nanoparticles. To confirm that catalase activity was maintained upon lyophilization according to the same ratio of the nanoparticles to trehalose employed in the previous study, the same experiment was conducted with the unstabilized nanoparticles instead of BSA-stabilized nanoparticles. Here it was also observed that the cryoprotection by trehalose with the ratio of 1:60, preserved enzymatic activity of the encapsulated catalase most efficiently alike previous studies. So, the formulation of 1:60 was selected as the cryoprotected sample and that of 1:0 selected as the sample not cryoprotected. It was also noticed in the study of chapter 2 that trehalose was not interfering with the enzymatic activity analysis

of lyophilized catalase-loaded nanoparticles, and accordingly it was not added any trehalose to the extraction process of enzymatic activity measurement of the formulations of 1:1, 1:20, 1:40 and 1:60 lyophilized nanoparticles.

Study of alterations in the secondary structure of catalase by ATR-FTIR spectroscopy showed that the α-helix band was shifted towards a slightly higher frequency from native catalase to catalase-loaded nanoparticles those were not cryoprotected and intensity of the band was dropped compared to the native catalase. In native catalase, the intermolecular β-sheet band appeared at 1686 cm^{-1} and this band shifted to 1684 cm^{-1} with an increased content for the 1:0 nanoparticles. This increment in the intensity of band near 1685 cm^{-1}, and hence rising of the intermolecular β-sheet content, could be attributed to increased aggregation of the protein.[356-358] Usually, lyophilization of proteins causes a reduction in the α-helix content with a concomitant increase in the β-sheet content. The augmentation in β-sheet content is possibly because of protein-protein interactions, which lead to formation of intermolecular β-sheets upon elimination of water by lyophilization. So, the β-sheet content of a lyophilized protein does not indicate its real intramolecular structural content. Therefore, α-helix content of a protein is regarded as a better indicator of its structural integrity.[359] PLGA and PVA do not interfere with the protein IR spectrum in the amide I region.[249,360]

The spectral similarity between trehalose and the cryoprotected 1:60 nanoparticles in this study could be attributed to the very high amount of trehalose that was added to the nanoparticles for cryoprotection. Due to this high ratio of nanoparticles to trehalose of 1:60, it was not possible to get absorption peak with the ATR-FTIR instrument. It was found in the current study that the α-helix content of catalase was

reduced upon lyophilization of the 1:0 nanoparticles with a concomitant rise in the intermolecular β-sheet content. It warrants further investigation to confirm whether the lyophilization process-induced alterations in the α-helix and the intermolecular β-sheet contents of the enzyme could be minimized by cryoprotection of the nanoparticles brought about by trehalose.

It was also attempted to investigate tertiary structural changes of the catalase-loaded into the PLGA nanoparticles by fluorescence spectroscopy. In the studies of proteins, intrinsic tryptophan fluorescence emission is a valuable approach.[242,261-263] To study alterations of the tertiary structure in the microenvironment of the tryptophan residues in proteins, fluorescence spectroscopy of protein solutions is widely used.[242,264] Among the fluorescence properties used in fluorescence spectroscopic study of proteins, fluorescence intensity and maximum emission wavelength are common.[264-267]

Guanidine hydrochloride-mediated unfolding study of catalase was performed by monitoring intrinsic tryptophan fluorescence of catalase at different GdnHCl concentrations. Fluorescence maximum emission wavelength (λ_{max}) of catalase solution observed was 334.7±0.6 nm in the absence of GdnHCl and the intensity was found to decline with increasing concentration of GdnHCl at 335 nm (Figure 48). But, the catalase solutions extracted from the formulation of 1:0 nanoparticles in presence of trehalose in the protein solutions produced no intensity at all at 335 nm. It is noteworthy that trehalose was added at an equivalent ratio of 1:60 nanoparticles in the extraction process of 1:0 catalase-loaded nanoparticles to rule out any possible effect of trehalose on the extraction process-induced loss of fluorescence intensity of catalase. Both types of nanoparticles produced maximum

intensity at around 328 nm. Fluorescence spectrum of GdnHCl-induced denaturation of catalase also showed a gradual diminution of fluorescence intensity at 328 nm (Figure 49), similar trend with that observed at 335 nm (Figure 48). The GdnHCl-induced unfolding study of catalase, a multi-tryptophan protein, confirmed that its fluorescence intensity declined with gradual increment of GdnHCl concentration. The intensity generated from the solutions of 1:60 nanoparticles was as high as six times of the intensity generated by the solutions of 1:0 nanoparticles at 328 nm (Figure 50). It was reported that fluorescence intensity was related with aggregation of proteins.[252,361] It has been shown by a simulation study that fluorescence intensity was directly linked with the folded/unfolded states of the protein.[242] Activity is considered as the most sensitive measure for studying conformational changes of an enzyme, because any minute change in the enzymatic activity reflects subtle restructuring at its active site which is related with conformational alteration of the enzyme. Prakash *et al.* reported that the enzymatic activity of catalase was lost in a concentration-dependent manner in the presence of GdnHCl.[274] Reduction of both catalase activity and fluorescence intensity of catalase solutions in presence of GdnHCl strongly indicate that the activity and conformational state of the catalase are proportionately correlated with the fluorescence intensity of catalase solution. From the comparative intensities of the nanoparticles, it could be inferred that lyophilization of the nanoparticles caused a structural alteration of the encapsulated enzyme with concomitant reduction in the fluorescence intensity of the nanoparticles which were not cryoprotected by trehalose. Trehalose added as a cryoprotectant minimized this structural changes of the encapsulated enzyme induced by lyophilization, and could help to preserve the structural integrity of the enzyme upon lyophilization. This ability of trehalose in

resisting conformational changes of catalase upon lyophilization of catalase-loaded nanoparticles is consistent with the catalase activity observed in Figure 45.

The tryptophan emission maximum was red-shifted with gradual denaturation of the catalase enzyme (Figure 51). Prakash *et al.* and Banerjee *et al.* reported that the Trp λ_{max} red-shifted similarly with increasing denaturation of catalase.[274,362] The red-shifted Trp λ_{max} for denatured catalase was reported to be 356 nm, which is close to the Trp λ_{max} observed in this study.[273] As it was observed that lyophilization caused a structural change in the native structure of the encapsulated catalase with concomitant loss of catalase activity of the catalase-loaded nanoparticles which were not cryoprotected by trehalose, it was supposed that the Trp λ_{max} of the 1:0 nanoparticles would appeared to be red-shifted in comparison to the native catalase solution and cryoprotected 1:60 nanoparticles-extracted solution. Rather it was found that the Trp λ_{max} of both the 1:0 and 1:60 nanoparticles-extracted solutions blue-shifted (Figure 52) and exhibited Trp λ_{max} at 328 nm, whereas the native catalase solution exhibited at 335 nm. The reason can be attributed to the presence of the same amount of trehalose in the solutions extracted from both of the nanoparticles, where trehalose was added as a cryoprotectant to the 1:60 nanoparticles and the same amount of trehalose was added to the extraction process of 1:0 nanoparticles. Instead of red-shifting of the Trp λ_{max}, the trehalose present in the extracted solutions caused to produce this blue-shift. Lakshmi *et al.* indicated an increased hydrophobicity in sugar solutions.[363] It can be inferred that trehalose present in the extracted solutions created more hydrophobic environment for catalase. Further investigations are warranted to see the effect of cryoprotection on the shifting of Trp λ_{max} of nanoparticles-extracted solutions.

4.5 Conclusion

The study of chapter 2 demonstrated that trehalose acting as a cryoprotectant could reduce the lyophilization-induced loss of enzymatic activity of catalase-loaded PLGA nanoparticles. In this work, structural alterations of the catalase encapsulated into the unstabilized catalase-loaded PLGA nanoparticles upon lyophilization with and without cryoprotection provided by trehalose were studied. For structural study of the encapsulated enzyme, catalase-loaded PLGA nanoparticles were formulated without adding another protein, bovine serum albumin, a stabilizer that was added to reduce loss of catalase activity induced by emulsification steps of the encapsulation process. It was shown in this study that trehalose could lessen the enzyme's activity loss induced by freeze-drying of the unstabilized nanoparticles.

Catalase and catalase-loaded PLGA nanoparticles were analysed by ATR-FTIR spectroscopy to investigate the encapsulated enzyme's secondary structural changes upon lyophilization with and without cryoprotection by trehalose. The baseline corrected and area-normalized IR spectra demonstrated that α-helix content of the enzyme was reduced and intermolecular β-sheet content of the enzyme was increased in the lyophilized nanoparticles when there was no cryoprotection of the nanoparticles by trehalose. Dropping of the α-helix content with concomitant rise in the intermolecular β-sheet content of the enzyme indicated denaturation of the enzyme upon freeze-drying of the catalase-loaded PLGA nanoparticles. But, it was not possible to obtain spectrum for the cryoprotected nanoparticles with the ATR-FTIR instrument due to a very high amount of trehalose present in the catalase-loaded nanoparticles. So, it could not be ascertained with this ATR-FTIR study, whether trehalose could minimize the changes in the secondary

structures of the encapsulated catalase upon lyophilization of the nanoparticles or not. Circular dichroism (CD) spectroscopy can be utilized to overcome this problem caused by this high amount of trehalose.

Conformational changes of the encapsulated catalase in the nanoparticles was studied by fluorescence spectroscopy. Guanidine hydrochloride-induced unfolding study of catalase confirmed that tryptophan fluorescence intensity was decreased with increasing concentration of GdnHCl. Using this observation of reducing fluorescence intensity with increasing concentration of GdnHCl was proportionately correlated with the enzymatic activity of catalase. Based on this correlation of fluorescence intensity and enzymatic activity of catalase, it was demonstrated that trehalose as a cryoprotectant could minimize the loss of tertiary structural integrity of the encapsulated catalase upon freeze-drying of the nanoparticles and, hence tried to stabilize the conformational state and enzymatic activity of the encapsulated catalase upon lyophilization.

Denaturation of catalase induced by GdnHCl was shown to cause a red-shift of the tryptophan emission maximum. Due to the increased hydrophobicity of the nanoparticles-extracted solutions incurred by a high amount of trehalose present in both types of the solutions used for fluorescence measurements, resulted in a blue-shift of the Trp λmax for both cryoprotected and non-cryoprotected nanoparticles, compared to native catalase solution. So, study of the Trp λ_{max} could not provide any conclusive evidence of the cryoprotection ability of trehalose in preserving conformational stability of the encapsulated catalase of catalase-loaded PLGA nanoparticles.

5 Summary and future work

5.1 Summary

Nanoparticle-based drug delivery systems offer advantages over conventional drug delivery systems. From small to large molecules including biomacromolecules can be successfully delivered using the approach of nanoparticles. Nonetheless, there are still some critical problems associated with the nanoparticle-based drug delivery systems which restrict the widespread use of nanoparticles. Physical instability like formation of the nanoparticle aggregates and particle fusion, chemical instability due to the degradation of the polymeric materials used in manufacturing of the nanoparticles, drug leakage from the nanoparticulate delivery systems, and reactivity of drugs during storage condition, are common when the nanoparticulate delivery systems are stored in the form of aqueous suspensions.

Use of proteins in medical field is rapidly expanding. Two virtues of proteins make them attractive as a therapeutic tool, potency and high specificity in their activities. But, the delivery of protein is challenging as they are labile in nature. They are in risk of easy inactivation by proteases, aggregation and natural inhibitors. During delivery of the proteins, they may face adverse environment that may cause denaturation or aggregation of the proteins. The denatured proteins may pose the threat of adverse reactions in the body. It is possible to minimize these delivery associated problems of proteins by encapsulating them into polymeric nanoparticles and then delivering the protein-loaded nanoparticles. Poly(lactic-co-glycolic acid)

(PLGA) is the mostly used synthetic polymer for producing nanoparticles because of possessing some favourable properties like biocompatibility and biodegradability, extended release profile, variable mechanical properties and above all non-toxicity. It is also approved by the USFDA for drug delivery.

Freeze-drying or lyophilization is a very useful technique to stabilize the nanoparticles by eliminating water from the nanoparticulate suspensions. In the freeze-drying process, water is eliminated by sublimation and desorption from a nanosuspension kept in its frozen state under vacuum in the freeze-drier chamber. Lyophilization can also reduce the loss of stability of the encapsulated protein alongside stabilizing the polymeric nanoparticles containing the protein. But, lyophilization itself is a stress for stability of the polymeric nanoparticles. Freeze-drying process creates stresses of freezing and dehydration that can destabilize a colloidal suspension of the nanoparticles. It is also a stress for the encapsulated protein, where it negatively influences the encapsulated protein's native conformational state. Cryoprotectants incorporated into the nanosuspensions of protein-loaded nanoparticles before freeze-drying, can minimize aggregation tendency of the nanoparticles, improve redispersibility of the reconstituted freeze-dried nanoparticles and reduce structural alterations of the protein encapsulated into the nanoparticles.

Nanoprecipitation is a very common method used to prepare nanoparticles. Sugars such as trehalose, mannitol, sucrose and glucose are the most commonly used cryoprotectants in freeze-drying of nanoparticles. Among the sugars, trehalose is a superior cryoprotectant. Before going to fabricate the protein-loaded PLGA nanoparticles, plain PLGA nanoparticles were prepared in this study following the

nanoprecipitation method and freeze-dried with trehalose in order to confirm that trehalose could successfully act as a cryoprotectant in lyophilization of this study's PLGA nanoparticles. It was observed that trehalose could minimize the lyophilization-induced aggregation of plain PLGA nanoparticles and helped in redispersibility of the reconstituted freeze-dried PLGA nanoparticles. Without cryoprotection by trehalose, a high degree of aggregation of the nanoparticles was observed after freeze-drying.

Following confirmation of the cryoprotection provided by trehalose in the lyophilization of plain PLGA nanoparticles, it was attempted to fabricate protein-loaded PLGA nanoparticles, targeting encapsulation of the body's endogenous antioxidant enzyme catalase, into PLGA nanoparticles. A two-step nanoprecipitation method reported in the literature for preparing protein-loaded PLGA nanoparticles was followed to fabricate catalase-loaded PLGA nanoparticles. This method could not produce any nanoparticles at all in our laboratory, even with lysozyme enzyme, the same protein of that study. Afterwards the most commonly used method, double emulsion method, was adopted for encapsulating the enzyme into PLGA nanoparticles.

Very low enzymatic activity was detected from the encapsulated catalase, when catalase-loaded PLGA nanoparticles were formulated without any stabilizer. Enzymatic activity of the encapsulated catalase was found to be only 1.47% of the activity of catalase, initially added to the inner aqueous phase. Because of this too low activity, it was attempted to investigate the reason and remedy of this massive loss of enzymatic activity upon the encapsulation process. There are two emulsification steps in the protein encapsulation process in double emulsion

method. Previous studies suggested that emulsification step, particularly the primary emulsification is the main step in the encapsulation process where denaturation of proteins occur maximally. In this study, it was observed that ultrasonication is more detrimental to the enzyme than vortexing in presence of the water/dichloromethane interface. It was also shown that vortexing and ultrasonication did not harm to the enzyme activity in absence of the interface between water and dichloromethane. In order to reduce the emulsification-induced damage to the enzymatic activity, two commonly used stabilizers, trehalose and bovine serum albumin were employed in the inner aqueous phase of primary emulsification step. It was observed that trehalose and BSA could minimize the emulsification-induced loss of enzymatic activity of catalase in a concentration-dependent manner. Among the four concentrations of each of the two additives used in this study, trehalose at the concentration of 50 mg/mL and BSA at the concentration of 25 mg/mL showed the best protection to the catalase activity upon emulsification process.

Incorporation of BSA into the inner aqueous phase at its most protective concentration reduced the loss of catalase activity in the formulation process of catalase-loaded PLGA nanoparticles. Enzymatic activity of the encapsulated catalase in the BSA-stabilized nanoparticles was about four times higher than that observed in the unstabilized catalase-loaded nanoparticles. Surprisingly, trehalose failed to show any such protective action in preserving the catalase activity in the trehalose-stabilized catalase-loaded nanoparticles.

Trehalose is a very good cryoprotectant of labile proteins alongside offering cryoprotection to PLGA nanoparticles. Accordingly, trehalose in this study

demonstrated its cryoprotection efficacy in minimizing the lyophilization-induced loss of enzymatic activity of encapsulated catalase in the BSA-stabilized catalase-loaded PLGA nanoparticles. This cryoprotection of trehalose observed in this study was concentration-dependent. The best cryoprotection was noticed when trehalose was added to the nanosuspension at a weight ratio of nanoparticles to trehalose of 1:60, and this amount of trehalose could preserve nearly 13.5% of the initial enzymatic activity of catalase that was added to the primary emulsification step of the encapsulation process.

After formulation of BSA-stabilized catalase-loaded PLGA nanoparticles cryoprotected by trehalose, efficacy of the cryoprotected nanoparticles in reducing oxidative stress-induced damage to cardiac myocytes was evaluated.

Myocardial infarction is a life-threating condition and needs immediate treatment and hospitalization. In myocardial infarction, two processes are involved in inflicting myocardial damage – ischemia and successive reperfusion therapy, and this damage is termed as myocardial ischemia/reperfusion injury. Reperfusion itself causes overproduction of ROS and these ROS damage cardiomyocytes through oxidation of nucleic acids, proteins and cellular machinery. Reperfusion injury has been suggested to be responsible for up to 50% of the final myocardial infarct size and this resultant infarct size is related with development of chronic heart failure.

Exposing cells to hydrogen peroxide is a recognized cellular model of inducing oxidative stress in cells. HL-1 cardiomyocytes is a useful model for studying features of cardiac physiology and pathophysiology due to having the same characteristics of differentiated cardiomyocytes while maintaining proliferation in

cell culture. Hydrogen peroxide was employed in this study to induce oxidative stress in HL-1 cardiomyocytes. 750µM of hydrogen peroxide was identified as sub-lethal concentration of H_2O_2 in this study. After injury with this sub-lethal concentration of H_2O_2, about 67% cells remained viable after 3 hours. This sub-lethal concentration of H_2O_2 has been employed in evaluating the therapeutic potential of the cryoprotected catalase-loaded PLGA nanoparticles in reducing oxidative stress-induced loss of cell viability of the cardiomyocytes. The nanoparticles demonstrated cardioprotective action in a pre-injury treatment model, where the cells were incubated with the nanoparticles for 3 hours before assaulting them with the sub-lethal concentration of H_2O_2 for next 24 hours. The nanoparticles were also evaluated in rescuing the cells in a post-injury treatment model, where the cells were assaulted with the sub-lethal concentration of H_2O_2 for 3 hours followed by treatment with the nanoparticles for the next 24 hours.

The nanoparticles demonstrated cardioprotective action in a dose-dependent manner in both pre- and post-injury models. Lowest dose of the nanoparticles employed in this study proved its insufficiency to elicit any cardioprotective response in both pre- and post-injury treatment models. The highest dose applied in this work showed the least cardioprotective action among the effective doses in pre-injury treatment case. In post-injury treatment case, the highest dose failed to show any cardioprotective action. The most effective dose of the nanoparticles observed in this study was 200 µg/well for both of pre- and post-injury treatment models. In the pre-injury treatment case, the cardioprotective action declined when the nanoparticles dose was increased from the most effective dose to the highest dose of this study which was 400 µg/well, and the protective action disappeared in post-

injury treatment when shifted from the most effective dose to the highest dose, 400 µg/well. This dose-responsive effects of the nanoparticles is suggestive of a tolerable limit of the nanoparticles for the cardiomyocytes beyond which the cells become more vulnerable and less capable to recover their metabolic activity from the damage effected by the oxidative insult. This is also reflected in the cytocompatibility study. All of the doses applied in this study were cytocompatible, compared to the control. But the highest dose caused a slight loss of cell viability although it was not statistically significant in comparison to the control.

It has also been compared the efficacies of the three formulations of cryoprotected nanoparticles where trehalose was added as a cryoprotectant at weight ratios of nanoparticles to trehalose of 1:60, 1:80 and 1:100. As there was no significant difference among enzymatic activities of the encapsulated catalase of the three formulations, their therapeutic efficacies using the pre-injury treatment model were evaluated and compared applying the most effective dose, 200 µg/well. This comparative study of the three formulations confirmed that the formulation of 1:60 was the right one to continue for further experiments.

Alongside necrosis, apoptosis also contributes to the total cell loss during myocardial ischemia/reperfusion. Studies suggested that apoptosis is mainly activated or increased during reperfusion after an episode of ischemia. Following ischemia/reperfusion, apoptosis is considered to be accountable for the ongoing loss of cardiomyocytes. Apoptotic cells in the peri-necrotic area is highly correlated with the development of myocardial infarction and expansion of the infarction area following reperfusion. Studies demonstrated that reduction of apoptosis could protect the myocardium after myocardial I/R injury. Efficacy of the cryoprotected

catalase-loaded PLGA nanoparticles in decreasing apoptosis in HL-1 cardiomyocytes was assessed, where apoptosis was induced by 200µM of H_2O_2. Apoptosis was measured by flow cytometric analysis using caspase-3 & -7 assay and annexin V-PI assay. Both assays demonstrated efficacy of the nanoparticles in reducing apoptosis of the cardiomyocytes, compared to the control. This study showed a large reduction in the percentages of apoptotic cells in HL-1 cardiomyocytes. Therefore, it is expected that the cryoprotected catalase-loaded PLGA nanoparticles might be an effective therapeutic approach in conserving the myocardial function after myocardial infarction, because of exerting a high anti-apoptotic effect by the nanoparticles. The nanoparticles could also be effective in preventing the development of heart failure or deteriorating the condition of the heart failure where apoptosis plays a critical role.

The ability of the catalase-loaded PLGA nanoparticles to neutralize the injurious agent, hydrogen peroxide, was also assessed in this study. It was observed that exposure of the cells to 1000µM H_2O_2 for 24 hours left around 81% of the cells viable in presence of the nanoparticles. In contrast, no viable cells were detected after assaulting them with this lethal concentration of H_2O_2 for 24 hours in absence of the nanoparticles.

Flow cytometric cellular uptake study suggested a significant uptake of the nanoparticles by the HL-1 cells. But, the uptake study by super resolution microscopic imaging revealed that all the nanoparticles observed over the cells were not internalized into the HL-1 cells. Only a small portion of the nanoparticles were internalized into the cells and most of the nanoparticles remained adsorbed and associated with the cell membrane of the HL-1 cells. Studies suggested that

nanoparticles could be internalized into the cardiomyocytes by enhanced endocytosis after reperfusion passively induced by hydrogen peroxide and exerted the cardioprotective action. The actual internalization of the nanoparticles was not reflected in the microscopic images, because the cells were not treated by hydrogen peroxide before obtaining microscopic samples.

Catalase is a major endogenous antioxidant enzyme and this enzyme is considered to be accountable for most of the peroxidase activities in the cardiac cells. The promising protective effect demonstrated by the cryoprotected catalase-loaded PLGA nanoparticles in rescuing the cardiomyocytes from oxidative stress-induced damage makes it a valuable candidate for effective therapeutic approach in myocardial ischemia/reperfusion injury and heart failure.

After confirming that trehalose could minimize lyophilization-induced loss of enzymatic activity of catalase loaded into the PLGA nanoparticles, and these trehalose-cryoprotected nanoparticles were effective in reducing oxidative stress-induced damage in a cell culture model of oxidative stress in HL-1 cardiomyocytes, the structural changes in the catalase loaded into the PLGA nanoparticles upon lyophilization of the nanoparticles and how the structural changes were influenced by the cryoprotection incurred by trehalose were investigated. For studying structural alterations of the encapsulated enzyme, catalase-loaded PLGA nanoparticles were prepared without using bovine serum albumin as a stabilizer in the encapsulation process as the second protein would interfere with the structural study of the encapsulated enzyme. Analysis of catalase activity of the unstabilized catalase-loaded PLGA nanoparticles also showed that cryoprotection by trehalose

could reduce the loss of enzymatic activity of the catalase-loaded nanoparticles upon freeze-drying.

ATR-FTIR spectroscopy was employed to study secondary structural alterations of the catalase encapsulated into the nanoparticles. The baseline corrected and area-normalized IR spectra showed that α-helix content of the enzyme was reduced in the lyophilized nanoparticles which were not cryoprotected by trehalose. On the contrary, compared to the native catalase, intermolecular β-sheet content was increased in the lyophilized nanoparticles in absence of cryoprotection, and this increased intermolecular β-sheet content indicated aggregation of the native protein. In absence of cryoprotection by trehalose, reduction in the α-helix content which is a better indicator of a protein's structural integrity, with concomitant rise in the intermolecular β-sheet content of the encapsulated catalase of the lyophilized nanoparticles suggested that the enzyme was subjected to denaturation upon lyophilization of the nanoparticles.

The secondary structure of the encapsulated catalase of the cryoprotected unstabilized catalase-loaded nanoparticles was also attempted to investigate. But, the spectrum of the cryoprotected nanoparticles and that of trehalose looked almost similar and this spectral similarity was attributed to the presence of an excessive amount of trehalose which was added as a cryoprotectant at a weight ratio of nanoparticles to trehalose of 1:60. In presence of this high amount of trehalose in the cryoprotected nanoparticles, the ATR-FTIR instrument could not produce detectable signal for secondary structure of the encapsulated catalase. Further investigations are needed to prove whether lyophilization-induced secondary

structural alterations could be minimized by cryoprotecting the nanoparticles with trehalose.

It was then attempted to investigate tertiary structural changes of the catalase loaded into the PLGA nanoparticles using fluorescence spectroscopy. In guanidine hydrochloride-mediated unfolding study of catalase, it was observed that tryptophan fluorescence intensity declined with increasing concentration of GdnHCl. This observation of decreasing fluorescence intensity with rising concentration of GdnHCl could be correlated with the findings of a study that showed that enzymatic activity of catalase was dropped with increasing concentration of GdnHCl. This correlation proved that intrinsic tryptophan fluorescence intensity of catalase solution is proportional to the enzymatic activity of catalase. The fluorescence intensity data of the nanoparticles demonstrated that the intensity generated by the cryoprotected nanoparticles was about six times of the intensity generated by the non-cryoprotected nanoparticles, and this higher fluorescence intensity of the cryoprotected nanoparticles confirmed that trehalose could preserve the structural integrity of catalase by resisting the enzyme's conformational alterations induced by lyophilization of the catalase-loaded nanoparticles.

Increasing denaturation of catalase by GdnHCl resulted in a red-shift of the tryptophan emission maximum. Accordingly, it was supposed that the Trp λ_{max} of the non-cryoprotected nanoparticles-extracted solution would be red-shifted compared to the native catalase solution and cryoprotected nanoparticles-extracted solution. In contrast, solutions extracted from both the cryoprotected and non-cryoprotected nanoparticles blue-shifted to 328 nm and the native catalase solution

exhibited the Trp λ_{max} at 335 nm. This blue-shifting of both of the nanoparticles was attributed to the presence of trehalose in both of the nanoparticles-extracted solutions which were used for fluorescence measurements. Trehalose present in the extracted solutions caused to create a more hydrophobic environment for the tryptophan residues of catalase. Therefore, comparison of Trp λ_{max} could not be used in this study to provide any decisive result of the cryoprotection incurred by trehalose in conserving tertiary structural integrity of the encapsulated catalase of the catalase-loaded PLGA nanoparticles.

5.2 Future work

In the cryoprotection study of catalase-loaded nanoparticles, trehalose was applied at weight ratios of nanoparticles to trehalose of 1:1, 1:20, 1:40, 1:60, 1:80 and 1:100 for cryoprotection of the nanoparticles. Addition of an equivalent weight of trehalose (1:1) preserved enzymatic activity of the encapsulated catalase by 1.9 times, compared to the non-cryoprotected nanoparticles. Increasing trehalose from the 1:1 ratio could produce a slight improvement in preserving the encapsulated catalase activity and showed the highest cryoprotection at 1:60 weight ratio where the activity was 2.6 times of that of the non-cryoprotected one. After 1:60 ratio, the cryoprotection ability of trehalose observed to be plateaued. Also, evaluating the ability of the 1:60 nanoparticles in reducing oxidative stress-induced damage to the cardiomyocytes demonstrated that the cells became less capable or incapable to recover from the oxidative stress-induced damage when the dose increased from 200 µg/well to 400 µg/well. These findings indicated that either the nanoparticles or trehalose or both might create an unfavourable environment for the cells after a certain limit. This observation warrants further investigations on oxidative stress-induced cardiomyocytes by applying the nanoparticles cryoprotected with a low amount of trehalose like 1:1 formulation and, also screening the sole effect of trehalose on cell survival of the oxidative stress-induced cardiomyocytes using equivalent amounts of trehalose present in the formulations of 1:1, 1:20, 1:40, 1:60, 1:80 and 1:100.

The same technique of small amount of trehalose-cryoprotected nanoparticles like 1:1 formulation could be employed in investigating secondary structural changes of the encapsulated protein, where ATR-FTIR spectroscopy could not produce

spectrum of the enzyme present in the nanoparticles in the presence of an excessive amount of trehalose in the formulation of 1:60. Along with the ATR-FTIR, circular dichroism (CD) spectroscopy can also be utilized to study secondary structural changes of the encapsulated catalase induced by lyophilization of the nanoparticles with and without cryoprotection.[199] Besides measuring enzymatic activity of the unstabilized catalase-loaded nanoparticles with and without cryoprotection by different amount of trehalose, protein concentrations of the respective nanoparticles-extracted catalase solutions could provide more detailed information about the changes associated with lyophilization and cryoprotection.

Intracellular measurement of reactive oxygen species (ROS) was not performed in this study. Intracellular ROS measurement in the HL-1 cardiomyocytes could be accomplished by using 2′,7′-dichlorofluorescin diacetate. This intracellular ROS measurement in the healthy, H_2O_2-injured and nanoparticles-treated HL-1 cells could provide an insight on the actual scenario of the protective effect of the nanoparticles.

In this study, anti-apoptotic effect of the catalase-loaded nanoparticles was evaluated in the pre-injury treatment model, where the cardiomyocytes were treated with the nanoparticles before inducing apoptosis in the HL-1 cells. The anti-apoptotic effect of the catalase-loaded nanoparticles could also be performed in the post-injury treatment model, where the cardiomyocytes would be treated with the nanoparticles after inducing apoptosis in the HL-1 cells. Finally, these cryoprotected catalase-loaded PLGA nanoparticles could be tried in the coronary artery ligation mouse model of myocardial ischemia/reperfusion injury.[364]

For studying cellular uptake of the nanoparticles, super resolution microscopic samples could be prepared from the stressed cardiomyocytes after injuring them with hydrogen peroxide in order to observe the actual scenario of internalization of the nanoparticles into the cardiomyocytes, because most of the nanoparticles were found to be associated with the plasma membrane and a very minute amount of the nanoparticles were internalized into the cells in this study, and studies suggested that nanoparticles could be internalized into the cardiomyocytes by enhanced endocytosis after reperfusion passively induced by hydrogen peroxide.

In a clinical setting, the cryoprotected BSA-stabilized catalase-loaded PLGA nanoparticles could be administered simultaneously with the reperfusion therapy. A potential dose of the nanoparticles may be 5 gm, which would be changed depending on the outcome of animal studies. The route of administration could be intracardiac or intravenous. If it is not possible to administer simultaneously with the reperfusion therapy which could provide the maximum benefit of the nanoparticles, the nanoparticles should be administered as soon as possible after the reperfusion therapy.

6 References

1 <http://www.who.int/mediacentre/factsheets/fs310/en/> (

2 Deljanin-Ilić, M. Ž. & Ilić, S. N. Prevalence and prognostic significance of silent myocardial ischemia in patients after myocardial infarction. *Vojnosanitetski pregled* **64**, 519-523 (2007).

3 Roger, V. L. *et al.* Heart disease and stroke statistics—2012 update a report from the American heart association. *Circulation* **125**, e2-e220 (2012).

4 Jennings, R. & Ganote, C. E. Structural changes in myocardium during acute ischemia. *Circulation Research* **35**, 156 (1974).

5 Thygesen, K. *et al.* Third universal definition of myocardial infarction. *Circulation* **126**, 2020-2035 (2012).

6 Frangogiannis, N. G. Pathophysiology of myocardial infarction. *Comprehensive Physiology* (2015).

7 White, H. D. & Chew, D. P. Acute myocardial infarction. *The Lancet* **372**, 570-584 (2008).

8 Reimer, K. A., Lowe, J. E., Rasmussen, M. M. & Jennings, R. B. The wavefront phenomenon of ischemic cell death. 1. Myocardial infarct size vs duration of coronary occlusion in dogs. *Circulation* **56**, 786-794 (1977).

9 Hausenloy, D. J. & Yellon, D. M. Myocardial ischemia-reperfusion injury: a neglected therapeutic target. *The Journal of clinical investigation* **123**, 92-100 (2013).

10 Konstantinidis, K., Whelan, R. S. & Kitsis, R. N. Mechanisms of cell death in heart disease. *Arteriosclerosis, thrombosis, and vascular biology* **32**, 1552-1562 (2012).

11 Kajstura, J. *et al.* Apoptotic and necrotic myocyte cell deaths are independent contributing variables of infarct size in rats. *Laboratory investigation; a journal of technical methods and pathology* **74**, 86-107 (1996).

12 Sam, F. *et al.* Progressive left ventricular remodeling and apoptosis late after myocardial infarction in mouse heart. *American Journal of Physiology-Heart and Circulatory Physiology* **279**, H422-H428 (2000).

13 Lenihan, C. R. & Taylor, C. T. The impact of hypoxia on cell death pathways. *Biochemical Society Transactions* **41**, 657-663 (2013).

14 Murphy, E. & Steenbergen, C. Mechanisms underlying acute protection from cardiac ischemia-reperfusion injury. *Physiological reviews* **88**, 581-609 (2008).

15 Rodrigo, R., Prieto, J. C. & Castillo, R. Cardioprotection against ischaemia/reperfusion by vitamins C and E plus n− 3 fatty acids: molecular mechanisms and potential clinical applications. *Clinical Science* **124**, 1-15 (2013).

16 Marsden, V. S. *et al.* Apoptosis initiated by Bcl-2-regulated caspase activation independently of the cytochrome c/Apaf-1/caspase-9 apoptosome. *Nature* **419**, 634-637 (2002).

17 Micheau, O. & Tschopp, J. Induction of TNF receptor I-mediated apoptosis via two sequential signaling complexes. *Cell* **114**, 181-190 (2003).

18 Boatright, K. M. *et al.* A unified model for apical caspase activation. *Molecular cell* **11**, 529-541 (2003).

19 Gottlieb, R. A. Cell death pathways in acute ischemia/reperfusion injury. *Journal of cardiovascular pharmacology and therapeutics* **16**, 233-238 (2011).

20 Gottlieb, R. A., Burleson, K., Kloner, R. A., Babior, B. & Engler, R. Reperfusion injury induces apoptosis in rabbit cardiomyocytes. *Journal of Clinical Investigation* **94**, 1621 (1994).

21 Crompton, M., Costi, A. & Hayat, L. Evidence for the presence of a reversible Ca2+-dependent pore activated by oxidative stress in heart mitochondria. *Biochemical Journal* **245**, 915-918 (1987).

22 Crompton, M., Ellinger, H. & Costi, A. Inhibition by cyclosporin A of a Ca2+-dependent pore in heart mitochondria activated by inorganic phosphate and oxidative stress. *Biochemical Journal* **255**, 357 (1988).

23 Halestrap, A. P. Calcium-dependent opening of a non-specific pore in the mitochondrial inner membrane is inhibited at pH values below 7. Implications for the protective effect of low pH against chemical and hypoxic cell damage. *Biochemical Journal* **278**, 715-719 (1991).

24 Baines, C. P. *et al.* Loss of cyclophilin D reveals a critical role for mitochondrial permeability transition in cell death. *Nature* **434**, 658-662 (2005).

25 Nakagawa, T. *et al.* Cyclophilin D-dependent mitochondrial permeability transition regulates some necrotic but not apoptotic cell death. *Nature* **434**, 652-658 (2005).

26 Yang, Z. & Klionsky, D. J. Eaten alive: a history of macroautophagy. *Nature cell biology* **12**, 814-822 (2010).

27 Sridhar, S., Botbol, Y., Macian, F. & Cuervo, A. M. Autophagy and disease: always two sides to a problem. *The Journal of pathology* **226**, 255-273 (2012).

28 Mizushima, N., Levine, B., Cuervo, A. M. & Klionsky, D. J. Autophagy fights disease through cellular self-digestion. *Nature* **451**, 1069-1075 (2008).

29 Matsui, Y. *et al.* Distinct Roles of Autophagy in the Heart During Ischemia and Reperfusion Roles of AMP-Activated Protein Kinase and Beclin 1 in Mediating Autophagy. *Circulation research* **100**, 914-922 (2007).

30 Lavandero, S. *et al.* Cardiovascular autophagy: concepts, controversies, and perspectives. *Autophagy* **9**, 1455-1466 (2013).

31 Karch, J. & Molkentin, J. D. Regulated Necrotic Cell Death The Passive Aggressive Side of Bax and Bak. *Circulation research* **116**, 1800-1809 (2015).

32 Kung, G., Konstantinidis, K. & Kitsis, R. N. Programmed necrosis, not apoptosis, in the heart. *Circulation research* **108**, 1017-1036 (2011).

33 Declercq, W., Berghe, T. V. & Vandenabeele, P. RIP kinases at the crossroads of cell death and survival. *Cell* **138**, 229-232 (2009).

34 He, S. *et al.* Receptor interacting protein kinase-3 determines cellular necrotic response to TNF-α. *Cell* **137**, 1100-1111 (2009).

35 Zhang, D.-W. *et al.* RIP3, an energy metabolism regulator that switches TNF-induced cell death from apoptosis to necrosis. *Science* **325**, 332-336 (2009).

36 Christofferson, D. E. & Yuan, J. Necroptosis as an alternative form of programmed cell death. *Current opinion in cell biology* **22**, 263-268 (2010).

37 Sun, L. *et al.* Mixed lineage kinase domain-like protein mediates necrosis signaling downstream of RIP3 kinase. *Cell* **148**, 213-227 (2012).

38 Li, J. *et al.* The RIP1/RIP3 necrosome forms a functional amyloid signaling complex required for programmed necrosis. *Cell* **150**, 339-350 (2012).

39 Cai, Z. *et al.* Plasma membrane translocation of trimerized MLKL protein is required for TNF-induced necroptosis. *Nature cell biology* **16**, 55-65 (2014).

40 Berghe, T. V., Linkermann, A., Jouan-Lanhouet, S., Walczak, H. & Vandenabeele, P. Regulated necrosis: the expanding network of non-apoptotic cell death pathways. *Nature reviews Molecular cell biology* **15**, 135-147 (2014).

41 Linkermann, A. & Green, D. R. Necroptosis. *New England Journal of Medicine* **370**, 455-465 (2014).

42 Keeley, E. C., Boura, J. A. & Grines, C. L. Primary angioplasty versus intravenous thrombolytic therapy for acute myocardial infarction: a quantitative review of 23 randomised trials. *The Lancet* **361**, 13-20 (2003).

43 Eapen, Z. J. *et al.* Defining Heart Failure End Points in ST-Segment Elevation Myocardial Infarction Trials. *Circulation: Cardiovascular Quality and Outcomes* **5**, 594-600 (2012).

44 Takemura, G. & Fujiwara, H. Role of apoptosis in remodeling after myocardial infarction. *Pharmacology & therapeutics* **104**, 1-16 (2004).

45 Baldi, A. *et al.* Apoptosis and post-infarction left ventricular remodeling. *Journal of molecular and cellular cardiology* **34**, 165-174 (2002).

46 Palojoki, E. *et al.* Cardiomyocyte apoptosis and ventricular remodeling after myocardial infarction in rats. *American Journal of Physiology-Heart and Circulatory Physiology* **280**, H2726-H2731 (2001).

47 Abbate, A., Biondi-Zoccai, G. G. & Baldi, A. Pathophysiologic role of myocardial apoptosis in post-infarction left ventricular remodeling. *Journal of cellular physiology* **193**, 145-153 (2002).

48 Abbate, A. *et al.* Increased myocardial apoptosis in patients with unfavorable left ventricular remodeling and early symptomatic post-infarction heart failure. *Journal of the American College of Cardiology* **41**, 753-760 (2003).

49 Saraste, A. *et al.* Cardiomyocyte apoptosis and progression of heart failure to transplantation. *European journal of clinical investigation* **29**, 380-386 (1999).

50 Wencker, D. *et al.* A mechanistic role for cardiac myocyte apoptosis in heart failure. *The Journal of clinical investigation* **111**, 1497-1504 (2003).

51 Dröge, W. Free radicals in the physiological control of cell function. *Physiological reviews* **82**, 47-95 (2002).

52 Thannickal, V. J. & Fanburg, B. L. Reactive oxygen species in cell signaling. *American Journal of Physiology-Lung Cellular and Molecular Physiology* **279**, L1005-L1028 (2000).

53 Xie, Z.-Z., Liu, Y. & Bian, J.-S. Hydrogen sulfide and cellular redox homeostasis. *Oxid Med Cell Longev* **2016**, 6043038 (2016).

54 Fridovich, I. Superoxide radical: an endogenous toxicant. *Annual Review of Pharmacology and Toxicology* **23**, 239-257 (1983).

55 Bielski, B. & Cabelli, D. Highlights of current research involving superoxide and perhydroxyl radicals in aqueous solutions. *International journal of radiation biology* **59**, 291-319 (1991).

56 Lü, J. M., Lin, P. H., Yao, Q. & Chen, C. Chemical and molecular mechanisms of antioxidants: experimental approaches and model systems. *Journal of cellular and molecular medicine* **14**, 840-860 (2010).

57 Cheng, F.-C., Jen, J.-F. & Tsai, T.-H. Hydroxyl radical in living systems and its separation methods. *Journal of Chromatography B* **781**, 481-496 (2002).

58 Kehrer, J. P. The Haber–Weiss reaction and mechanisms of toxicity. *Toxicology* **149**, 43-50 (2000).

59 Agnez-Lima, L. F. *et al.* DNA damage by singlet oxygen and cellular protective mechanisms. *Mutation Research/Reviews in Mutation Research* **751**, 15-28 (2012).

60 Freeman, B. A. & Crapo, J. D. Biology of disease: free radicals and tissue injury. *Laboratory investigation; a journal of technical methods and pathology* **47**, 412-426 (1982).

61 Atalay, M. & Laaksonen, D. E. Diabetes, oxidative stress and physical exercise. *Journal of sports science and medicine* **1**, 1-14 (2002).

62 Perrin, S. *et al.* HIV-1 infection and first line ART induced differential responses in mitochondria from blood lymphocytes and monocytes: the ANRS EP45 "Aging" study. *PloS one* **7**, e41129 (2012).

63 Hoyal, C. R., Gozal, E., Zhou, H., Foldenauer, K. & Forman, H. J. Modulation of the rat alveolar macrophage respiratory burst by hydroperoxides is calcium dependent. *Archives of biochemistry and biophysics* **326**, 166-171 (1996).

64 Jones, O. The mechanism of the production of superoxide by phagocytes. *Molecular and chemical neuropathology* **19**, 177-184 (1993).

65 Murphy, M. S. C., Britigan, B. E., Hassett, D. J. & Rosen, G. M. Phagocytes, O2 reduction, and hydroxyl radical. *Review of Infectious Diseases* **10**, 1088-1096 (1988).

66 Nishino, T., Okamoto, K., Eger, B. T., Pai, E. F. & Nishino, T. Mammalian xanthine oxidoreductase–mechanism of transition from xanthine dehydrogenase to xanthine oxidase. *FEBS journal* **275**, 3278-3289 (2008).

67 Kelley, E. E. *et al.* Hydrogen peroxide is the major oxidant product of xanthine oxidase. *Free Radical Biology and Medicine* **48**, 493-498 (2010).

68 Thompson-Gorman, S. L. & Zweier, J. L. Evaluation of the role of xanthine oxidase in myocardial reperfusion injury. *Journal of Biological Chemistry* **265**, 6656-6663 (1990).

69 Minhas, K. M. *et al.* Xanthine oxidoreductase inhibition causes reverse remodeling in rats with dilated cardiomyopathy. *Circulation research* **98**, 271-279 (2006).

70 Saavedra, W. F. *et al.* Imbalance between xanthine oxidase and nitric oxide synthase signaling pathways underlies mechanoenergetic uncoupling in the failing heart. *Circulation research* **90**, 297-304 (2002).

71 Miller, J. W., Selhub, J. & Joseph, J. A. Oxidative damage caused by free radicals produced during catecholamine autoxidation: protective effects of O-methylation and melatonin. *Free Radical Biology and Medicine* **21**, 241-249 (1996).

72 Kowaltowski, A. J., de Souza-Pinto, N. C., Castilho, R. F. & Vercesi, A. E. Mitochondria and reactive oxygen species. *Free Radical Biology and Medicine* **47**, 333-343 (2009).

73 St-Pierre, J., Buckingham, J. A., Roebuck, S. J. & Brand, M. D. Topology of superoxide production from different sites in the mitochondrial electron transport chain. *Journal of Biological Chemistry* **277**, 44784-44790 (2002).

74 Santos, C. X., Anilkumar, N., Zhang, M., Brewer, A. C. & Shah, A. M. Redox signaling in cardiac myocytes. *Free Radical Biology and Medicine* **50**, 777-793 (2011).

75 Kurian, G. A., Rajagopal, R., Vedantham, S. & Rajesh, M. The Role of Oxidative Stress in Myocardial Ischemia and Reperfusion Injury and Remodeling: Revisited. *Oxidative Medicine and Cellular Longevity* **2016** (2016).

76 Auten, R. L. & Davis, J. M. Oxygen toxicity and reactive oxygen species: the devil is in the details. *Pediatric research* **66**, 121-127 (2009).

77 Zhang, X., Azhar, G., Nagano, K. & Wei, J. Y. Differential vulnerability to oxidative stress in rat cardiac myocytes versus fibroblasts. *Journal of the American College of Cardiology* **38**, 2055-2062 (2001).

78 Hassan, H. M. Microbial superoxide dismutases. *Advances in genetics* **26**, 65-97 (1989).

79 Tappel, A. [53] Glutathione peroxidase and hydroperoxides. *Methods in enzymology* **52**, 506-513 (1978).

80 Finosh, G. T. & Jayabalan, M. Reactive oxygen species-Control and management using amphiphilic biosynthetic hydrogels for cardiac applications. *Advances in Bioscience and Biotechnology* **4**, 1134 (2013).

81 Kim, S.-J. *et al.* Glutathione reductase plays an anti-apoptotic role against oxidative stress in human hepatoma cells. *Biochimie* **92**, 927-932 (2010).

82 Wolff, C. B. in *Oxygen Transport to Tissue XXVIII* 169-182 (Springer, 2008).

83 Raedschelders, K., Ansley, D. M. & Chen, D. D. The cellular and molecular origin of reactive oxygen species generation during myocardial ischemia and reperfusion. *Pharmacology & therapeutics* **133**, 230-255 (2012).

84 Ansley, D. M. & Wang, B. Oxidative stress and myocardial injury in the diabetic heart. *The Journal of pathology* **229**, 232-241 (2013).

85 Couto, N., Malys, N., Gaskell, S. J. & Barber, J. Partition and turnover of glutathione reductase from Saccharomyces cerevisiae: a proteomic approach. *Journal of proteome research* **12**, 2885-2894 (2013).

86 Marklund, S. L., Westman, N. G., Lundgren, E. & Roos, G. Copper-and zinc-containing superoxide dismutase, manganese-containing superoxide dismutase, catalase, and glutathione peroxidase in normal and neoplastic human cell lines and normal human tissues. *Cancer Research* **42**, 1955-1961 (1982).

87 Doroshow, J. H., Locker, G. Y. & Myers, C. Enzymatic defenses of the mouse heart against reactive oxygen metabolites: alterations produced by doxorubicin. *Journal of Clinical Investigation* **65**, 128 (1980).

88 Ishikawa, T., Akerboom, T. P. & Sies, H. Role of Key Defense Systems in Target Organ Toxicity. *Cohen, GM (ed.) Target Organ Toxicity, CRC Press, London.*, 129-144 (1986).

89 Thayer, W. S. Role of catalase in metabolism of hydrogen peroxide by the perfused rat heart. *FEBS letters* **202**, 137-140 (1986).

90 Eefting, F. *et al.* Role of apoptosis in reperfusion injury. *Cardiovascular Research* **61**, 414-426 (2004).

91 van Empel, V. P. *et al.* Myocyte apoptosis in heart failure. *Cardiovascular research* **67**, 21-29 (2005).

92 Ambrosio, G. *et al.* Evidence that mitochondrial respiration is a source of potentially toxic oxygen free radicals in intact rabbit hearts subjected to ischemia and reflow. *Journal of Biological Chemistry* **268**, 18532-18541 (1993).

93 Andreadou, I., Iliodromitis, E. K., Farmakis, D. & Kremastinos, D. T. To prevent, protect and save the ischemic heart: antioxidants revisited. *Expert opinion on therapeutic targets* **13**, 945-956 (2009).

94 Park, J.-W., Chun, Y.-S., Kim, Y.-H., Kim, C.-H. & Kim, M.-S. Ischemic preconditioning reduces O 2.-generation and prevents respiratory impairment in the mitochondria of post-ischemic reperfused heart of rat. *Life sciences* **60**, 2207-2219 (1997).

95 Kevin, L. G., Novalija, E. & Stowe, D. F. Reactive oxygen species as mediators of cardiac injury and protection: the relevance to anesthesia practice. *Anesthesia & Analgesia* **101**, 1275-1287 (2005).

96 Tavazzi, B. *et al.* Lipid peroxidation, tissue necrosis, and metabolic and mechanical recovery of isolated reperfused rat heart as a function of increasing ischemia. *Free radical research* **28**, 25-37 (1998).

97 Hill, M. F. & Singal, P. K. Antioxidant and oxidative stress changes during heart failure subsequent to myocardial infarction in rats. *The American journal of pathology* **148**, 291 (1996).

98 Hill, M. F. & Singal, P. K. Right and left myocardial antioxidant responses during heart failure subsequent to myocardial infarction. *Circulation* **96**, 2414-2420 (1997).

99 Ibáñez, B., Heusch, G., Ovize, M. & Van de Werf, F. Evolving therapies for myocardial ischemia/reperfusion injury. *Journal of the American College of Cardiology* **65**, 1454-1471 (2015).

100 Arai, A. E. Magnetic resonance imaging for area at risk, myocardial infarction, and myocardial salvage. *Journal of Cardiovascular Pharmacology and Therapeutics* **16**, 313-320 (2011).

101 Lewis, E. F. *et al.* Predictors of late development of heart failure in stable survivors of myocardial infarction: the CARE study. *Journal of the American College of Cardiology* **42**, 1446-1453 (2003).

102 Miura, T., Yellon, D. M., Hearse, D. J. & Downey, J. M. Determinants of infarct size during permanent occlusion of a coronary artery in the closed chest dog. *Journal of the American College of Cardiology* **9**, 647-654 (1987).

103 Reimer, K. & Jennings, R. The" wavefront phenomenon" of myocardial ischemic cell death. II. Transmural progression of necrosis within the framework of ischemic bed size (myocardium at risk) and collateral flow. *Laboratory investigation; a journal of technical methods and pathology* **40**, 633-644 (1979).

104 Duncker, D. J. *et al.* Effect of temperature on myocardial infarction in swine. *American Journal of Physiology-Heart and Circulatory Physiology* **270**, H1189-H1199 (1996).

105 Penna, C., Mancardi, D., Rastaldo, R. & Pagliaro, P. Cardioprotection: a radical view Free radicals in pre and postconditioning. *Biochimica et biophysica acta* **1787**, 781-793, doi:10.1016/j.bbabio.2009.02.008 (2009).

106 Penna, C., Mancardi, D., Raimondo, S., Geuna, S. & Pagliaro, P. The paradigm of postconditioning to protect the heart. *Journal of cellular and molecular medicine* **12**, 435-458 (2008).

107 Pagliaro, P., Moro, F., Tullio, F., Perrelli, M. G. & Penna, C. Cardioprotective pathways during reperfusion: focus on redox signaling and other modalities of cell signaling. *Antioxidants & redox signaling* **14**, 833-850, doi:10.1089/ars.2010.3245 (2011).

108 Vinten-Johansen, J. *et al.* The multidimensional physiological responses to postconditioning. *Antioxidants & redox signaling* **14**, 791-810 (2011).

109 Golstein, P. & Kroemer, G. Cell death by necrosis: towards a molecular definition. *Trends in biochemical sciences* **32**, 37-43, doi:10.1016/j.tibs.2006.11.001 (2007).

110 Zong, W.-X. & Thompson, C. B. Necrotic death as a cell fate. *Genes & development* **20**, 1-15 (2006).

111 Takagi, H., Matsui, Y. & Sadoshima, J. The role of autophagy in mediating cell survival and death during ischemia and reperfusion in the heart. *Antioxidants & redox signaling* **9**, 1373-1382 (2007).

112 Moens, A., Claeys, M., Timmermans, J. & Vrints, C. Myocardial ischemia/reperfusion-injury, a clinical view on a complex pathophysiological process. *International journal of cardiology* **100**, 179-190 (2005).

113 Hashmi, S. & Al-Salam, S. Acute myocardial infarction and myocardial ischemia-reperfusion injury: a comparison. *International journal of clinical and experimental pathology* **8**, 8786 (2015).

114 Perrelli, M.-G., Pagliaro, P. & Penna, C. Ischemia/reperfusion injury and cardioprotective mechanisms: role of mitochondria and reactive oxygen species. *World J Cardiol* **3**, 186-200 (2011).

115 Miyamae, M., Camacho, S. A., Weiner, M. W. & Figueredo, V. M. Attenuation of postischemic reperfusion injury is related to prevention of [Ca2+] m overload in rat hearts. *American Journal of Physiology-Heart and Circulatory Physiology* **271**, H2145-H2153 (1996).

116 Herzog, W. R. *et al.* Short-term low dose intracoronary diltiazem administered at the onset of reperfusion reduces myocardial infarct size. *International journal of cardiology* **59**, 21-27 (1997).

117 Jeremias, I. *et al.* Involvement of CD95/Apo1/Fas in cell death after myocardial ischemia. *Circulation* **102**, 915-920 (2000).

118 Lee, P. *et al.* Fas pathway is a critical mediator of cardiac myocyte death and MI during ischemia-reperfusion in vivo. *American Journal of Physiology-Heart and Circulatory Physiology* **284**, H456-H463 (2003).

119 Brocheriou, V. *et al.* Cardiac functional improvement by a human Bcl-2 transgene in a mouse model of ischemia/reperfusion injury. *Journal of Gene Medicine* **2**, 326 (2000).

120 Chen, Z., Chua, C. C., Ho, Y.-S., Hamdy, R. C. & Chua, B. H. Overexpression of Bcl-2 attenuates apoptosis and protects against myocardial I/R injury in transgenic mice. *American Journal of Physiology-Heart and Circulatory Physiology* **280**, H2313-H2320 (2001).

121 Hochhauser, E. *et al.* Bax ablation protects against myocardial ischemia-reperfusion injury in transgenic mice. *American Journal of Physiology-Heart and Circulatory Physiology* **284**, H2351-H2359 (2003).

122 Hochhauser, E. *et al.* Bax deficiency reduces infarct size and improves long-term function after myocardial infarction. *Cell biochemistry and biophysics* **47**, 11-19 (2007).

123 Baines, C. P. & Molkentin, J. D. STRESS signaling pathways that modulate cardiac myocyte apoptosis. *Journal of molecular and cellular cardiology* **38**, 47-62 (2005).

124 Chen, M. *et al.* Bid is cleaved by calpain to an active fragment in vitro and during myocardial ischemia/reperfusion. *Journal of Biological Chemistry* **276**, 30724-30728 (2001).

125 Imahashi, K., Schneider, M. D., Steenbergen, C. & Murphy, E. Transgenic expression of Bcl-2 modulates energy metabolism, prevents cytosolic acidification during ischemia, and reduces ischemia/reperfusion injury. *Circulation research* **95**, 734-741 (2004).

126 McCully, J. D., Wakiyama, H., Hsieh, Y.-J., Jones, M. & Levitsky, S. Differential contribution of necrosis and apoptosis in myocardial ischemia-reperfusion injury. *American Journal of Physiology-Heart and Circulatory Physiology* **286**, H1923-H1935 (2004).

127 Shimizu, S. *et al.* Role of Bcl-2 family proteins in a non-apoptotic programmed cell death dependent on autophagy genes. *Nature cell biology* **6**, 1221-1228 (2004).

128 Yaoita, H., Ogawa, K., Maehara, K. & Maruyama, Y. Attenuation of ischemia/reperfusion injury in rats by a caspase inhibitor. *Circulation* **97**, 276-281 (1998).

129 Holly, T. A. *et al.* Caspase inhibition reduces myocyte cell death induced by myocardial ischemia and reperfusion in vivo. *Journal of molecular and cellular cardiology* **31**, 1709-1715 (1999).

130 Huang, J.-Q., Radinovic, S., Rezaiefar, P. & Black, S. C. In vivo myocardial infarct size reduction by a caspase inhibitor administered after the onset of ischemia. *European journal of pharmacology* **402**, 139-142 (2000).

131 Yang, W. *et al.* MX1013, a dipeptide caspase inhibitor with potent in vivo antiapoptotic activity. *British journal of pharmacology* **140**, 402-412 (2003).

132 Gottlieb, R. ICE-ing the heart. *Circulation research* **96**, 1036-1038 (2005).

133 Mocanu, M., Baxter, G. & Yellon, D. Caspase inhibition and limitation of myocardial infarct size: protection against lethal reperfusion injury. *British journal of pharmacology* **130**, 197-200 (2000).

134 Stephanou, A. *et al.* Distinct initiator caspases are required for the induction of apoptosis in cardiac myocytes during ischaemia versus reperfusion injury. *Cell death and differentiation* **8**, 434-435 (2001).

135 Clarke, S. J., McStay, G. P. & Halestrap, A. P. Sanglifehrin A acts as a potent inhibitor of the mitochondrial permeability transition and reperfusion injury of the heart by binding to cyclophilin-D at a different site from cyclosporin A. *Journal of Biological Chemistry* **277**, 34793-34799 (2002).

136 Griffiths, E. J. & Halestrap, A. P. Protection by Cyclosporin A of ischemia/reperfusion-induced damage in isolated rat hearts. *Journal of molecular and cellular cardiology* **25**, 1461-1469 (1993).

137 Hausenloy, D. J., Duchen, M. R. & Yellon, D. M. Inhibiting mitochondrial permeability transition pore opening at reperfusion protects against ischaemia–reperfusion injury. *Cardiovascular research* **60**, 617-625 (2003).

138 Argaud, L. *et al.* Specific inhibition of the mitochondrial permeability transition prevents lethal reperfusion injury. *Journal of molecular and cellular cardiology* **38**, 367-374 (2005).

139 Golstein, P. & Kroemer, G. Cell death by necrosis: towards a molecular definition. *Trends in biochemical sciences* **32**, 37-43 (2007).

140 Dosenko, V. E., Nagibin, V. S., Tumanovska, L. V. & Moibenko, A. A. Protective effect of autophagy in anoxia-reoxygenation of isolated cardiomyocyte? *Autophagy* **2**, 305-306 (2006).

141 Yan, L. *et al.* Autophagy in chronically ischemic myocardium. *Proceedings of the National Academy of Sciences of the United States of America* **102**, 13807-13812 (2005).

142 Sciarretta, S. *et al.* Rheb is a critical regulator of autophagy during myocardial ischemia pathophysiological implications in obesity and metabolic syndrome. *Circulation* **125**, 1134-1146 (2012).

143 Zhai, P., Sciarretta, S., Galeotti, J., Volpe, M. & Sadoshima, J. Differential roles of GSK-3β during myocardial ischemia and ischemia/reperfusion. *Circulation research* **109**, 502-511 (2011).

144 Luedde, M. *et al.* RIP3, a kinase promoting necroptotic cell death, mediates adverse remodelling after myocardial infarction. *Cardiovascular research* **103**, 206-216 (2014).

145 Wu, J. *et al.* Mlkl knockout mice demonstrate the indispensable role of Mlkl in necroptosis. *Cell research* **23**, 994-1006 (2013).

146 Smith, C. C. *et al.* Necrostatin: a potentially novel cardioprotective agent? *Cardiovascular Drugs and Therapy* **21**, 227-233 (2007).

147 Koshinuma, S., Miyamae, M., Kaneda, K., Kotani, J. & Figueredo, V. M. Combination of necroptosis and apoptosis inhibition enhances cardioprotection against myocardial ischemia–reperfusion injury. *Journal of anesthesia* **28**, 235-241 (2014).

148 Oerlemans, M. I. *et al.* Inhibition of RIP1-dependent necrosis prevents adverse cardiac remodeling after myocardial ischemia–reperfusion in vivo. *Basic research in cardiology* **107**, 1-13 (2012).

149 Habener, A. *et al.* MitoNEET Protects HL-1 Cardiomyocytes from Oxidative Stress Mediated Apoptosis in an In Vitro Model of Hypoxia and Reoxygenation. *PloS one* **11**, e0156054 (2016).

150 Rodrigo, R., Libuy, M., Feliú, F. & Hasson, D. Molecular basis of cardioprotective effect of antioxidant vitamins in myocardial infarction. *BioMed research international* **2013** (2013).

151 Evans, C. W., Iyer, K. S. & Hool, L. C. The potential for nanotechnology to improve delivery of therapy to the acute ischemic heart. *Nanomedicine* **11**, 817-832 (2016).

152 Chen, Z. *et al.* Overexpression of MnSOD protects against myocardial ischemia/reperfusion injury in transgenic mice. *Journal of molecular and cellular cardiology* **30**, 2281-2289 (1998).

153 Yoshida, T. *et al.* Transgenic mice overexpressing glutathione peroxidase are resistant to myocardial ischemia reperfusion injury. *Journal of molecular and cellular cardiology* **28**, 1759-1767 (1996).

154 Chen, Y., Yu, A., Saari, J. T. & Kang, Y. J. Repression of hypoxia-reoxygenation injury in the catalase-overexpressing heart of transgenic mice. *Experimental Biology and Medicine* **216**, 112-116 (1997).

155 Kang, Y. J., Chen, Y. & Epstein, P. N. Suppression of doxorubicin cardiotoxicity by overexpression of catalase in the heart of transgenic mice. *Journal of Biological Chemistry* **271**, 12610-12616 (1996).

156 Li, G., Chen, Y., Saari, J. T. & Kang, Y. J. Catalase-overexpressing transgenic mouse heart is resistant to ischemia-reperfusion injury. *American Journal of Physiology-Heart and Circulatory Physiology* **273**, H1090-H1095 (1997).

157 Pendergrass, K. D. *et al.* Temporal effects of catalase overexpression on healing after myocardial infarction. *Circulation: Heart Failure* **4**, 98-106 (2011).

158 Liu, M. *et al.* Heart-targeted nanoscale drug delivery systems. *Journal of biomedical nanotechnology* **10**, 2038-2062 (2014).

159 Buxton, D. B. The impact of nanotechnology on myocardial infarction treatment. *Nanomedicine* **7**, 173-175 (2012).

160 Godin, B. & Ferrari, M. Cardiovascular Nano Medicine: A Posse Ad Esse. *Methodist DeBakey cardiovascular journal* **8**, 2 (2012).

161 Suarez, S., Almutairi, A. & Christman, K. Micro-and nanoparticles for treating cardiovascular disease. *Biomaterials science* **3**, 564-580 (2015).

162 Cote, B., Carlson, L. J., Rao, D. A. & Alani, A. W. Combinatorial resveratrol and quercetin polymeric micelles mitigate doxorubicin induced cardiotoxicity in vitro and in vivo. *Journal of Controlled Release* **213**, 128-133 (2015).

163 Kang, J. Y. *et al.* Pharmacokinetics, antitumor and cardioprotective effects of liposome-encapsulated phenylaminoethyl selenide in human prostate cancer rodent models. *Pharmaceutical research* **32**, 852-862 (2015).

164 Simón-Yarza, T. *et al.* Functional benefits of PLGA particulates carrying VEGF and CoQ 10 in an animal of myocardial ischemia. *International journal of pharmaceutics* **454**, 784-790 (2013).

165 Ikeda, G. *et al.* Nanoparticle-Mediated Targeting of Cyclosporine A Enhances Cardioprotection Against Ischemia-Reperfusion Injury Through Inhibition of Mitochondrial Permeability Transition Pore Opening. *Scientific reports* **6** (2016).

166 Clemons, T. D., Viola, H. M., House, M. J., Iyer, K. S. & Hool, L. C. Examining Efficacy of "TAT-less" Delivery of a Peptide against the L-Type Calcium Channel in Cardiac Ischemia–Reperfusion Injury. *ACS nano* **7**, 2212-2220 (2013).

167 Hardy, N. *et al.* Nanoparticle-Mediated Dual Delivery of an Antioxidant and a Peptide against the L-Type Ca2+ Channel Enables Simultaneous Reduction of Cardiac Ischemia-Reperfusion Injury. *ACS nano* **9**, 279-289 (2014).

168 Nakano, Y. *et al.* Nanoparticle-Mediated Delivery of Irbesartan Induces Cardioprotection from Myocardial Ischemia-Reperfusion Injury by Antagonizing Monocyte-Mediated Inflammation. *Scientific Reports* **6** (2016).

169 Nagaoka, K. *et al.* A new therapeutic modality for acute myocardial infarction: nanoparticle-mediated delivery of pitavastatin induces cardioprotection from ischemia-reperfusion injury via activation of PI3K/Akt pathway and anti-inflammation in a rat model. *PloS one* **10**, e0132451 (2015).

170 Couvreur, P. & Vauthier, C. Nanotechnology: intelligent design to treat complex disease. *Pharmaceutical research* **23**, 1417-1450 (2006).

171 Hans, M. & Lowman, A. Biodegradable nanoparticles for drug delivery and targeting. *Current Opinion in Solid State and Materials Science* **6**, 319-327 (2002).

172 Hillaireau, H. & Couvreur, P. Nanocarriers' entry into the cell: relevance to drug delivery. *Cellular and Molecular Life Sciences* **66**, 2873-2896 (2009).

173 Fernandez-Urrusuno, R., Calvo, P., Remuñán-López, C., Vila-Jato, J. L. & Alonso, M. J. Enhancement of nasal absorption of insulin using chitosan nanoparticles. *Pharmaceutical research* **16**, 1576-1581 (1999).

174 Luppi, B. *et al.* Albumin nanoparticles carrying cyclodextrins for nasal delivery of the anti-Alzheimer drug tacrine. *European Journal of Pharmaceutical Sciences* **44**, 559-565 (2011).

175 Machado, A. H. *et al.* Preparation of calcium alginate nanoparticles using water-in-oil (W/O) nanoemulsions. *Langmuir* **28**, 4131-4141 (2012).

176 Moradhaseli, S. *et al.* Preparation and characterization of sodium alginate nanoparticles containing ICD-85 (venom derived peptides). (2013).

177 Joachim, E. *et al.* Gelatin nanoparticles enhance the neuroprotective effects of intranasally administered osteopontin in rat ischemic stroke model. *Drug delivery and translational research* **4**, 395-399 (2014).

178 Wasiak, I. *et al.* Dextran Nanoparticle Synthesis and Properties. *PloS one* **11**, e0146237 (2016).

179 Mo, X., Iwata, H., Matsuda, S. & Ikada, Y. Soft tissue adhesive composed of modified gelatin and polysaccharides. *Journal of Biomaterials Science, Polymer Edition* **11**, 341-351 (2000).

180 Ikada, Y. & Tsuji, H. Biodegradable polyesters for medical and ecological applications. *Macromolecular rapid communications* **21**, 117-132 (2000).

181 Hino, M. *et al.* Transmission of symptomatic parvovirus B19 infection by fibrin sealant used during surgery. *British journal of haematology* **108**, 194-195 (2000).

182 Lü, J.-M. *et al.* Current advances in research and clinical applications of PLGA-based nanotechnology. *Expert review of molecular diagnostics* (2014).

183 Marin, E., Briceño, M. I. & Caballero-George, C. Critical evaluation of biodegradable polymers used in nanodrugs. *International journal of nanomedicine* **8**, 3071 (2013).

184 Azizi, M. *et al.* Fabrication of protein-loaded PLGA nanoparticles: effect of selected formulation variables on particle size and release profile. *Journal of Polymer Research* **20**, 1-14 (2013).

185 Makadia, H. K. & Siegel, S. J. Poly lactic-co-glycolic acid (PLGA) as biodegradable controlled drug delivery carrier. *Polymers* **3**, 1377-1397 (2011).

186 Kumari, A., Yadav, S. K. & Yadav, S. C. Biodegradable polymeric nanoparticles based drug delivery systems. *Colloids and Surfaces B: Biointerfaces* **75**, 1-18 (2010).

187 Gentile, P., Chiono, V., Carmagnola, I. & Hatton, P. V. An overview of poly (lactic-co-glycolic) acid (PLGA)-based biomaterials for bone tissue engineering. *International journal of molecular sciences* **15**, 3640-3659 (2014).

188 Wu, X. S. & Wang, N. Synthesis, characterization, biodegradation, and drug delivery application of biodegradable lactic/glycolic acid polymers. Part II: biodegradation. *Journal of Biomaterials Science, Polymer Edition* **12**, 21-34 (2001).

189 Lu, L. *et al.* In vitro degradation of porous poly (L-lactic acid) foams. *Biomaterials* **21**, 1595-1605 (2000).

190 Holy, C. E., Dang, S. M., Davies, J. E. & Shoichet, M. S. In vitro degradation of a novel poly (lactide-co-glycolide) 75/25 foam. *Biomaterials* **20**, 1177-1185 (1999).

191 Panagi, Z. *et al.* Effect of dose on the biodistribution and pharmacokinetics of PLGA and PLGA–mPEG nanoparticles. *International journal of pharmaceutics* **221**, 143-152 (2001).

192 Semete, B. *et al.* In vivo evaluation of the biodistribution and safety of PLGA nanoparticles as drug delivery systems. *Nanomedicine: Nanotechnology, Biology and Medicine* **6**, 662-671 (2010).

193 Zambaux, M., Bonneaux, F., Gref, R., Dellacherie, E. & Vigneron, C. Preparation and characterization of protein C-loaded PLA nanoparticles. *Journal of controlled release* **60**, 179-188 (1999).

194 Sahana, D., Mittal, G., Bhardwaj, V. & Kumar, M. PLGA nanoparticles for oral delivery of hydrophobic drugs: influence of organic solvent on nanoparticle formation and release behavior in vitro and in vivo using estradiol as a model drug. *Journal of pharmaceutical sciences* **97**, 1530-1542 (2008).

195 Barichello, J. M., Morishita, M., Takayama, K. & Nagai, T. Encapsulation of hydrophilic and lipophilic drugs in PLGA nanoparticles by the nanoprecipitation method. *Drug development and industrial pharmacy* **25**, 471-476 (1999).

196 Niwa, T., Takeuchi, H., Hino, T., Kunou, N. & Kawashima, Y. Preparations of biodegradable nanospheres of water-soluble and insoluble drugs with D, L-lactide/glycolide copolymer by a novel spontaneous emulsification solvent diffusion method, and the drug release behavior. *Journal of Controlled Release* **25**, 89-98 (1993).

197 Nagavarma, B., Yadav, H. K., Ayaz, A., Vasudha, L. & Shivakumar, H. Different techniques for preparation of polymeric nanoparticles—a review. *Asian J. Pharm. Clin. Res* **5**, 16-23 (2012).

198 Kobsa, S. & Saltzman, W. M. Bioengineering approaches to controlled protein delivery. *Pediatric research* **63**, 513-519 (2008).

199 Fonte, P. *et al.* Co-encapsulation of lyoprotectants improves the stability of protein-loaded PLGA nanoparticles upon lyophilization. *International journal of pharmaceutics* **496**, 850-862 (2015).

200 Fonte, P. *et al.* Stability study perspective of the effect of freeze-drying using cryoprotectants on the structure of insulin loaded into PLGA nanoparticles. *Biomacromolecules* **15**, 3753-3765 (2014).

201 Pirooznia, N., Hasannia, S., Lotfi, A. S. & Ghanei, M. Encapsulation of alpha-1 antitrypsin in PLGA nanoparticles: in vitro characterization as an effective aerosol formulation in pulmonary diseases. *Journal of nanobiotechnology* **10**, 1 (2012).

202 Chacon, M., Molpeceres, J., Berges, L., Guzman, M. & Aberturas, M. Stability and freeze-drying of cyclosporine loaded poly (D, L lactide–glycolide) carriers. *European Journal of Pharmaceutical Sciences* **8**, 99-107 (1999).

203 Dimitrov, D. S. Therapeutic proteins. *Therapeutic Proteins: Methods and Protocols*, 1-26 (2012).

204 Simone, E., Dziubla, T., Shuvaev, V. & Muzykantov, V. R. Synthesis and characterization of polymer nanocarriers for the targeted delivery of therapeutic enzymes. *Free Radicals and Antioxidant Protocols*, 145-164 (2010).

205 Leader, B., Baca, Q. J. & Golan, D. E. Protein therapeutics: a summary and pharmacological classification. *Nature Reviews Drug Discovery* **7**, 21-39 (2008).

206 Simone, E. A., Dziubla, T. D., Discher, D. E. & Muzykantov, V. R. Filamentous polymer nanocarriers of tunable stiffness that encapsulate the therapeutic enzyme catalase. *Biomacromolecules* **10**, 1324-1330 (2009).

207 Fonte, P. *et al.* Effect of cryoprotectants on the porosity and stability of insulin-loaded PLGA nanoparticles after freeze-drying. *Biomatter* **2**, 329-339 (2012).

208 van de Weert, M., Hennink, W. E. & Jiskoot, W. Protein instability in poly (lactic-co-glycolic acid) microparticles. *Pharmaceutical research* **17**, 1159-1167 (2000).

209 Hood, E., Simone, E., Wattamwar, P., Dziubla, T. & Muzykantov, V. Nanocarriers for vascular delivery of antioxidants. *Nanomedicine* **6**, 1257-1272 (2011).

210 Raghuvanshi, R. S., Goyal, S., Singh, O. & Panda, A. K. Stabilization of dichloromethane-induced protein denaturation during microencapsulation. *Pharmaceutical development and technology* **3**, 269-276 (1998).

211 Li, X. *et al.* Influence of process parameters on the protein stability encapsulated in poly-DL-lactide–poly (ethylene glycol) microspheres. *Journal of Controlled Release* **68**, 41-52 (2000).

212 van de Weert, M., Hoechstetter, J., Hennink, W. E. & Crommelin, D. J. The effect of a water/organic solvent interface on the structural stability of lysozyme. *Journal of controlled release* **68**, 351-359 (2000).

213 Chen, L., Apte, R. N. & Cohen, S. Characterization of PLGA microspheres for the controlled delivery of IL-1α for tumor immunotherapy. *Journal of controlled release* **43**, 261-272 (1997).

214 Suslick, K. S., Hammerton, D. A. & Cline, R. E. Sonochemical hot spot. *Journal of the American Chemical Society* **108**, 5641-5642 (1986).

215 Stanwick, J. C., Baumann, M. D. & Shoichet, M. S. Enhanced neurotrophin-3 bioactivity and release from a nanoparticle-loaded composite hydrogel. *Journal of controlled release* **160**, 666-675 (2012).

216 Wong, D. & Parasrampuria, J. Pharmaceutical excipients for the stabilisation of proteins. *Pharmaceutical technology* **21**, 34-50 (1997).

217 Wolf, M., Wirth, M., Pittner, F. & Gabor, F. Stabilisation and determination of the biological activity of L-asparaginase in poly (D, L-lactide-co-glycolide) nanospheres. *International journal of pharmaceutics* **256**, 141-152 (2003).

218 Cleland, J. L. & Jones, A. J. Stable formulations of recombinant human growth hormone and interferon-γ for microencapsulation in biodegradable mircospheres. *Pharmaceutical research* **13**, 1464-1475 (1996).

219 Gentile, P. *et al.* Influence of parathyroid hormone-loaded PLGA nanoparticles in porous scaffolds for bone regeneration. *International journal of molecular sciences* **16**, 20492-20510 (2015).

220 Meinel, L. *et al.* Stabilizing insulin-like growth factor-I in poly (D, L-lactide-co-glycolide) microspheres. *Journal of controlled release* **70**, 193-202 (2001).

221 Danhier, F. *et al.* PLGA-based nanoparticles: an overview of biomedical applications. *Journal of controlled release* **161**, 505-522 (2012).

222 Konan, Y. N., Gurny, R. & Allémann, E. Preparation and characterization of sterile and freeze-dried sub-200 nm nanoparticles. *International journal of pharmaceutics* **233**, 239-252 (2002).

223 De Jaeghere, F. *et al.* Formulation and lyoprotection of poly (lactic acid-co-ethylene oxide) nanoparticles: influence on physical stability and in vitro cell uptake. *Pharmaceutical research* **16**, 859-866 (1999).

224 Date, P. V., Samad, A. & Devarajan, P. V. Freeze thaw: a simple approach for prediction of optimal cryoprotectant for freeze drying. *AAPS PharmSciTech* **11**, 304-313 (2010).

225 Kesisoglou, F., Panmai, S. & Wu, Y. Nanosizing—oral formulation development and biopharmaceutical evaluation. *Advanced drug delivery reviews* **59**, 631-644 (2007).

226 Heller, M. C., Carpenter, J. F. & Randolph, T. W. Protein formulation and lyophilization cycle design: Prevention of damage due to freeze-concentration induced phase separation. *Biotechnology and bioengineering* **63**, 166-174 (1999).

227 Kadoya, S. *et al.* Freeze-drying of proteins with glass-forming oligosaccharide-derived sugar alcohols. *International journal of pharmaceutics* **389**, 107-113 (2010).

228 Abdelwahed, W., Degobert, G., Stainmesse, S. & Fessi, H. Freeze-drying of nanoparticles: formulation, process and storage considerations. *Advanced drug delivery reviews* **58**, 1688-1713 (2006).

229 Kaushik, J. K. & Bhat, R. Why is trehalose an exceptional protein stabilizer? An analysis of the thermal stability of proteins in the presence of the compatible osmolyte trehalose. *Journal of Biological Chemistry* **278**, 26458-26465 (2003).

230 Crowe, L. M., Reid, D. S. & Crowe, J. H. Is trehalose special for preserving dry biomaterials? *Biophysical journal* **71**, 2087 (1996).

231 Lynch, I., Dawson, K. A. & Linse, S. Detecting cryptic epitopes created by nanoparticles. *Sci. Stke* **2006**, pe14-pe14 (2006).

232 Yang, H., Yang, S., Kong, J., Dong, A. & Yu, S. Obtaining information about protein secondary structures in aqueous solution using Fourier transform IR spectroscopy. *Nature protocols* **10**, 382-396 (2015).

233 Van Stokkum, I. H., Spoelder, H. J., Bloemendal, M., Van Grondelle, R. & Groen, F. C. Estimation of protein secondary structure and error analysis from circular dichroism spectra. *Analytical biochemistry* **191**, 110-118 (1990).

234 Matsuo, K., Yonehara, R. & Gekko, K. Improved estimation of the secondary structures of proteins by vacuum-ultraviolet circular dichroism spectroscopy. *Journal of biochemistry* **138**, 79-88 (2005).

235 Greenfield, N. J. Using circular dichroism spectra to estimate protein secondary structure. *Nature protocols* **1**, 2876-2890 (2006).

236 Kong, J. & Yu, S. Fourier transform infrared spectroscopic analysis of protein secondary structures. *Acta biochimica et biophysica Sinica* **39**, 549-559 (2007).

237 Arrondo, J. L. R. & Goñi, F. M. Structure and dynamics of membrane proteins as studied by infrared spectroscopy. *Progress in biophysics and molecular biology* **72**, 367-405 (1999).

238 Goormaghtigh, E., Raussens, V. & Ruysschaert, J.-M. Attenuated total reflection infrared spectroscopy of proteins and lipids in biological membranes. *Biochimica et Biophysica Acta (BBA)-Reviews on Biomembranes* **1422**, 105-185 (1999).

239 Barth, A. Infrared spectroscopy of proteins. *Biochimica et Biophysica Acta (BBA)-Bioenergetics* **1767**, 1073-1101 (2007).

240 Liu, K.-Z., Shaw, R. A., Man, A., Dembinski, T. C. & Mantsch, H. H. Reagent-free, simultaneous determination of serum cholesterol in HDL and LDL by infrared spectroscopy. *Clinical chemistry* **48**, 499-506 (2002).

241 Lenk, T. J., Horbett, T. A., Ratner, B. D. & Chittur, K. K. Infrared spectroscopic studies of time-dependent changes in fibrinogen adsorbed to polyurethanes. *Langmuir* **7**, 1755-1764 (1991).

242 Eftink, M. R. The use of fluorescence methods to monitor unfolding transitions in proteins. *Biophysical journal* **66**, 482 (1994).

243 Ladokhin, A. S., Jayasinghe, S. & White, S. H. How to measure and analyze tryptophan fluorescence in membranes properly, and why bother? *Analytical biochemistry* **285**, 235-245 (2000).

244 Royer, C. A. Probing protein folding and conformational transitions with fluorescence. *Chemical reviews* **106**, 1769-1784 (2006).

245 Carpenter, J. F., Prestrelski, S. J. & Dong, A. Application of infrared spectroscopy to development of stable lyophilized protein formulations. *European Journal of Pharmaceutics and Biopharmaceutics* **45**, 231-238 (1998).

246 Byler, D. M. & Susi, H. Examination of the secondary structure of proteins by deconvolved FTIR spectra. *Biopolymers* **25**, 469-487 (1986).

247 Krimm, S. & Bandekar, J. Vibrational spectroscopy and conformation of peptides, polypeptides, and proteins. *Advances in protein chemistry* **38**, 181-364 (1986).

248 Bandekar, J. Amide modes and protein conformation. *Biochimica et Biophysica Acta (BBA)-Protein Structure and Molecular Enzymology* **1120**, 123-143 (1992).

249 Fu, K., Griebenow, K., Hsieh, L., Klibanov, A. M. & Langera, R. FTIR characterization of the secondary structure of proteins encapsulated within PLGA microspheres. *Journal of Controlled Release* **58**, 357-366 (1999).

250 Carrasquillo, K. G. *et al.* Non-aqueous encapsulation of excipient-stabilized spray-freeze dried BSA into poly (lactide-co-glycolide) microspheres results in release of native protein. *Journal of Controlled Release* **76**, 199-208 (2001).

251 Castellanos, I. J., Cruz, G., Crespo, R. & Griebenow, K. Encapsulation-induced aggregation and loss in activity of γ-chymotrypsin and their prevention. *Journal of controlled release* **81**, 307-319 (2002).

252 Ramachander, R. *et al.* Solid state fluorescence of lyophilized proteins. *Analytical biochemistry* **376**, 173-182 (2008).

253 Ptitsyn, O. Molten globule and protein folding. *Advances in protein chemistry* **47**, 83-229 (1995).

254 Ptitsyn, O. B. Structures of folding intermediates. *Current opinion in structural biology* **5**, 74-78 (1995).

255 Ghisaidoobe, A. B. & Chung, S. J. Intrinsic tryptophan fluorescence in the detection and analysis of proteins: a focus on Förster resonance energy transfer techniques. *International journal of molecular sciences* **15**, 22518-22538 (2014).

256 Eftink, M. Fluorescence techniques for studying protein structure. *Methods of biochemical analysis* **35**, 127 (1991).

257 Lakowicz, J. Principles of Fluorescence Spectroscopy, 3rd edn, 2006. *Search PubMed*, 63-95.

258 Ruan, K. *et al.* A rare protein fluorescence behavior where the emission is dominated by tyrosine: case of the 33-kDa protein from spinach photosystem II. *Biochemical and biophysical research communications* **293**, 593-597 (2002).

259 Ross, J. A., Laws, W. R., Rousslang, K. W. & Wyssbrod, H. R. Tyrosine Fluorescence and Phosphorescence from Proteins and Polypeptides. *Biochemical Applications* **3**, 1 (1992).

260 Chattopadhyay, A. & Haldar, S. Dynamic insight into protein structure utilizing red edge excitation shift. *Accounts of chemical research* **47**, 12-19 (2013).

261 Tcherkasskaya, O. & Uversky, V. N. Denatured collapsed states in protein folding: example of apomyoglobin. *Proteins: Structure, Function, and Bioinformatics* **44**, 244-254 (2001).

262 Royer, C. A., Mann, C. J. & Matthews, C. R. Resolution of the fluorescence equilibrium unfolding profile of trp aporepressor using single tryptophan mutants. *Protein Science* **2**, 1844-1852 (1993).

263 Szpikowska, B. K., Beechem, J. M., Sherman, M. A. & Mas, M. T. Equilibrium unfolding of yeast phosphoglycerate kinase and its mutants lacking one or both native tryptophans: a circular dichroism and steady-state and time-resolved fluorescence study. *Biochemistry* **33**, 2217-2225 (1994).

264 Sharma, V. K. & Kalonia, D. S. Steady-state tryptophan fluorescence spectroscopy study to probe tertiary structure of proteins in solid powders. *Journal of pharmaceutical sciences* **92**, 890-899 (2003).

265 Shortle, D., Meeker, A. K. & Freire, E. Stability mutants of staphylococcal nuclease: large compensating enthalpy-entropy changes for the reversible denaturation reaction. *Biochemistry* **27**, 4761-4768 (1988).

266 Eftink, M. R., Ghiron, C. A., Kautz, R. A. & Fox, R. O. Fluorescence and conformational stability studies of Staphylococcus nuclease and its mutants, including the less stable nuclease-concanavalin A hybrids. *Biochemistry* **30**, 1193-1199 (1991).

267 Schwehm, J. M. & Stites, W. E. [8] Application of automated methods for determination of protein conformational stability. *Methods in enzymology* **295**, 150-170 (1998).

268 Gryczynski, I., Eftink, M. & Lakowicz, J. R. Conformation heterogeneity in proteins as an origin of heterogeneous fluorescence decays, illustrated by native and denatured ribonuclease T 1. *Biochimica et Biophysica Acta (BBA)-Protein Structure and Molecular Enzymology* **954**, 244-252 (1988).

269 Callis, P. R. & Burgess, B. K. Tryptophan fluorescence shifts in proteins from hybrid simulations: an electrostatic approach. *The Journal of Physical Chemistry B* **101**, 9429-9432 (1997).

270 Szabo, A., Stepanik, T., Wayner, D. & Young, N. Conformational heterogeneity of the copper binding site in azurin. A time-resolved fluorescence study. *Biophysical journal* **41**, 233 (1983).

271 Royer, C. A. *et al.* Effects of amino acid substitutions on the pressure denaturation of staphylococcal nuclease as monitored by fluorescence and nuclear magnetic resonance spectroscopy. *Biochemistry* **32**, 5222-5232 (1993).

272 Lakowicz, J. Principles of fluorescence spectroscopy. 3rd edn Springer. *New York* (2006).

273 Jiao, M. *et al.* Structural and functional alterations of two multidomain oxidoreductases induced by guanidine hydrochloride. *Acta biochimica et biophysica Sinica* **42**, 30-38 (2010).

274 Prakash, K., Prajapati, S., Ahmad, A., Jain, S. & Bhakuni, V. Unique oligomeric intermediates of bovine liver catalase. *Protein science* **11**, 46-57 (2002).

275 Gaudana, R., Khurana, V., Parenky, A. & Mitra, A. K. Encapsulation of protein-polysaccharide HIP complex in polymeric nanoparticles. *Journal of drug delivery* **2011** (2011).

276 Swed, A., Cordonnier, T., Fleury, F. & Boury, F. Protein encapsulation into PLGA nanoparticles by a novel phase separation method using non-toxic solvents. *Journal of Nanomedicine & Nanotechnology* **2014** (2014).

277 Singhal, A., Morris, V., Labhasetwar, V. & Ghorpade, A. Nanoparticle-mediated catalase delivery protects human neurons from oxidative stress. *Cell death & disease* **4**, e903 (2013).

278 Fessi, H., Puisieux, F., Devissaguet, J. P., Ammoury, N. & Benita, S. Nanocapsule formation by interfacial polymer deposition following solvent displacement. *International journal of pharmaceutics* **55**, R1-R4 (1989).

279 Morales-Cruz, M. *et al.* Two-step nanoprecipitation for the production of protein-loaded PLGA nanospheres. *Results in pharma sciences* **2**, 79-85 (2012).

280 Reddy, D. S., Reddy, B., Gunasekhar, K. & Reddy, P. S. Nanostructured Cd1− xMnxS Films for Spintronics and Optoelectronic Device Applications: Synthesis and

Characterization. *Journal of nanoscience and nanotechnology* **8**, 6487-6490 (2008).

281 Bergmeyer, H., Gawehn, K. & Grassl, M. Enzymes as biochemical reagents. *Methods of enzymatic analysis* **1**, 425-522 (1974).

282 Aebi, H. [13] Catalase in vitro. *Methods in enzymology* **105**, 121-126 (1984).

283 Zhou, Z. & Kang, Y. J. Cellular and subcellular localization of catalase in the heart of transgenic mice. *Journal of Histochemistry & Cytochemistry* **48**, 585-594 (2000).

284 Bai, J., Rodriguez, A. M., Melendez, J. A. & Cederbaum, A. I. Overexpression of catalase in cytosolic or mitochondrial compartment protects HepG2 cells against oxidative injury. *Journal of Biological Chemistry* **274**, 26217-26224 (1999).

285 Goth, L. A simple method for determination of serum catalase activity and revision of reference range. *Clinica Chimica Acta* **196**, 143-151 (1991).

286 Kaszuba, M., McKnight, D., Connah, M. T., McNeil-Watson, F. K. & Nobbmann, U. Measuring sub nanometre sizes using dynamic light scattering. *Journal of Nanoparticle Research* **10**, 823-829 (2008).

287 Marshall, F. H. *et al.* Diffusion and reactivity in ultraviscous aerosol and the correlation with particle viscosity. *Chemical Science* **7**, 1298-1308 (2016).

288 Bihari, P. *et al.* Optimized dispersion of nanoparticles for biological in vitro and in vivo studies. *Particle and fibre toxicology* **5**, 14 (2008).

289 Ramadan, E., Borg, T., Abdelghani, G. & Saleh, N. M. Transdermal microneedle-mediated delivery of polymeric lamivudine-loaded nanoparticles. *journal of Pharmaceutical Technology and Drug Research* **5**, 1 (2016).

290 Yan, C. *et al.* Characterization and morphological analysis of protein-loaded poly (lactide-co-glycolide) microparticles prepared by water-in-oil-in-water emulsion technique. *Journal of Controlled Release* **32**, 231-241 (1994).

291 Sah, H. Stabilization of proteins against methylene chloride/water interface-induced denaturation and aggregation. *Journal of controlled release* **58**, 143-151 (1999).

292 Sturesson, C. & Carlfors, J. Incorporation of protein in PLG-microspheres with retention of bioactivity. *Journal of Controlled Release* **67**, 171-178 (2000).

293 Abdelwahed, W., Degobert, G. & Fessi, H. Investigation of nanocapsules stabilization by amorphous excipients during freeze-drying and storage. *European Journal of Pharmaceutics and Biopharmaceutics* **63**, 87-94 (2006).

294 Abdelwahed, W., Degobert, G. & Fessi, H. A pilot study of freeze drying of poly (epsilon-caprolactone) nanocapsules stabilized by poly (vinyl alcohol): formulation and process optimization. *International journal of pharmaceutics* **309**, 178-188 (2006).

295 Pikal, M. J. Mechanisms of protein stabilization during freeze-drying and storage: The relative importance of thermodynamic stabilization and glassy state relaxation dynamics. *Freeze-drying/lyophilization of pharmaceutical and biological products* **96**, 161-198 (1999).

296 Angell, C. & Franks, F. Water: A comprehensive treatise. *by F. Franks, Plenum, New York* **7**, 1 (1982).

297 Carpenter, J. F. & Crowe, J. H. An infrared spectroscopic study of the interactions of carbohydrates with dried proteins. *Biochemistry* **28**, 3916-3922 (1989).

298 Allison, S. D., Dong, A. & Carpenter, J. F. Counteracting effects of thiocyanate and sucrose on chymotrypsinogen secondary structure and aggregation during freezing, drying, and rehydration. *Biophysical journal* **71**, 2022 (1996).

299 Gopalakrishnan, B., Nash, K. M., Velayutham, M. & Villamena, F. A. Detection of nitric oxide and superoxide radical anion by electron paramagnetic resonance spectroscopy from cells using spin traps. *JoVE (Journal of Visualized Experiments)*, e2810-e2810 (2012).

300 Raha, S., McEachern, G. E., Myint, A. T. & Robinson, B. H. Superoxides from mitochondrial complex III: the role of manganese superoxide dismutase. *Free Radical Biology and Medicine* **29**, 170-180 (2000).

301 White, S. M., Constantin, P. E. & Claycomb, W. C. Cardiac physiology at the cellular level: use of cultured HL-1 cardiomyocytes for studies of cardiac muscle cell structure and function. *American Journal of Physiology-Heart and Circulatory Physiology* **286**, H823-H829 (2004).

302 Claycomb, W. C. *et al.* HL-1 cells: a cardiac muscle cell line that contracts and retains phenotypic characteristics of the adult cardiomyocyte. *Proceedings of the National Academy of Sciences* **95**, 2979-2984 (1998).

303 Xueping, W. & Valen, G. GW24-e1418 Protective effect of bone morphogenetic protein 4 (BMP4) on oxidative stress induced cardiomyocyte death. *Heart* **99**, A15-A15 (2013).

304 He, H. *et al.* Calcineurin suppresses AMPK-dependent cytoprotective autophagy in cardiomyocytes under oxidative stress. *Cell death & disease* **5**, e997 (2014).

305 Koumangoye, R. B. *et al.* Reduced annexin A6 expression promotes the degradation of activated epidermal growth factor receptor and sensitizes invasive breast cancer cells to EGFR-targeted tyrosine kinase inhibitors. *Molecular cancer* **12**, 1 (2013).

306 Fadok, V. A. *et al.* Exposure of phosphatidylserine on the surface of apoptotic lymphocytes triggers specific recognition and removal by macrophages. *The Journal of Immunology* **148**, 2207-2216 (1992).

307 Vermes, I., Haanen, C., Steffens-Nakken, H. & Reutellingsperger, C. A novel assay for apoptosis flow cytometric detection of phosphatidylserine expression on early

apoptotic cells using fluorescein labelled annexin V. *Journal of immunological methods* **184**, 39-51 (1995).

308 Breu, A., Rosenmeier, K., Kujat, R., Angele, P. & Zink, W. The cytotoxicity of bupivacaine, ropivacaine, and mepivacaine on human chondrocytes and cartilage. *Anesthesia & Analgesia* **117**, 514-522 (2013).

309 Wei, C., Kumar, S., Kim, I.-K. & Gupta, S. Thymosin beta 4 protects cardiomyocytes from oxidative stress by targeting anti-oxidative enzymes and anti-apoptotic genes. *PloS one* **7**, e42586 (2012).

310 Malhi, S. S. & Murthy, R. S. R. Delivery to mitochondria: a narrower approach for broader therapeutics. *Expert opinion on drug delivery* **9**, 909-935 (2012).

311 Yellon, D. M. & Hausenloy, D. J. Myocardial reperfusion injury. *New England Journal of Medicine* **357**, 1121-1135 (2007).

312 Heusch, G. *et al.* Cardiovascular remodelling in coronary artery disease and heart failure. *The Lancet* **383**, 1933-1943 (2014).

313 Ambrosio, G., Becker, L. C., Hutchins, G. M., Weisman, H. & Weisfeldt, M. Reduction in experimental infarct size by recombinant human superoxide dismutase: insights into the pathophysiology of reperfusion injury. *Circulation* **74**, 1424-1433 (1986).

314 Chi, L. *et al.* Effect of superoxide dismutase on myocardial infarct size in the canine heart after 6 hours of regional ischemia and reperfusion: a demonstration of myocardial salvage. *Circulation research* **64**, 665-675 (1989).

315 Kilgore, K. *et al.* Protective effects of the SOD-mimetic SC-52608 against ischemia/reperfusion damage in the rabbit isolated heart. *Journal of molecular and cellular cardiology* **26**, 995-1006 (1994).

316 Näslund, U. *et al.* Superoxide dismutase and catalase reduce infarct size in a porcine myocardial occlusion-reperfusion model. *Journal of molecular and cellular cardiology* **18**, 1077-1084 (1986).

317 Downey, J. M., Omar, B., Ooiwa, H. & McCord, J. Superoxide dismutase therapy for myocardial ischemia. *Free radical research communications* **13**, 703-720 (1991).

318 Gallagher, K., Buda, A. J., Pace, D., Gerren, R. & Shlafer, M. Failure of superoxide dismutase and catalase to alter size of infarction in conscious dogs after 3 hours of occlusion followed by reperfusion. *Circulation* **73**, 1065-1076 (1986).

319 Nejima, J. *et al.* Superoxide dismutase reduces reperfusion arrhythmias but fails to salvage regional function or myocardium at risk in conscious dogs. *Circulation* **79**, 143-153 (1989).

320 Ooiwa, H., Stanley, A., Felaneous-Bylund, A. C., Wilborn, W. & Downey, J. M. Superoxide dismutase conjugated to polyethylene glycol fails to limit myocardial

infarct size after 30 min ischemia followed by 72h of reperfusion in the rabbit. *Journal of molecular and cellular cardiology* **23**, 119-125 (1991).

321 Uraizee, A., Reimer, K. A., Murry, C. E. & Jennings, R. B. Failure of superoxide dismutase to limit size of myocardial infarction after 40 minutes of ischemia and 4 days of reperfusion in dogs. *Circulation* **75**, 1237-1248 (1987).

322 Vanhaecke, J. *et al.* Effect of superoxide dismutase on infarct size and postischemic recovery of myocardial contractility and metabolism in dogs. *Journal of the American College of Cardiology* **18**, 224-230 (1991).

323 Bulluck, H., Yellon, D. M. & Hausenloy, D. J. Reducing myocardial infarct size: challenges and future opportunities. *Heart*, heartjnl-2015-307855 (2015).

324 Paradis, M., Gagné, J., Mateescu, M.-A. & Paquin, J. The effects of nitric oxide-oxidase and putative glutathione-peroxidase activities of ceruloplasmin on the viability of cardiomyocytes exposed to hydrogen peroxide. *Free Radical Biology and Medicine* **49**, 2019-2027 (2010).

325 Liang, Q., Yu, X., Qu, S., Xu, H. & Sui, D. Acanthopanax senticosides B ameliorates oxidative damage induced by hydrogen peroxide in cultured neonatal rat cardiomyocytes. *European journal of pharmacology* **627**, 209-215 (2010).

326 Zhu, Y. *et al.* Salidroside protects against hydrogen peroxide-induced injury in cardiac H9c2 cells via PI3K-Akt dependent pathway. *DNA and cell biology* **30**, 809-819 (2011).

327 Keene, A. M., Balasubramanian, R., Lloyd, J., Shainberg, A. & Jacobson, K. A. Multivalent dendrimeric and monomeric adenosine agonists attenuate cell death in HL-1 mouse cardiomyocytes expressing the A 3 receptor. *Biochemical pharmacology* **80**, 188-196 (2010).

328 Saraste, A. *et al.* Apoptosis in human acute myocardial infarction. *Circulation* **95**, 320-323 (1997).

329 Silverman, H. S. & Stern, M. D. Ionic basis of ischaemic cardiac injury: insights from cellular studies. *Cardiovascular research* **28**, 581-597 (1994).

330 Itoh, G. *et al.* DNA fragmentation of human infarcted myocardial cells demonstrated by the nick end labeling method and DNA agarose gel electrophoresis. *The American journal of pathology* **146**, 1325 (1995).

331 Hoek, T. L. V. *et al.* Reperfusion, not simulated ischemia, initiates intrinsic apoptosis injury in chick cardiomyocytes. *American Journal of Physiology-Heart and Circulatory Physiology* **284**, H141-H150 (2003).

332 Li, C. & Jackson, R. M. Reactive species mechanisms of cellular hypoxia-reoxygenation injury. *American Journal of Physiology-Cell Physiology* **282**, C227-C241 (2002).

333 Cheng, W. *et al.* Programmed myocyte cell death affects the viable myocardium after infarction in rats. *Experimental cell research* **226**, 316-327 (1996).

334 Zhao, Z.-Q. & Vinten-Johansen, J. Myocardial apoptosis and ischemic preconditioning. *Cardiovascular research* **55**, 438-455 (2002).

335 Hearse, D. J. & Bolli, R. Reperfusion induced injury: manifestations, mechanisms, and clinical relevance. *Cardiovascular research* **26**, 101-108 (1992).

336 Sosnovik, D. E. *et al.* Molecular MRI of cardiomyocyte apoptosis with simultaneous delayed-enhancement MRI distinguishes apoptotic and necrotic myocytes in vivo potential for midmyocardial salvage in acute ischemia. *Circulation: Cardiovascular Imaging* **2**, 460-467 (2009).

337 Gao, E. *et al.* Darbepoetin alfa, a long-acting erythropoietin analog, offers novel and delayed cardioprotection for the ischemic heart. *American Journal of Physiology-Heart and Circulatory Physiology* **293**, H60-H68 (2007).

338 Wang, K. *et al.* miR-874 regulates myocardial necrosis by targeting caspase-8. *Cell death & disease* **4**, e709 (2013).

339 Wang, J.-X. *et al.* MicroRNA-103/107 regulate programmed necrosis and myocardial ischemia/reperfusion injury through targeting FADD. *Circulation research* **117**, 352-363 (2015).

340 Ali, M. A., Kandasamy, A. D., Fan, X. & Schulz, R. Hydrogen peroxide-induced necrotic cell death in cardiomyocytes is independent of matrix metalloproteinase-2. *Toxicology in Vitro* **27**, 1686-1692 (2013).

341 Fabbri, F. *et al.* Sequential events of apoptosis involving docetaxel, a microtubule-interfering agent: a cytometric study. *BMC Cell Biology* **7**, 1 (2006).

342 Ravassa, S., Zudaire, A., Carr, R. D. & Díez, J. Antiapoptotic effects of GLP-1 in murine HL-1 cardiomyocytes. *American Journal of Physiology-Heart and Circulatory Physiology* **300**, H1361-H1372 (2011).

343 Suzuki, K., Kostin, S., Person, V., Elsässer, A. & Schaper, J. Time course of the apoptotic cascade and effects of caspase inhibitors in adult rat ventricular cardiomyocytes. *Journal of molecular and cellular cardiology* **33**, 983-994 (2001).

344 Bailey, R. W. *et al.* Sequence of physical changes to the cell membrane during glucocorticoid-induced apoptosis in S49 lymphoma cells. *Biophysical journal* **96**, 2709-2718 (2009).

345 Seshadri, G. *et al.* The delivery of superoxide dismutase encapsulated in polyketal microparticles to rat myocardium and protection from myocardial ischemia-reperfusion injury. *Biomaterials* **31**, 1372-1379 (2010).

346 Lin, M.-J. *et al.* Massive palmitoylation-dependent endocytosis during reoxygenation of anoxic cardiac muscle. *Elife* **2**, e01295 (2013).

347 Von Harsdorf, R., Li, P.-F. & Dietz, R. Signaling pathways in reactive oxygen species–induced cardiomyocyte apoptosis. *Circulation* **99**, 2934-2941 (1999).

348 Jamnicki-Abegg, M. *et al.* Isoflurane inhibits cardiac myocyte apoptosis during oxidative and inflammatory stress by activating Akt and enhancing Bcl-2 expression. *The Journal of the American Society of Anesthesiologists* **103**, 1006-1014 (2005).

349 Movahed, A., Yu, L., Thandapilly, S., Louis, X. & Netticadan, T. Resveratrol protects adult cardiomyocytes against oxidative stress mediated cell injury. *Archives of biochemistry and biophysics* **527**, 74-80 (2012).

350 Boncler, M., Różalski, M., Krajewska, U., Podsędek, A. & Watala, C. Comparison of PrestoBlue and MTT assays of cellular viability in the assessment of anti-proliferative effects of plant extracts on human endothelial cells. *Journal of pharmacological and toxicological methods* **69**, 9-16 (2014).

351 Owusu-Ansah, E., Yavari, A. & Banerjee, U. A protocol for in vivo detection of reactive oxygen species. *Protocol Exchange* **10** (2008).

352 Lu, Z.-x. *et al.* RETRACTED ARTICLE: Cardioprotective activity of placental growth factor in a rat model of acute myocardial infarction: nanoparticle-based delivery versus direct myocardial injection. *BMC cardiovascular disorders* **14**, 1 (2014).

353 Arrondo, J. L. R., Muga, A., Castresana, J. & Goñi, F. M. Quantitative studies of the structure of proteins in solution by Fourier-transform infrared spectroscopy. *Progress in biophysics and molecular biology* **59**, 23-56 (1993).

354 Barth, A. & Zscherp, C. What vibrations tell about proteins. *Quarterly reviews of biophysics* **35**, 369-430 (2002).

355 Vonhoff, S., Condliffe, J. & Schiffter, H. Implementation of an FTIR calibration curve for fast and objective determination of changes in protein secondary structure during formulation development. *Journal of pharmaceutical and biomedical analysis* **51**, 39-45 (2010).

356 Tanaka, M., Morishima, I., Akagi, T., Hashikawa, T. & Nukina, N. Intra-and intermolecular β-pleated sheet formation in glutamine-repeat inserted myoglobin as a model for polyglutamine diseases. *Journal of Biological Chemistry* **276**, 45470-45475 (2001).

357 Prestrelski, S., Arakawa, T. & Carpenter, J. Separation of freezing-and drying-induced denaturation of lyophilized proteins using stress-specific stabilization: II. Structural studies using infrared spectroscopy. *Archives of Biochemistry and Biophysics* **303**, 465-473 (1993).

358 Prestrelski, S. J., Pikal, K. A. & Arakawa, T. Optimization of lyophilization conditions for recombinant human interleukin-2 by dried-state conformational analysis using Fourier-transform infrared spectroscopy. *Pharmaceutical research* **12**, 1250-1259 (1995).

359 Griebenow, K. & Klibanov, A. M. On protein denaturation in aqueous-organic mixtures but not in pure organic solvents. *Journal of the American Chemical Society* **118**, 11695-11700 (1996).

360 Mansur, H. S., Sadahira, C. M., Souza, A. N. & Mansur, A. A. FTIR spectroscopy characterization of poly (vinyl alcohol) hydrogel with different hydrolysis degree and chemically crosslinked with glutaraldehyde. *Materials Science and Engineering: C* **28**, 539-548 (2008).

361 Park, J. *et al.* Effect of pH and excipients on structure, dynamics, and long-term stability of a model IgG1 monoclonal antibody upon freeze-drying. *Pharmaceutical research* **30**, 968-984 (2013).

362 Banerjee, S., Zamocky, M., Furtmüller, P. G. & Obinger, C. Probing the two-domain structure of homodimeric prokaryotic and eukaryotic catalase–peroxidases. *Biochimica et Biophysica Acta (BBA)-Proteins and Proteomics* **1804**, 2136-2145 (2010).

363 Lakshmi, T. & Nandi, P. Effects of sugar solutions on the activity coefficients of aromatic amino acids and their N-acetyl esters. *Journal of Physical Chemistry* **80**, 249-252 (1976).

364 Gao, E. *et al.* A novel and efficient model of coronary artery ligation and myocardial infarction in the mouse. *Circulation research* **107**, 1445-1453 (2010).